Building Integrated Solar Concentrators for Façade Applications

Piratheepan Mahendran

A thesis submitted to

Auckland University of Technology

in fulfilment of the requirements for the degree of

Doctor of Philosophy (PhD)

2016

School of Engineering, Computer and Mathematical Sciences

ABSTRACT

In this study a novel building façade integrated photovoltaic/thermal (BIPVT) collector was designed to produce both electricity and hot water. Based on the shortcomings of concepts presented in the literature, a simple robust façade integrated collector using flat plate reflectors was developed, modelled and tested both experimentally and theoretically.

In developing the BIPVT collector, an optical study comparing façade integrated collectors incorporated with parabolic and flat plate reflectors was carried out using a non-imaging ray tracing analysis and experiments. It concluded that, flat plate reflectors rather than parabolic reflectors for façade applications offer significant potential. It was shown that flat reflectors avoid uneven illumination profiles and hence the need for special photovoltaic absorber materials. Subsequently a generalised expression for the concentration ratio of the proposed collector was determined.

Furthermore, the absence of natural convection heat transfer relationships for façade integrated solar concentrators was realized. To address this, a computational fluid dynamics analysis was carried out to deduce a relationship, and this was validated by an experimental test rig. The relationship showed that the heat transfer, expressed in terms on the Nusselt number, is strongly dependent on the Rayleigh number and the aspect ratio (A/H), and can be expressed in the form $Nu=a\ Ra^{b}\ (A/H)^{c}$.

Having characterised the heat loss, ways of improving the thermal transport properties of the heat transfer media were examined. For this study multi-walled

carbon nanotube (MWCNT) nanofluids were examined. It was found that these impaired the turbulent forced convection heat transfer coefficient, needed more pumping power compared to water and would not be suitable for use in a BIPVT collector.

Finally, a conceptual collector was designed and analysed using a one-dimensional thermal network. This numerical model was coupled with the generalised geometric relationship for the concentration ratio and was validated with an outdoor experiment.

Using the model, a number of parameters affecting the collector performance were identified. It was found that when the thermal conductance between the silicon cells and thermal absorber was doubled, the combined efficiency of the collector was improved by 10%. Increasing the flow rate of the working fluid only marginally improved the efficiency; however, increasing the number of cooling channels across the absorber improved it significantly, due to increasing fin efficiency. It was also found that, the power generated by the collectors was strongly dependant on the reflectance of the reflectors. In summary, the results show the potential opportunity for concentrating BIPVT collectors in façade applications.

ACKNOWLEDGEMENTS

This thesis would not have been possible without the generous support of the wonderful people around me. Firstly, I would like to thank my supervisor Dr Timothy Anderson for letting me undertake this work and his continuous support throughout these three years. I would like to acknowledge his patience and commitment in guiding me to the finishing line by gently nudging my ideas towards clarity and form. Also a big thank to my secondary supervisor Prof John Raine for his continuous support and thoughts regarding the work despite his busy schedule.

My gratitude goes to AUT and the School of Engineering who supported this research in many ways. In particular, Head of research Prof Zhan Chen for continuous meetings and general advice in making a successful PhD journey. My sincere thanks also goes to the school manager and the administrative staff for arranging me a comfortable working space and taking care of the rest.

I thank Jim Crossen and Tim Luton from the workshop for their help in making my test rigs and continuous support throughout the installations. Also thanks must go to, Dave Crofts and Clayton Lines for their thoughts on all things electrical and helping get my test rig running on the roof against the odds.

Thanks also go to my solar research colleagues Reza, Aziz, and Uzair for the valuable discussions during the course of my studies. Thanks must also go to dear friend Thayaparan for his thoughts and support.

I thank my Primary School principal Mr Selvakumar and high school teacher Mr Shivakumar and my extended family for making me who I am today.

I thank my mother Nageswary, for her love and being there with me during my ups and downs through my life, my father Mahendran and brothers Pirabakar and Shivashanker for being there in case I needed anything morally or financially.

Finally, my heartfelt thanks to my lovely wife Layani, for patiently putting up with me during the hardship of these three years and my beautiful daughter Rathinii who was born and has grown with my PhD.

LIST OF PUBLICATIONS

The following papers have been published over the course of this research. Though covered by this thesis, they form an additional body of work the reader may wish to refer to.

Journal papers:

Piratheepan, M. and Anderson, T., 2015, "Natural Convection Heat Transfer in Façade Integrated Solar Concentrators", *Solar Energy*, Vol 122, pp. 271-276, December 2015

Piratheepan, M. and Anderson, T., 2014, "An experimental investigation of turbulent forced convection heat transfer by a multi-walled carbon-nanotube nanofluid", *International Communications in Heat and Mass Transfer*, Vol 57, pp. 286-290, October 2014

Conference papers:

Piratheepan, M and Anderson, T.N, 2015 "Optical Properties of Low Concentration Ratio Façade Integrated Solar Collectors" Asia- Pacific Solar Research Conference, Brisbane, Australia

Piratheepan, M. and Anderson, T.N, 2015, "Evaluation of a Facade Integrated Concentrating Solar Collector System" Solar World Congress 2015, Daegu, South Korea

Piratheepan, M. and Anderson, T.N, 2014, "Experimental Evaluation of Natural Heat Transfer in Façade Integrated Triangular Enclosures" Asia- Pacific Solar Research Conference, Sydney, Australia

Piratheepan, M. and Anderson, T.N, 2014, “Experimental Evaluation of Low Concentration Collectors for Façade Applications”, Australian Solar Council Scientific Conference 2014, Melbourne, Australia

Piratheepan, M. and Anderson, T.N., 2013, “Optical Characteristics of Low Concentration Ratio Solar Collectors for Façade Applications”, Proceedings of ENZCON13, 20th Electronics New Zealand Conference, Auckland, September 2013

TABLE OF CONTENTS

ABSTRACT ii

ACKNOWLEDGEMENTS iv

LIST OF PUBLICATIONS vi

TABLE OF CONTENTS viii

LIST OF FIGURES xii

LIST OF TABLES xvi

ATTESTATION OF AUTHORSHIP xvii

Chapter 1: Introduction 1

1.1 Overview 1

1.2 Solar energy 2

1.3 Solar energy conversion 3

1.3.1 Solar thermal collectors 4

1.3.2 Solar photovoltaic collectors 8

1.3.3 Photovoltaic/thermal collectors (PVT) 12

1.3.4 Concentrating solar PVT collectors 17

1.4 Building integrated solar energy systems (BISES) 19

1.5 Low concentration ratio collectors for building integration 21

1.6 Thesis objective 24

Chapter 2: Optical assessment on the geometry of the collector 25

2.1 Reflector design 25

2.1.1 Parabolic collectors 26

2.1.2 Flat plate collectors 27

2.2 Simulation method 28

2.3 Simulation results 30

2.4 Experimental method 33

2.5 Experimental results 35

2.6 Remarks 38

Chapter 3: Development of the collector geometry 39

3.1 Ray tracing and concentration ratio 39

3.2 Mathematical expression for concentration ratio at different elevation angles. 43

3.3 Sun-Earth geometric relationship 47

3.4 Experimental validation 49

3.5 Modelling results and analysis 51

3.6 Remarks 53

Chapter 4: Determination of thermal losses 55

4.1 Introduction 56

4.2 Computational fluid dynamics analysis 57

4.3 Experimental validation method 59

4.4 Experimental analysis 62

4.5 Results 64

4.5.1 CFD results 64

4.5.2 Experimental results 68

4.6 Empirical relationship 69

Chapter 5: Determination of appropriate heat transfer media 71

5.1 Overview 71

5.2. Experiment and the validation of the test rig 73

5.2.1 Method 73

5.2.2 Validation of experimental apparatus 74

5.3 Nanofluid preparation 77

5.3.1 Pre-preparation 77

5.3.2 Bulk nanofluid preparation 83

5.4 Analysis of nanofluid and results 83

5.5 Remarks 87

Chapter 6: Development of a combined analytical PVT system model 89

6.1 Overview 89

6.2 Mathematical model 90

6.3 Development of a prototype collector and the model validation 99

6.4 Model results 105

6.4.1 Effect of design variables 107

6.4.2 Performance of collector under various weather conditions 113

6.5 Remarks 116

Chapter 7: Conclusions and recommendations for future work 118

7.1 Conclusions 118

7.2 Future recommendations 120

References 123

Appendix A: Uncertainty analysis 138

A.1 Uncertainty analysis of the experiment relation to the geometrical concentration ratio confirmation 138

A.2 Uncertainty analysis in natural convection heat transfer coefficient measurements 140

A.3 Uncertainties associated with final module testing 143

A.4 EES code used for the simulation of the collector 146

LIST OF FIGURES

Figure 1 Classification of solar thermal technologies 5

Figure 2 Evacuated tube collector 6

Figure 3 Flat plate collector 7

Figure 4 Photovoltaic solar collectors 9

Figure 5 Classification of PV technologies (Petter, Breivik and Drolsum 2012) . 10

Figure 6 Schematic diagram of air cooled PVT collector with dual air flow 14

Figure 7 Schematic diagram of water-cooled PVT collector 15

Figure 8 Classification of solar concentrators 18

Figure 9 Facade integrated low concentration collector incorporated with flat reflectors 23

Figure 10 Cross section of a symmetrical CPC 26

Figure 11 Flat reflector booster collector 28

Figure 12 Façade integrated concentrator profiles 29

Figure 13 Number of rays hitting the absorber vs elevation angle (α) of the source 30

Figure 14 Elevation angle vs effective concentration ratio 31

Figure 15 Illumination on the absorber module at various elevation angles under parabolic reflector 32

Figure 16 Illumination on the absorber module at various elevation angles under flat reflector 33

Figure 17 Schematic diagrams of the parabolic and flat reflectors 34

Figure 18 Schematic diagram of the absorber 34

Figure 19 Local concentration ratios across the absorber at 30 degree elevation angle 36
Figure 20 Local concentration ratios across the absorber at 45 degree elevation angle 36
Figure 21 Local concentration ratios across the absorber at 60 degree elevation angle 37
Figure 22 Angle of rotation of reflector and the absorber combination 40
Figure 23 Number of rays received by the absorber at different elevation and reflector angles when the absorber is fixed at 0° 41
Figure 24 Number of rays received by the absorber at different elevation and reflector angles when the absorber is fixed angle at 10° 42
Figure 25 Number of rays received by the absorber at different elevation and reflector angles when the absorber is fixed angle at 20° 42
Figure 26 Number of rays received by the absorber at different elevation and reflector angles when the absorber is fixed angle at 30° 43
Figure 27 Geometrical representation of the collector 45
Figure 28 Optical ray tracing at different elevation angles 46
Figure 29 Schematic diagram of the test rig 49
Figure 30 Experimental concentration ratio and calculated concentration ratio ... 50
Figure 31 Concentration ratios over the year 51
Figure 32 Change in radiation on absorber on 9th of January 52
Figure 33 Change in radiation on absorber on 30th of June 53
Figure 34 Façade integrated solar concentrator 55
Figure 35 Enclosures modelled in CFD 59

Figure 36 Module to be used for the heat transfer experiment 60
Figure 37 Schematic of the experimental setup 61
Figure 38 Natural convection heat transfer coefficient vs Temperature difference for enclosures with varying aspect ratios 65
Figure 39 Nusselt vs Rayleigh number for enclosures with varying aspect ratios 66
Figure 40 Natural convection heat transfer coefficient vs Temperature difference in enclosures i and iv 67
Figure 41 Nusselt vs Rayleigh number for experimental and CFD analysis 69
Figure 42 Test rig to measure the heat transfer coefficient of the fluid under constant temperature 74
Figure 43 Experimental vs empirical Nusselt number values 77
Figure 44 Samples without surfactant with different sonication time 79
Figure 45 Sonicated samples with surfactant as shown in table 1 80
Figure 46 Surfactant treated MWCNT sample 81
Figure 47 Untreated MWCNT sample 82
Figure 48 Magnified view of surfactant treated MWCNT sample 82
Figure 49 Comparison of water and nanofluid heat transfer characteristics 87
Figure 50 Façade integrated concentrator 90
Figure 51 Schematic arrangement of the collector and the thermal energy balance 91
Figure 52 Simple thermal network of the proposed module 91
Figure 53 Façade integrated PVT collector outdoor test rig 101
Figure 54 Experimental test rig and the circuit diagram for electrical measurements 102

Figure 55 Experimental and theoretical efficiencies of façade integrated collector 104
Figure 56 Combined efficiency by varying flow rate 108
Figure 57 Combined efficiency by varying tube spacing 109
Figure 58 Combined efficiency by varying cell to absorber heat transfer coefficient 110
Figure 59 Thermal efficiency varying packing factor..... 111
Figure 60 Combined efficiency varying packing factor 112
Figure 61 Performance of the collector varying the reflectance of the reflector 113
Figure 62 Combined efficiency varying wind speed 114
Figure 63 Performance of the collector on 9th of January..... 115
Figure 64 Performance of the collector on 30th of June..... 116
Figure 65 Experimental concentration ratio and calculated concentration ratio with the uncertainty values..... 139
Figure 66 Nusselt vs Rayleigh number for experimental and CFD analysis with the uncertainty values..... 143
Figure 67 Experimental and theoretical efficiencies of façade integrated collector 145

LIST OF TABLES

Table 1 Composition of the sample experiments 78

Table 2 Physical characteristics of experimental prototype 103

Table 3: Parameters used for the sensitivity analysis 105

ATTESTATION OF AUTHORSHIP

I hereby declare that this submission is my own work and that, to the best of my knowledge and belief, it contains no material previously published or written by another person (except where explicitly defined in the acknowledgements), nor material which to a substantial extent has been submitted for the award of any other degree or diploma of a university or other institution of higher learning.

Auckland Signature_____

Chapter 1: Introduction

1.1 Overview

Energy and water are two primary concerns of modern society in its desire to sustain its recent technological growth in the future. Modern technological advances, conveniences, global population growth and modern mechanised food production techniques would not be possible without humanity having taken advantage of cheap non-renewable fossil fuels in the past. Thus, rising energy prices, rapidly diminishing non-renewable energy sources, rapid increase in population, energy scarcity and security, and growing environmental concerns are challenging the existing global energy paradigm (IEA 2012). According to the census by the United States Census Bureau (2013), the global population at the present time is nearly 7.1 billion, while every 13 seconds it is increasing by one person and it may approach 10 billion by 2050 (United Nations Population Division 2004). But contemporary improvement in the global energy networks is increasingly insufficient to meet the growing energy demand.

According to the International Energy Agency, buildings represent 40% of global energy consumption (IEA 2013). In many parts of the world, energy consumption for heating and cooling in buildings, domestic appliances and lighting are the major portion of the energy demand. With the recent advancement in consumable electronics technologies and living standards, energy consumption in buildings is expected to increase sharply in the near future.

In many locations a significant portion of the building energy demand is met by energy produced from fossil fuels. Therefore, reducing or offsetting the energy

consumption in the built environment may relieve the burden on the overall fossil fuel consumption. Energy efficient building design and advanced materials for building construction may be also a way forward in addressing this issue.

The primary purpose of the building envelope is to provide shelter from the weather, security, privacy and comfort for the occupants. If the materials used to provide these comforts can be seamlessly merged, or replaced, with energy harnessing materials without compromising the primary requirements, this will reduce the energy dependency of the building on the grid power supply. One possible option may be materials that harness solar energy to provide the energy required in the buildings.

The key challenge in doing this is to optimise the design of these types of advanced building materials without significantly altering the traditional building practices.

1.2 Solar energy

Solar energy is the source of energy that has supported life on earth since the early ages of the earth. It is a clean, environmentally friendly, widely abundant and sustainable energy resource that is comparatively well-spread over the world, unlike fossil fuels. Solar energy reaches the earth as electromagnetic radiation that can be represented as photons. The earth can therefore be seen as a huge collector of solar energy where, naturally, plants absorb the energy via photosynthesis, the warm air causes the wind and the evaporated ocean results in the rain. This natural phenomenon has been happening for millions of years. Without the sun providing a near constant source of energy input into Earth's thermodynamic system, it is

unlikely that such a complex ecosystem would have been capable of existing and thriving into the many forms seen around the globe today.

The sun mostly produces its energy by changing four million tonnes of hydrogen, into helium every second via a continuous fusion reaction. The estimated amount of energy produced by sun per second is $3.8x10^{23}$ kW while only a fraction i.e. $1.8x10^{14}$ kW reaches the earth (IEA 2011a). The amount of solar energy striking the earth every hour ($4.3x10^{20}$ J) would be enough to power the whole planet for a year (Foster, et al., 2010). Even if 1% of the energy reaching the world is converted with 10% efficiency it would be enough to meet the energy demand of the world comprehensively. In recent years, methods to harness the solar energy either directly, in the form of photovoltaic and solar thermal devices, or indirectly in the form of hydropower, wind power and bio-mass have been widely used in energy production.

1.3 Solar energy conversion

Since prehistoric times, radiation from the sun has been directly used for heating and lighting the surrounding while indirectly used for fresh water and food production and preservation. It is recorded by Greek philosopher Socrates (470-399 BC) that having the correct orientation of a house means it will be warmer during the winter and cooler during the summer. In 212 BC, it is believed, the scientist Archimedes proposed, and succeeded, in setting fire to a Roman naval fleet using a large number of concave mirrors (Anderson 1977). Although the ways of collecting solar energy evolved with time, the basic idea of capturing the electromagnetic rays remains the same.

In the modern world solar energy collection methods are classified into two different categories, passive and active. Passive collection methods are mostly achieved by innovative building design. This allows the occupant to take advantage of solar energy purely by changing the initial design of the building without any special collectors or instruments retrofitted. The usage of a thermal chimney to enhance cooling and appropriate window placement to allow the natural light to enter are classical examples of passive collection methods. In contrast to the passive collection methods, active methods make use of special collectors that employ active mechanical/electrical components to collect and transfer heat and generate electrical energy. Widely available photovoltaic panels and solar thermal collectors are examples of active collection methods (Goswami, Kreith and Kreider 2000).

1.3.1 Solar thermal collectors

Solar thermal collection is achieved by using a surface to intercept the solar radiation from the sun. Some of the radiation falling on this surface is absorbed while some of it is reflected. The absorbed radiation will increase the surface temperature and this heat can be removed using a working fluid.

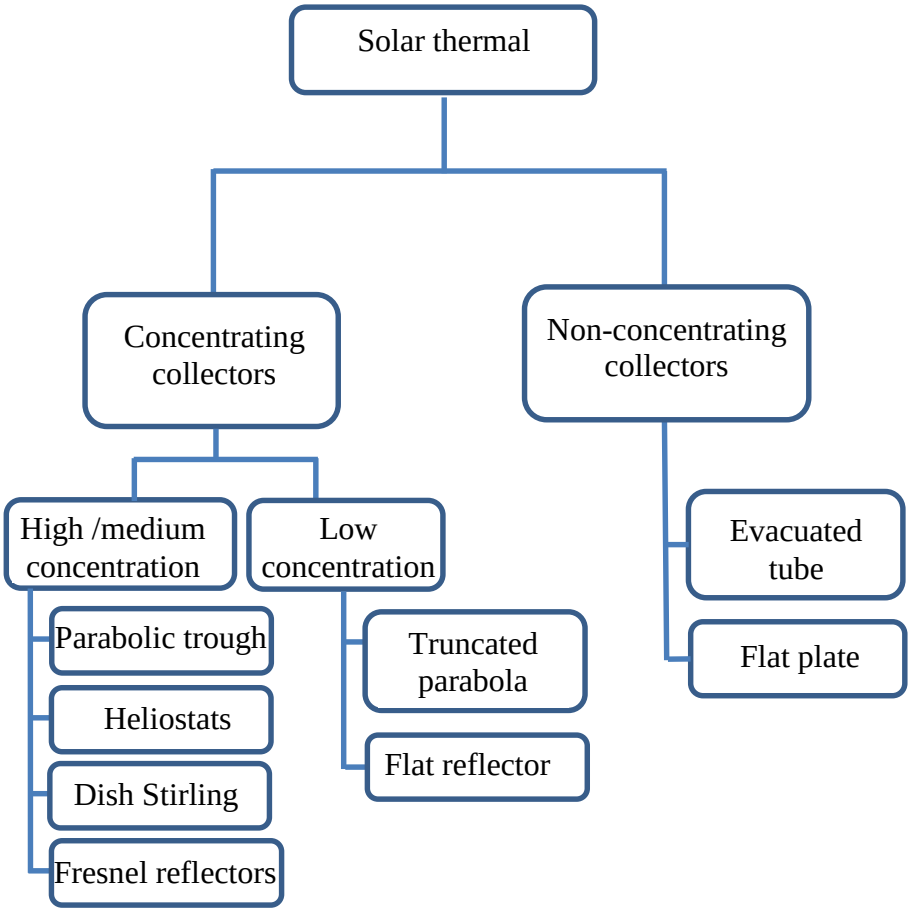

Figure 1 Classification of solar thermal technologies

As shown in Figure 1, these collectors can be classified into two categories: non-concentrating collectors and concentrating collectors. The former category has a receiver and an absorber of equal area while the later has a reflector or lens surface, which receives the radiation and concentrates it on to a small absorber area, thereby increasing the radiation flux per unit area.

Non-concentrating collectors are usually stationary and do not need any tracking mechanisms. There are two main types of stationary collectors available in the market, evacuated tube collectors and flat plate collectors.

A typical evacuated tube collector features a heat pipe inside a sealed vacuum tube as shown in Figure 2. The heat pipe contains a small amount of fluid that undergoes

a phase change cycle every time it is warm enough. It is vaporised and flows along the heat sink to lose its latent heat and become a liquid again. The condensed liquid returns to the collector tube to collect the heat again. The maximum/minimum temperature it can reach is a phase change temperature, which eliminates the risk of the overheating or freezing of the collector during adverse conditions (Norton 2014). This is one of the main advantages of evacuated tube collector as it means that, unlike conventional flat plate collectors, evacuated tube collectors are suitable for robust weather changes.

Figure 2 Evacuated tube collector

The flat plate collector is based on a simple mechanism of harnessing the heat energy by obstructing the solar radiation with a surface of high absorptivity as

shown in Figure 3. When solar radiation passes through the glazing material and is incident on the absorber, this absorber absorbs a large portion of energy and transfers it to the working fluid flowing underneath the absorber through the riser tubes. These riser tubes are connected to a header tube or manifold that carries the warm fluid away.

Figure 3 Flat plate collector

Usually absorber plates are well insulated at the base and the sides to reduce conduction losses from the rear and sides of the absorber. Glass covers reduce the convection and radiation losses from the top of the absorber plate. These covers prevent convection losses by restricting the air movement between the absorber and

ambient environment, while radiation losses are reduced by the optical characteristics of the glass cover. Transmittance of the glass will allow the short wave radiation from the sun to pass through while preventing long wave thermal radiation emitted by the absorber plate from escaping (Kalogirou 2004).

Both evacuated tube and flat plate collectors are commonly used in domestic water heating, pool heating and space heating where very high temperatures are not required.

1.3.2 Solar photovoltaic collectors

Although the photovoltaic effect was discovered in the 19th century by French physicist Edmond Becquerel, the first modern silicon based semi-conductors were manufactured only in 1954 (Chapin, Fuller and Pearson 1954). Initially photovoltaic (PV) modules were only used in space shuttles and remote locations where there were no other alternative energy sources available. In the initial stages it needed more energy to build one of these devices than it could deliver over its life time (Rittner 1954). However, the space race between the USA and the USSR in the 1960s led to tremendous improvements in efficiencies and manufacturing methods of photovoltaic modules (Goswami et al. 2000). From the year 2000, large scale silicon based PV production started, followed by financial incentives given by many countries to reduce the carbon footprints and to achieve independence from fossil fuel based energy politics (IEA 2011b).

Photovoltaic solar cells are made up of semi-conductor materials that can convert solar radiation in to electricity without any heat engine between them. Most photovoltaic devices consist of solid-state stationary modules; they are generally

robust and need very little maintenance. These advantages promote the use of solar cells in a wide variety of applications ranging, in recent years, from calculators, watches, remote communication systems, power generation in remote areas and grid connected power generation (Parida, Iniyan and Goic 2011).

Photovoltaic panels such as the one shown in Figure 4 consist of cells made from silicon. However, there is a large range of materials that produce the photoelectric effect, as shown in Figure 5.

Figure 4 Photovoltaic solar collectors

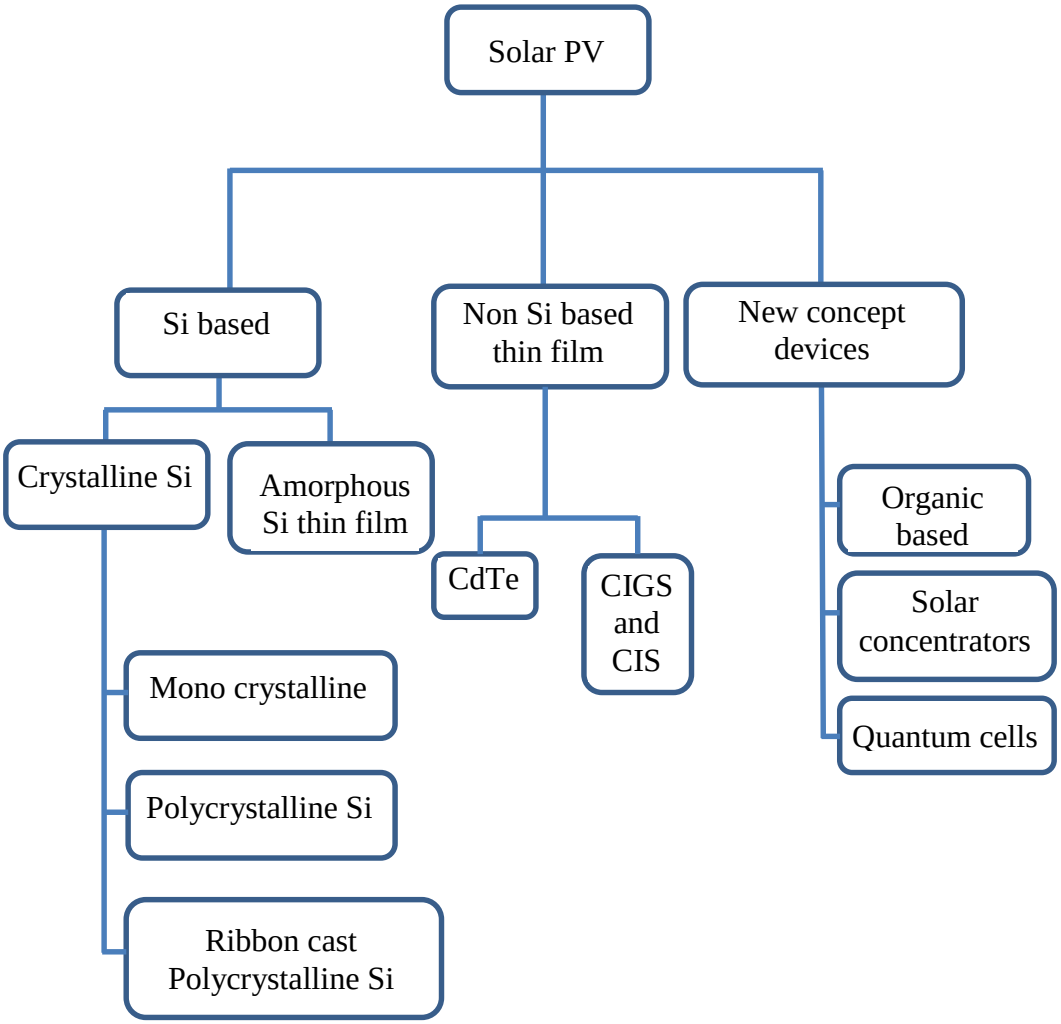

Figure 5 Classification of PV technologies (Petter, Breivik and Drolsum 2012)

Despite the recent improvements and latest manufacturing advancements in the PV industry, one of the shortcomings of photovoltaic energy generation is that the devices tend to have relatively low efficiencies. However, as the latest silicon based semiconductor cells have reached efficiencies of up to 23% (Green et al. 2013), photovoltaic energy generation may possibly have moved one step closer to solar being one of the primary energy resources of modern society.

The basic physics of the photovoltaic effect are well understood. Irradiation from the sun is a flux of photons carrying different amounts of energy with them. When

these photons interact with a semiconductor material, if the energy of the photon is larger than or equal to the band gap of the semiconductor, electrons on the valence shells will move to the conduction band and thus facilitate the photovoltaic effect. Notably, one electron can only gain energy from one photon. If the energy of the particular photon is higher than the band gap, the balance of the energy available will be used to increase the kinetic energy of the electron. If the energy of the photon is lower than the band gap, it may either be reflected off or absorbed by the free carriers and metal contacts, consequently increasing the temperature of the solar cells (Goswami et al. 2000).

Notably, as the temperature of the cell increases, the band gap of the semiconductor will decrease. Hence more photons will have enough energy to induce the electrons through reduced bandgap to increase the short circuit current. However as more and more electrons move between the conduction band and valence band, it will decrease the open circuit voltage (Wenham et al. 2012) and fill factor significantly. As the efficiency of the photovoltaic cell is proportional to the product of these factors, ultimately temperature increase will have a negative cumulative effect on the overall efficiency of the cell.

Research has shown that an increase in cell temperatures of a typical crystalline silicon cell lowers the power output by 0.3 to 0.5% per degree centigrade of temperature increase (Skoplaki and Palyvos 2009). The increase in temperature not only decreases the overall efficiency of the photovoltaic cells, it can also physically damage the cells and lead to premature failure. To overcome this issue, it is vital to integrate a cooling mechanism that can keep the temperature of the cell at a desired limit especially for concentrating PV. A number of studies (Andrews 1981, Cox

and Raghuraman 1985, Florschuetz 1979) have investigated ways to use the waste heat removed by the cooling mechanism in some useful manner, thus forming a combined photovoltaic and thermal system.

1.3.3 Photovoltaic/thermal collectors (PVT)

As an increase in temperature will limit the performance of the photovoltaic collector, attempts to reduce the temperature of such devices by introducing a cooling element into the collector were not promising until a way was found to carry away the heat from the collectors (Kern Jr and Russell 1978). This heat can be used as an energy source for purposes otherwise produced using electricity. The concept of a PVT collector offers a way to generate both electrical and thermal energy simultaneously by allowing photovoltaic and thermal conversion methods to complement each other. This approach also improves the overall efficiency of the photovoltaic output because of the available active cooling (Dubey, Sarvaiya and Seshadri 2013). Among several early studies, Kern Jr and Russell (1978) were one of the earliest researchers to model and test the combined PVT system using water or air as a heat transfer fluid, and found this combination achieved a promising output.

The combination of PV technology and solar thermal technology offers a new hybrid collector. This gives the convenience of having both collectors together in one: thereby saving the cost and space of installing them separately, while producing electrical and thermal energy simultaneously and improving the PV efficiency (IEA 2014). This is particularly useful where the available space is limited. Significant savings in material used, reduction in overall cost and uniform appearance are additional benefits of having both systems together.

In their study (Zondag et al. 2002) explained that despite 80% of solar radiation being absorbed by a conventional PV module, only a small percentage (up to 15%) is converted into electrical energy and the rest heats the module. Further, in their studies (Zondag et al. 2003) found that a PVT system has the potential to produce a higher combined efficiency than separate photovoltaic and thermal modules. They achieved up to 65% combined theoretical efficiency considering the energy losses and other parameters such as the ambient temperature and flow rate of the working fluid.

In a recent study, Zhang and Xu (2015) demonstrated a novel thin PVT collector consisting of an extruded thermal absorber laser welded to the rear of a PV absorber can potentially increase the efficiency up to 71%.

Dealing with the electrical output of the system is comparatively straightforward as produced electrical energy can be either used up straight away or fed back to the grid, as many countries have introduced a feed-in tariff system to the national grid. However, the thermal output of the system not only depends on the collector system but also on other parameters. As the collector is just one part of the system, a complete heat supply system may consist of many subsystems, including auxiliary heaters, storage tanks, flow piping and other instrumentation, which affect the overall efficiency (Chow, He and Ji 2006).

Furthermore, total energy (electrical and thermal) output depends on the solar insolation, wind speed, ambient temperature, type of collector (glazed, unglazed), operating temperature of the system and the type of cells used in the system. For such a system it is vital to prioritise the demand and design accordingly. Higher

temperature may be desirable for a better thermal output but it will be undesirable for better PV output. Hence there should be a compromise made between the total output, type of energy demand and cost of the collector.

The simplest and cheapest hybrid energy modules in the literature are air heating collectors. Air is circulated either on one side of the PV module or above and below to increase the effective heat pick up. The warm air that comes out of the collector could be utilised in desiccant air-conditioning systems. Tiwari and Sodha (2007) found that introducing an additional air gap between the PV module and the glass cover improved the thermal efficiency significantly. Unlike a collector with single airflow, dual air flow collectors, such as the one shown in Figure 6, have shown promising combined efficiency (Hegazy 2000).

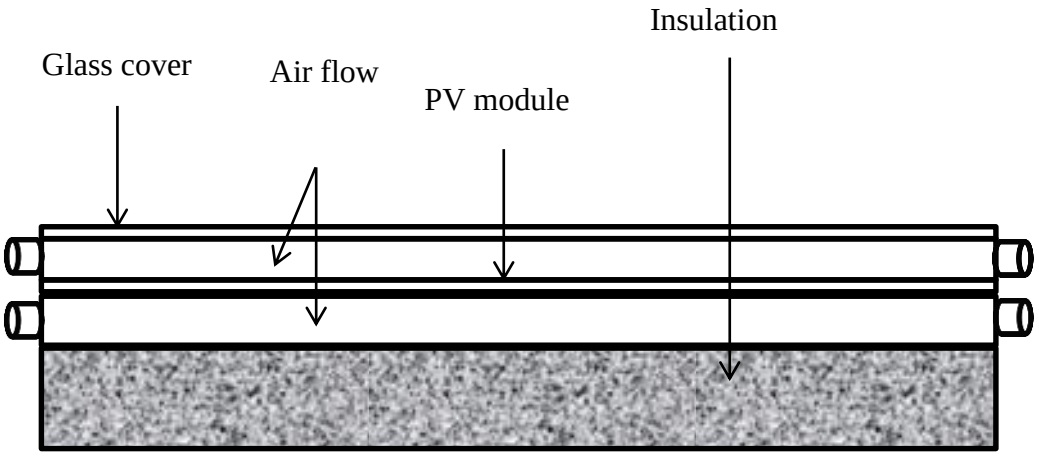

Figure 6 Schematic diagram of air cooled PVT collector with dual air flow

In addition to their system Tripanagnostopoulos, et al. (2002) used stationary reflectors to increase the solar insolation on the module. They found that a combination of reflectors with glazing improved the system efficiency from 59% to 75%. However, glazing may reduce the electrical efficiency due to optical losses

during the transmission through the glass cover. In another study (Tripanagnostopoulos 2007) proposed some cheap alterations such as the addition of fins or the addition of a thin metal sheet in the air duct behind the PV module to improve the performance of PVT air systems.

From a heating perspective, the low density and low thermal capacity of air means, it needs higher volume flowrate to transfer a significant amount of heat energy. Hence, air collectors require a large space for the ducts and thermal storage is not as easy as it is with liquid based collectors. Therefore, air collectors are usually used for space heating applications, as mentioned by (Duffie and Beckman 2006).

PVT water/liquid heating collectors use liquid working fluids instead of air. The most common PVT water collector look similar to a flat plate thermal collector, except a PV module is laminated on top of the riser tubes as shown in Figure 7. The PV module on the top of the riser tubes will generate the electrical energy, while the absorbed heat will be carried away by the liquid flowing through the riser tubes.

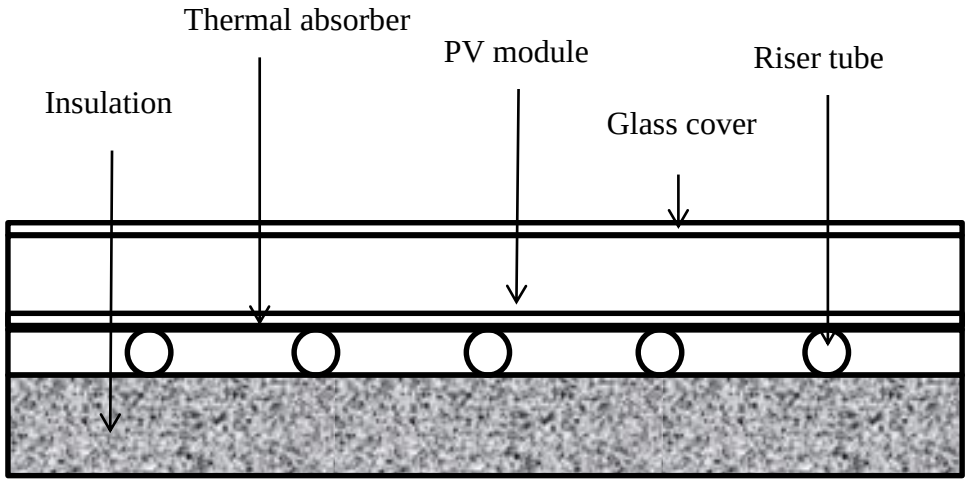

Figure 7 Schematic diagram of water-cooled PVT collector

The theoretical model proposed by (Florschuetz 1979) is one of the earliest studies of PVT solar collectors based on water. He used an extended version of the Hottel-Whillier model to replicate the performance of hybrid collectors. Andrews (1981) found that use of PVT collector was not cost effective at that time due to cheaper alternative energy sources. However, with the increase in the cost of energy in the late 1990s and improvements in solar technology in the early 2000s, the interest in PVT water heating systems was renewed.

Sandnes and Rekstad (2002) examined a PVT water solar collector with a polymer thermal absorber and found that the presence of solar cells reduced the heat absorption by 10%. (Tiwari and Sodha 2007) examined the effect of the packing factor of solar cells (Ratio between the area covered by the solar cells and total absorber area) on the PVT collector. Vokas et al (2006) tested PVT collectors at 3 different locations and showed that the thermal efficiency of the water based domestic PVT system was well suited for lower temperature domestic applications.

Liquid based thermal collectors offer some advantages over air-collectors. The higher heat transport energy density and better heat transfer properties ease the complications in designs of thermal storage. They are also suitable for space heating and cooling while they just need smaller diameter piping rather than the larger ducts for the air collectors (Duffie and Beckman 2006). This is important, especially when space is limited for the collectors.

However, the down sides of the PVT collector technology in general are, they need a large number of PVT receivers to generate enough electricity. The high absorber

costs, trade-off between the electrical output of the collector and the quality of the thermal energy has to be addressed.

1.3.4 Concentrating solar PVT collectors

Although the potential of concentrating hybrid collectors was realised in the 1980s (Gibart 1981), they have been gaining increasing attention from the scientific community due to their potential to produce higher value energy compared to the non-concentrating collectors. There are several solar concentrators described in the literature that have been designed and demonstrated both theoretically and experimentally, as classified in Figure 8.

The range benefits of concentrating PVT solar collectors include high efficiencies, up to 65% (Kandilli 2013), low energy cost, down to 8.7c€ per kWh, (Quaia et al. 2012) and an energy and greenhouse gas payback period of around one year (Cellura et al. 2011).

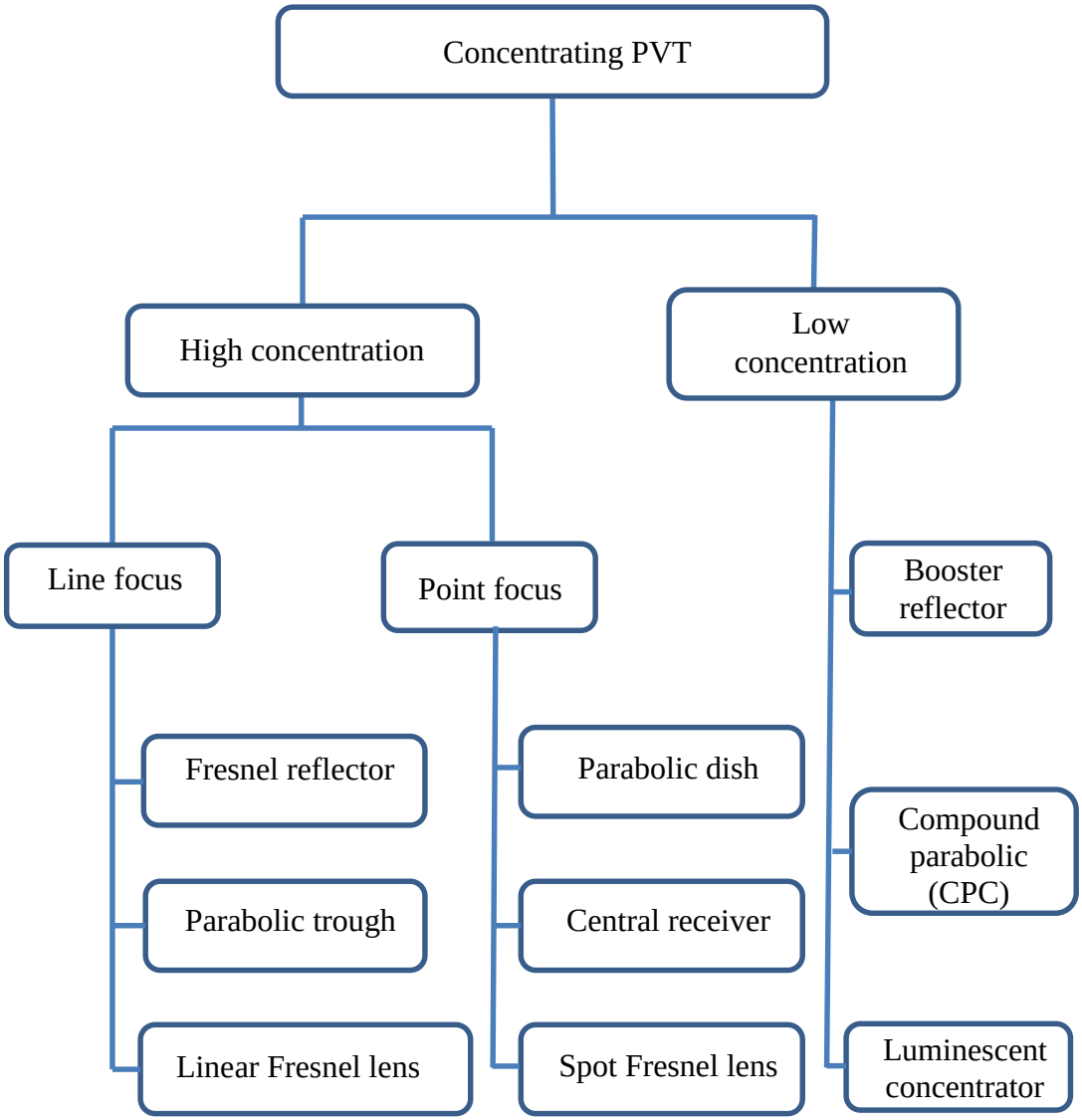

Figure 8 Classification of solar concentrators

Arguably the concentrator collectors avoid many of the disadvantages of non-concentrator collectors, namely by their:

- High electrical efficiency (given that appropriate PV cells are used)
- High thermal efficiency
- Less absorber area required
- Comparatively lower investment cost and high design flexibility (Sharaf and Orhan 2015)

- Low PV cell temperatures and high quality thermal energy
- Enable large capacity

In the literature (Coventry 2005) studied the Combined Heat and Power System (CHAPS) module using antifreeze as a cooling liquid at Australian National University. With a two axis tracking system and mono crystalline solar cells, the system successfully achieved 70 % overall efficiency with a concentration ratio of 37 from parabolic trough reflectors. However, due to high complexity namely, non-uniform illumination, risk of overheating, high PV series resistance and lost diffuse radiation (Da Silva and Fernandes 2010) such collectors are less likely to be adopted in a domestic environment. Furthermore, due to high concentration ratios in these collectors, traditional silicon PV cells which are often suitable for single sun illumination cannot be used (Rosell et al. 2005).

On the other hand, low concentrations collectors do not need tracking hence do not need any moving parts, though they have lower acceptance angle ranges than tracking collectors (Rabl 1976). Unlike high concentrating collectors, low concentration ratio collectors have the advantage of collecting diffuse radiation as well (Petter et al. 2012). Furthermore, low concentration ratio reflectors increase the possibility of using the traditional single sun silicon PV absorber with less need for precise optics.

1.4 Building integrated solar energy systems (BISES)

In recent years there has been increased interest in building solar PV modules that can be integrated within buildings. Such collectors will be an embodiment of the building, as a roof or as a façade element rather than retrofitted to the building. With

the increasing number of solar panels used in urban environments, building integrated PVT (BIPVT) offers high combined efficiency while using up less space, and hence increases the energy density (useful power generated per unit area) from such solar systems.

Furthermore, the cost of the BIPVT can offset the cost of the building structure it replaces, and the electrical energy generated offsets the cost of electricity otherwise purchased at commercial rates for use in the building. The recent advancement in grid connectable solar systems makes the overall system cheaper while ensuring a continuous supply of electricity (IEA 2011b).

However, even with the advantages of a building integrated solar PVT system, they have not been widely commercialized because of the challenges they bring to the architecture and aesthetics of the building. In general, such systems are less appealing to architects and end-users because of the challenges and constraints they bring in to the building design. In support of this, a study by (Munari Probst and Roecker 2007) explains that the primary challenge in developing a new building integrated module is that it should not only be "accepted" by the architects but be "desirable" to be considered as part of a construction system. To achieve these factors such as the geographic location, the limited roof space, and the shading of highly dense city buildings force the designer to think beyond the roof and on to the façade (Quesada et al. 2012).

Furthermore, the concept of building integrated solar energy systems (building integrated thermal for water and/or air heating, building integrated PV and building integrated PV/thermal for water and/or air heating as well as electricity generation)

(Anderson and Duke 2007, Ibrahim et al. 2011, Ibrahim et al. 2014, Daghigh et al. 2009) has been of interest to the research community and the building industry. However, there are very few examples of commercially available products that display "true" integration and those that do exist tend to be particularly specialised and made to order.

1.5 Low concentration ratio collectors for building integration

In an attempt to further reduce the cost associated with BIPVT collectors, increasing the radiation falling on the absorber using low concentrating elements could be a key aspect.

Compared to the currently available BIPVT designs, collectors incorporating reflectors with modules not only increase the output per unit area of the absorbers, but also decreases the architectural burden on designers, as they could deal with cheap reflectors rather than relatively expensive solar modules.

In an urban environment, with limited supply of roof space, low concentrating façade integration opens an innovative way of designing the BIPVT. Systems of this premise have been discussed by researchers in the UK (Zacharopoulos et al. 2000) using non imaging compound parabolic reflectors without any tracking devices. Later in 2004 (Mallick et al.) used an asymmetric compound parabolic photovoltaic concentrator to achieve the optical efficiencies up to 86%. In another experimental study Hall, et al (2005) developed a facade integrated collector to generate electricity suitable for high latitude locations and demonstrated that off-the-shelf silicon modules and static parabolic reflectors made of rolled aluminium could be used for potential cost reductions.

Earlier in 2002 (Brogren and Karlsson) developed a low concentrating water cooled PVT hybrid system based on the MaReCo design (Karlsson and Wilson 2000), using a bifacial absorber. They reported the possible thermal energy extraction, in the form of hot water, suitable for domestic heating purposes. In a more detailed study on the optical efficiency of low concentrating solar energy systems with parabolic reflectors, Brogren (2004) realised the uneven illumination profiles on the absorber and the potential problem it presented to using standard silicon solar cells. Furthermore, although this study explored the importance of having a PVT hybrid absorber, the potential thermal performance was not investigated.

Later in 2008 (Gajbert) explored the various configurations of parabolic reflector systems for both roof and façade integration. The study focused on the thermal analysis of such systems and suggested an optimum configuration based on three different configurations.

On an interesting note, Zanesco and Lorenzo (2002) carried out a cost analysis on a similar system consisting of PV arrays and reported a 38% cost reduction potential compared to standard modules.

Hall, et al (2005) also used a parabolic reflector and reported a 20-30% increase in electrical output compared to a conventional collector. Similarly, in another study Gajbert, Hall and Karlsson (2007) noted that although the concentration ratio of their collector was up to 3.0, the electrical output compared to the vertical reference was only 1.9. Apart from these studies, there is little research done concerning façade integration, while thermal aspects of the absorber plate appear to be ignored or not properly portrayed.

In addition to being technically and structurally robust, solar concentrators suitable for the building integration must fulfil the following requirements formulated by IEA PVPS Task 7 (Schoen et al. 2001, Reijenga 2000) workgroup for the aesthetic quality of building integrated photovoltaics:

- Natural integration
- Architecturally pleasing design
- Good composition of colours and material
- Dimension that fit the gridula, harmony and composition
- Well engineered and innovative design

On that note, modules incorporated with flat reflectors for façade applications, such as the one conceptually represented in Figure 9, appear to have been ignored.

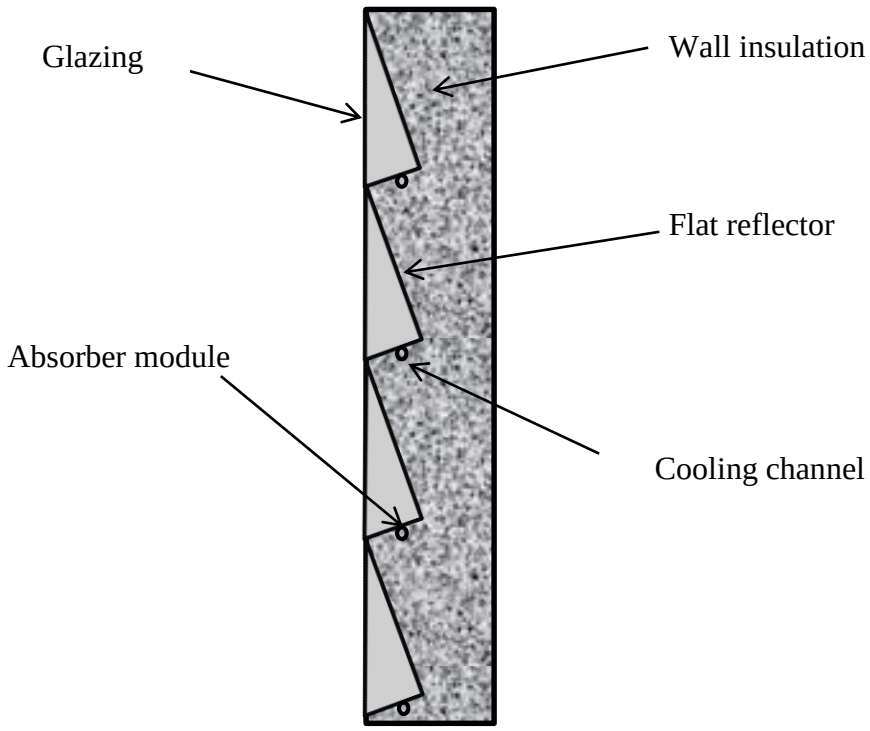

Figure 9 Facade integrated low concentration collector incorporated with flat reflectors

Furthermore, to understand possibilities of using the façade integrated collectors as the skin of a building, it is essential to understand its performance at the design phase. The absence of a combined mathematical model for glazed façade integrated solar concentrator collectors in general appears to be one of the hurdles that the research community may have to overcome to achieve this.

1.6 Thesis objective

The literature has shown that the prospect of using building integrated systems for concentrating radiation to achieve medium temperature heating and electricity generation appears to have been ignored. These factors suggest that there is an opportunity for the design of a cost effective, visually appealing building integrated concentrator system for façade integration. In addressing this, the central question for this work is:

How should a facade integrated concentrating solar collector be designed so that maximum combined electric/thermal efficiency is achieved?

This will be answered through the following steps:

- Finding the most suitable optical arrangement of the collector/absorber system
- Developing an expression for concentration ratio in terms of geometrical relationships
- Determining the heat losses from it
- Examining heat transfer media for use in it
- Developing a combined analytical PVT collector model in order to determine the collector efficiency
- Validating the results with physical testing

Chapter 2: Optical assessment on the geometry of the collector

Based on the literature review, a complete design of a proposed collector has several challenges at the design phase; in particular, a suitable optical arrangement needs to be found. This is best done with the aid of non-imaging ray tracing software that can rapidly inform the design of reflectors.

In considering a solar concentrator, the most common defining characteristic is the concentration ratio, defined by the ratio of the aperture area to the receiver area. Obviously it is desirable to maximize this parameter in order to improve the performance of the collector. The most practical solution to take advantage of this in façade integrated collectors is to use static solar concentrators with medium to low concentration ratios.

As mentioned in Chapter 1, with low concentrating system, it is not necessary to track the sun, thus does not have any moving parts involved. Hence it is possible to use them in building integrated solar collectors where often collectors are the part of the building and hardly movable.

2.1 Reflector design

Compared to the other concentrating techniques, low concentrator reflectors were often overlooked in the past due to the fact that they did not produce the high concentration ratio needed for industrial large scale energy production. However, low concentration modules may also work with an absorber, equipped with conventional silicon solar cells to produce significant amount of energy. These absorbers are comparatively cheap, readily available in the market and do not need the precise optical design of high/medium concentrator devices. Research on low

concentration reflectors conducted in the mid-70's (McDaniels et al. 1975, Rabl 1976) was mainly around two distinctly different reflectors; one a modified compound parabolic reflector and the other based on a simple flat plate reflector often referred to a booster reflector.

2.1.1 Parabolic collectors

Parabolic reflectors are one of the widely used non-imaging concentrator concept in linear and trough type concentrator collectors. As shown in Figure 9, the angle between the axis of the CPC and the line connecting the focus of the parabola with the edge of the aperture is the acceptance half angle (θ_c).

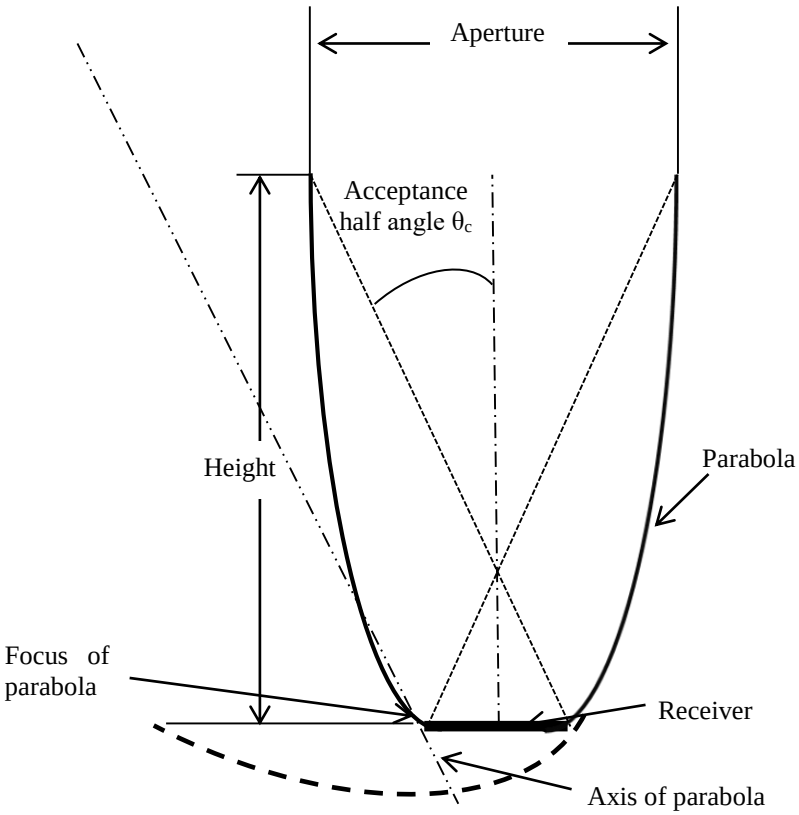

Figure 10 Cross section of a symmetrical CPC

If the reflector is perfect, any radiation entering within this acceptance angle will be funnelled down to the receiver. The theoretical maximum containing the acceptance half angle expression (θ_c) is given in Equation 1 (Welford, Winston and Sinclair 1980).

$$C_{max} = \frac{1}{\sin \theta_c} \quad (1)$$

By modifying the reflectors (either by truncating or extending) higher concentration ratios at a particular angle can be achieved. Changing the area of the reflector material allows variation of the acceptance angle without changing the concentration ratio for a particular range of angles.

Systems of similar truncated semi parabolic concentrators have been proposed for building facade integrated collectors in the past (Gajbert et al. 2007, Brogren 2004).

2.1.2 Flat plate collectors

Flat plate reflectors are one of the easiest ways to increase the insolation incident on a solar collector. Figure 11 shows a typical flat booster reflector collector design with an absorber inclination angle θ_a and a reflector inclination angle of θ_r.

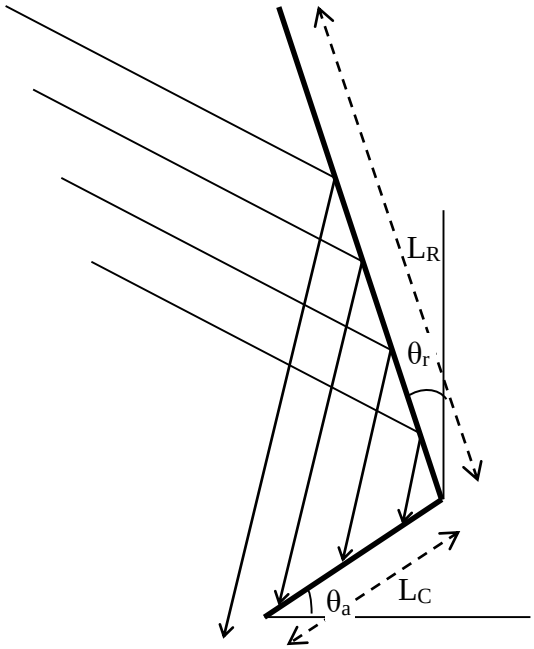

Figure 11 Flat reflector booster collector

Here L_R and L_C are the lengths of the booster reflector and the collector respectively. By changing the size of the reflector plate, the geometric concentration ratio (L_R/L_C) can be manipulated to achieve a higher level of solar radiation on the absorber. Unlike a flat plate collector, inclination angles of both the absorber and reflector can be manipulated to achieve the optimum results (Tanaka 2011).

Although concentrating systems with booster reflective elements have been used in different applications, the possibility of using them in façade applications as highlighted in Chapter 1 appears to have been ignored due to their low concentration ratios.

2.2 Simulation method

Based on the suitability of CPC and flat reflectors for static concentrators, it was decided to examine the concentration ratio of these two possible configurations for a façade integrated concentrator. As such, a collector with a parabolic reflector

incorporated similar to that described in (Gajbert et al. 2007) and a second with a flat reflector, as shown in Figure 12, were examined.

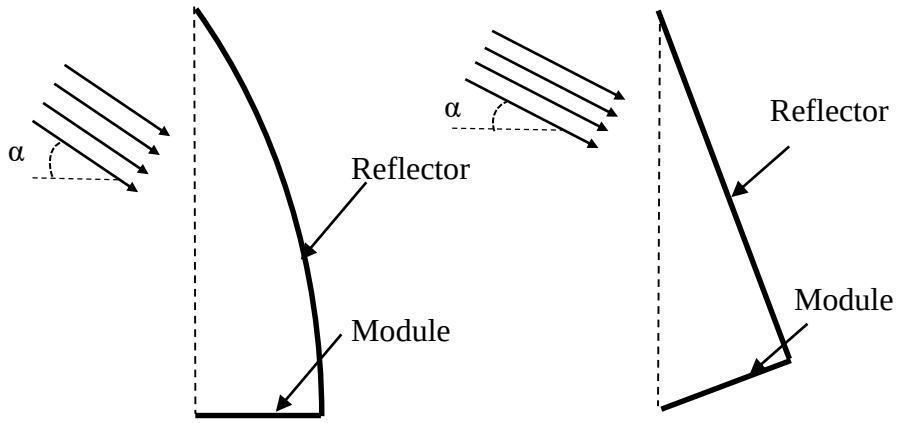

Figure 12 Façade integrated concentrator profiles

To characterize the performance of the two systems it was decided to use the ray-tracing program FRED followed by an experimental comparison. FRED is an optical engineering software program that is capable of performing non-sequential ray tracing analysis of non-imaging optics, such as solar concentrators (FRED 2014). To simplify the ray tracing, it was decided to perform a one dimensional ray tracing study with a collimated optical source of rays, as an approximation of the beam component of solar radiation. It was assumed that the reflectors were perfect reflectors while the absorbers (analysed surface) were perfect absorbers.

To make a fair comparison of the two concentrators, the length of each reflector was kept constant as was the width of the absorber module. The geometrical concentration ratio for both was kept at approximately 3.6. In addition, a horizontal absorber of the same dimensions as that in the concentrators was modelled to serve as a benchmark.

2.3 Simulation results

With each system the illumination pattern on the absorber plate was observed while varying the solar elevation angle (α – measured up from horizon) of the rays between 0 and 90°.

Figure 13 shows the total number of rays received by the absorbers from both modules compared to the reference module for different elevation angles of the source. If the number of rays incident on the absorbers are then normalised against the number of rays incident on the horizontal reference we can determine a relative concentration ratio, as shown in Figure 14.

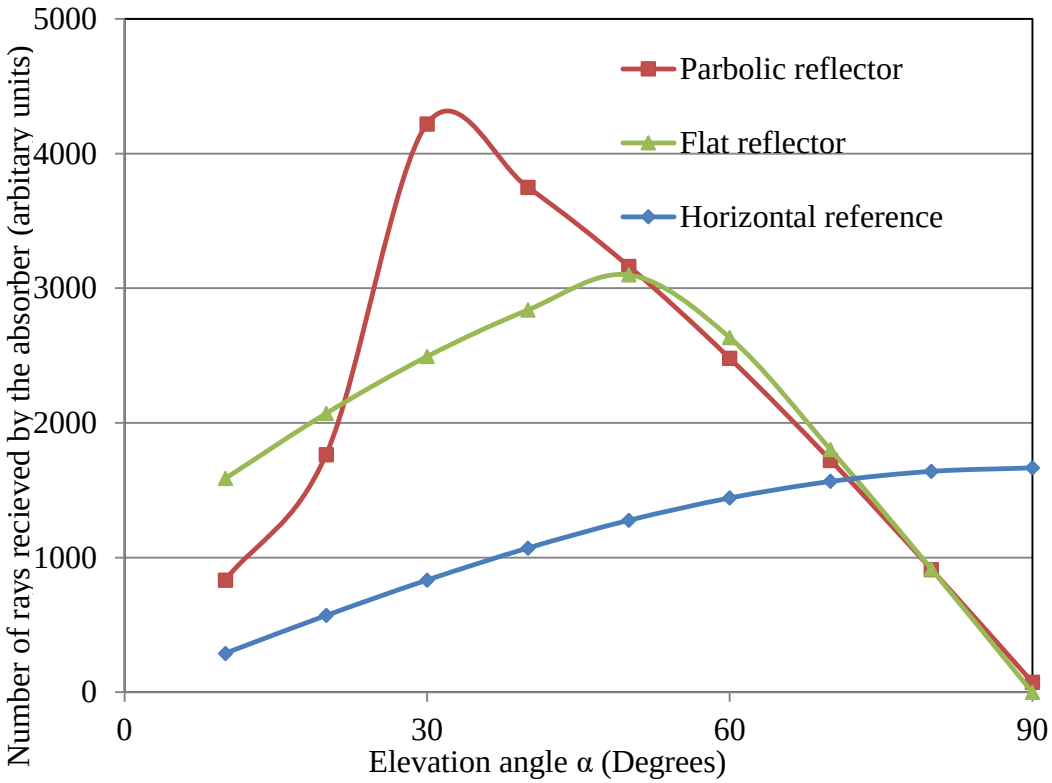

Figure 13 Number of rays hitting the absorber vs elevation angle (α) of the source

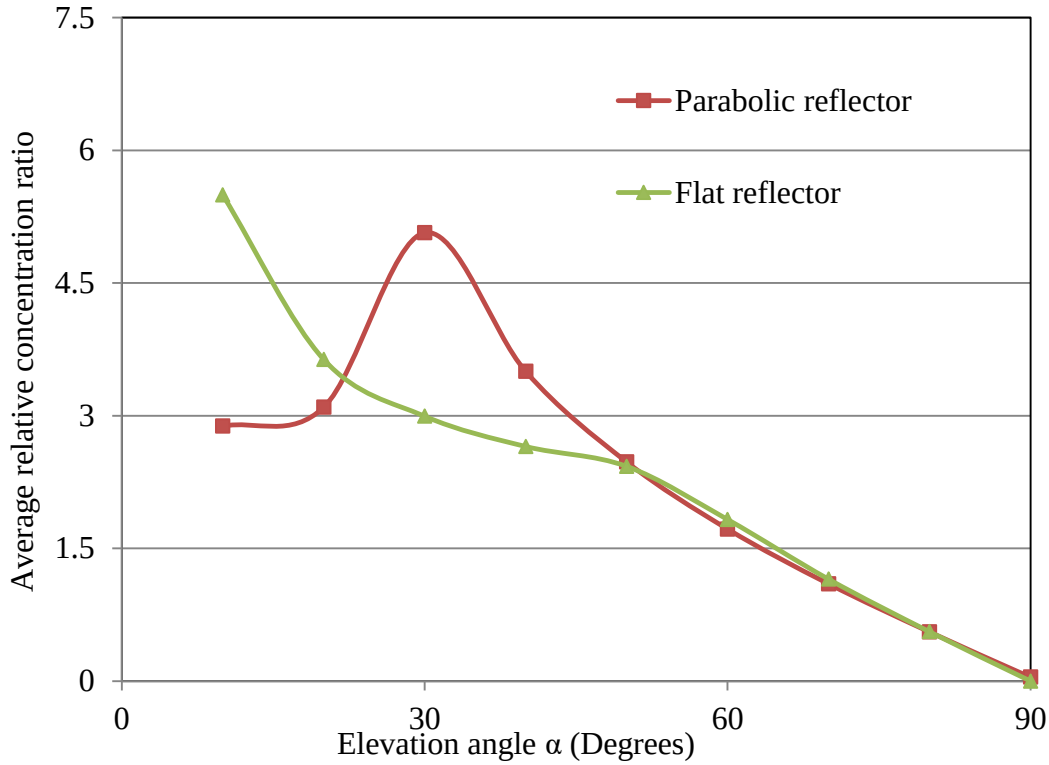

Figure 14 Elevation angle vs effective concentration ratio

By considering both Figure 13 and Figure 14, the conclusion could be drawn that the parabolic reflectors give better performance at a range of elevation angles compared to the flat reflector, as (Brogren and Karlsson 2002) suggested. However, in drawing this conclusion it is important to also consider the local concentration ratio (illumination pattern) on the absorber.

Figure 15 shows the variation in illumination across the width of the absorber with the parabolic reflector (taking the junction of absorber and reflector as the origin). From this, for the mid-range elevation angles, there is a significant non-uniformity in the intensity on the absorber. For example, at an elevation angle of 60° the illumination near the apex is over seven times that at the edge of the absorber. This shows that the illumination profile of parabolic reflectors tends to be non-uniform

and the patterns are discrete and discontinuous in nature due to them focusing the light to a line.

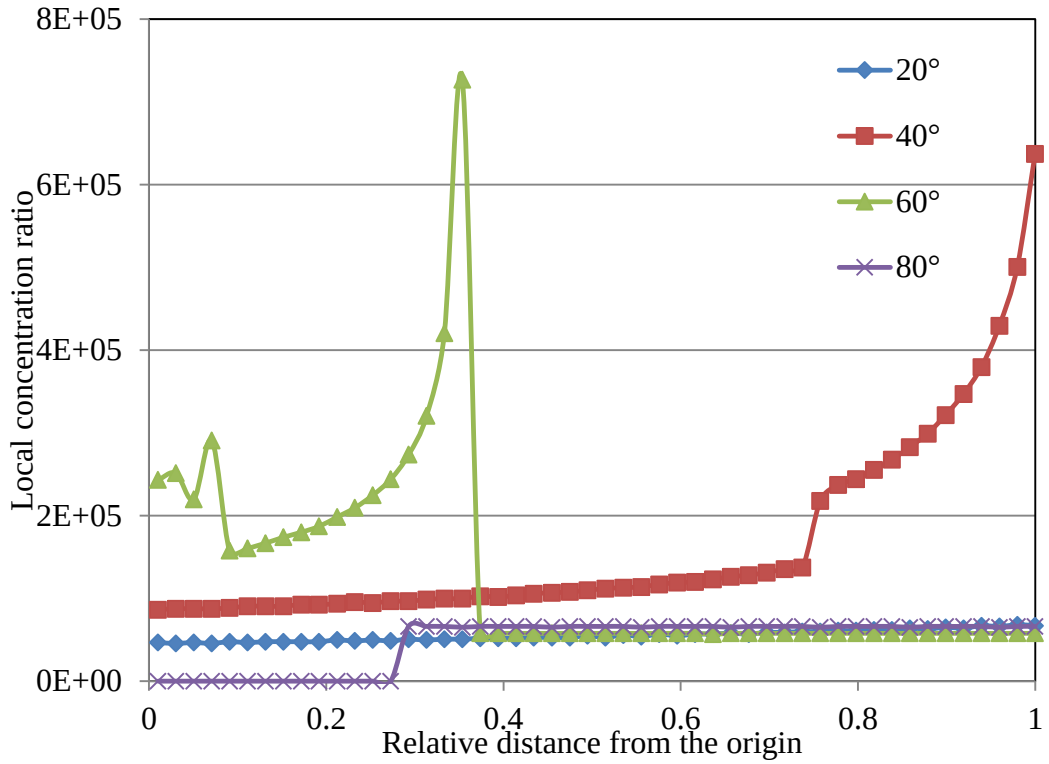

Figure 15 Illumination on the absorber module at various elevation angles under parabolic reflector

Now if we consider the illumination profile from a flat plate reflector, as shown in Figure 16 we can see that the magnitude of the average illumination (flux concentration ratio) is significantly lower than that of a parabolic reflector. This is interesting, because they have the same dimensions but the illumination is more uniform in its distribution. That is to say, the local concentration ratio across the absorber is far more consistent at a particular elevation angle across the absorber surface. Hence each part of the module will produce similar electric current output, so that the undesirable effect of hotspots and thermal energy dissipation otherwise caused under the parabolic reflectors can be avoided.

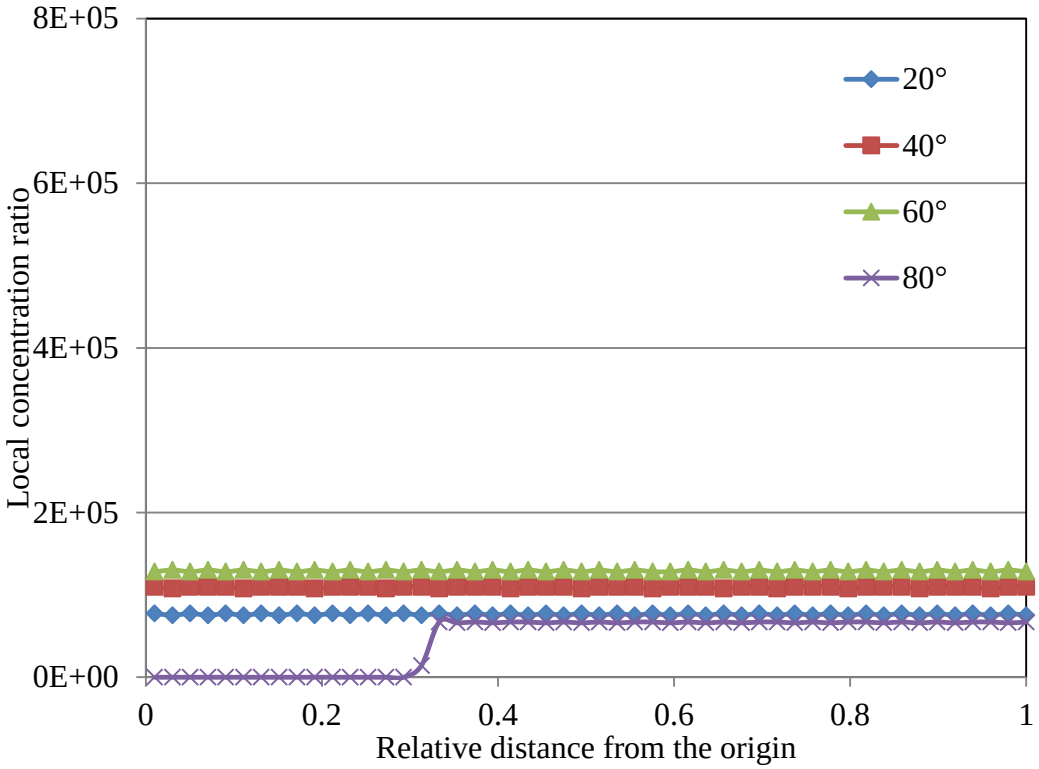

Figure 16 Illumination on the absorber module at various elevation angles under flat reflector

This supports the hypothesis that flat mirror type reflectors could be considered as circular mirror with an infinite radius that will focus on a plane.

2.4 Experimental method

In order to validate the results obtained from the ray tracing it was decided to build two experimental test rigs corresponding to those modelled in the ray tracing analysis. One featured a truncated parabola and the other a flat reflector. Both reflectors were made with silver metallized films with 94% reflectance (3M Solar Mirror Film 1100) affixed to a supporting frame to form the respective shapes. The parabola was made with a focal length of 600mm while the flat reflector was built with the dimensions shown in Figure 17.

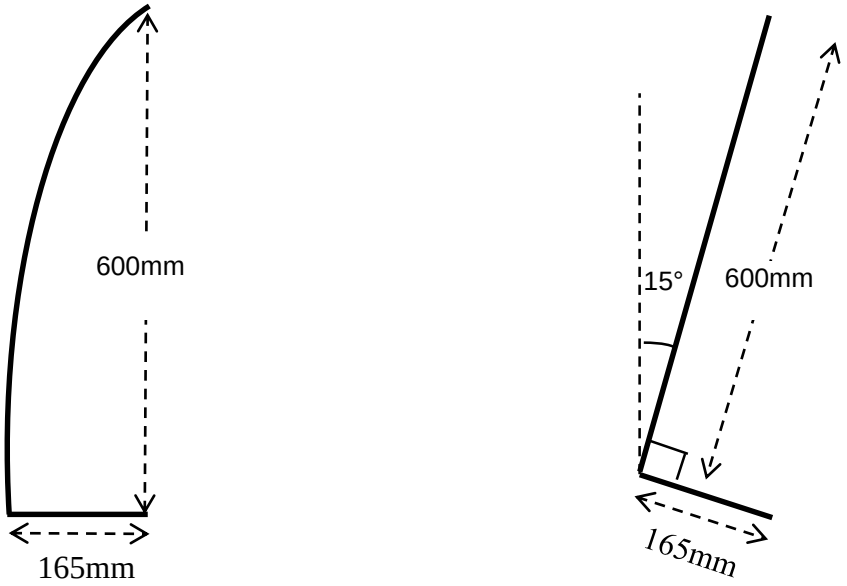

Figure 17 Schematic diagrams of the parabolic and flat reflectors

To determine the illumination profile the absorber plates were fabricated with a series of small solar cells on them, as shown in Figure 18 . Seven thin mono-crystalline solar cells with a width of 20mm were affixed uniformly across the absorber next to a larger (156mm x 156mm) mono-crystalline solar cell. In addition, two reference cells were placed adjacent to the concentrators to measure the non-concentrated radiation output.

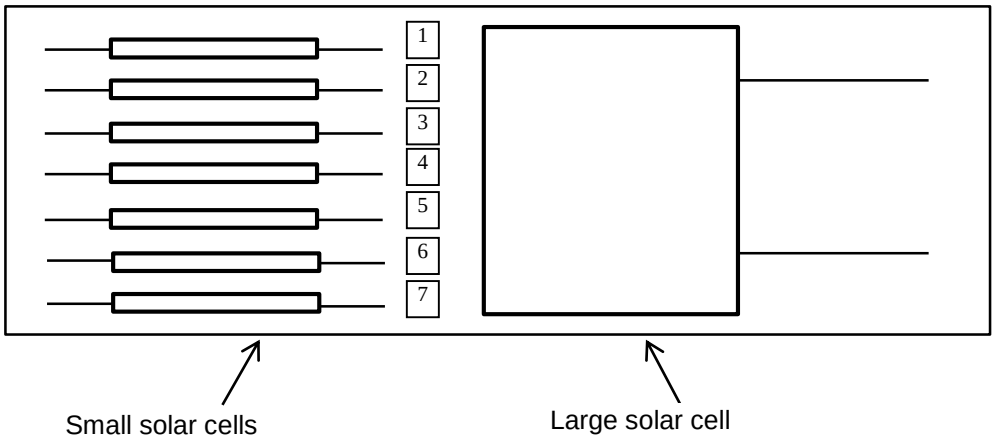

Figure 18 Schematic diagram of the absorber

When radiation falls on the absorber plate, each small solar cell produces a current proportional to the radiation falling on them that can be compared to that of the reference cell. By dividing the short circuit current of the concentrated cells with that of the reference cell, the local concentration ratio across the absorber can be determined. Similarly, the short circuit current from the larger cells should correspond to the average flux falling over the width of the absorber, allowing determination of the overall optical concentration ratio. For the experiments the short circuit current from the solar cells was recorded under outdoor conditions at solar elevation angles of 30, 45 and 60 degrees by tracking the sun manually.

2.5 Experimental results

In order to analyse the local concentration ratio across the absorber the relative concentration ratios at solar elevation angles of 30°, 45°, and 60° were compared. Under these conditions the local concentration ratio changes across the absorber as shown in Figure 19-20.

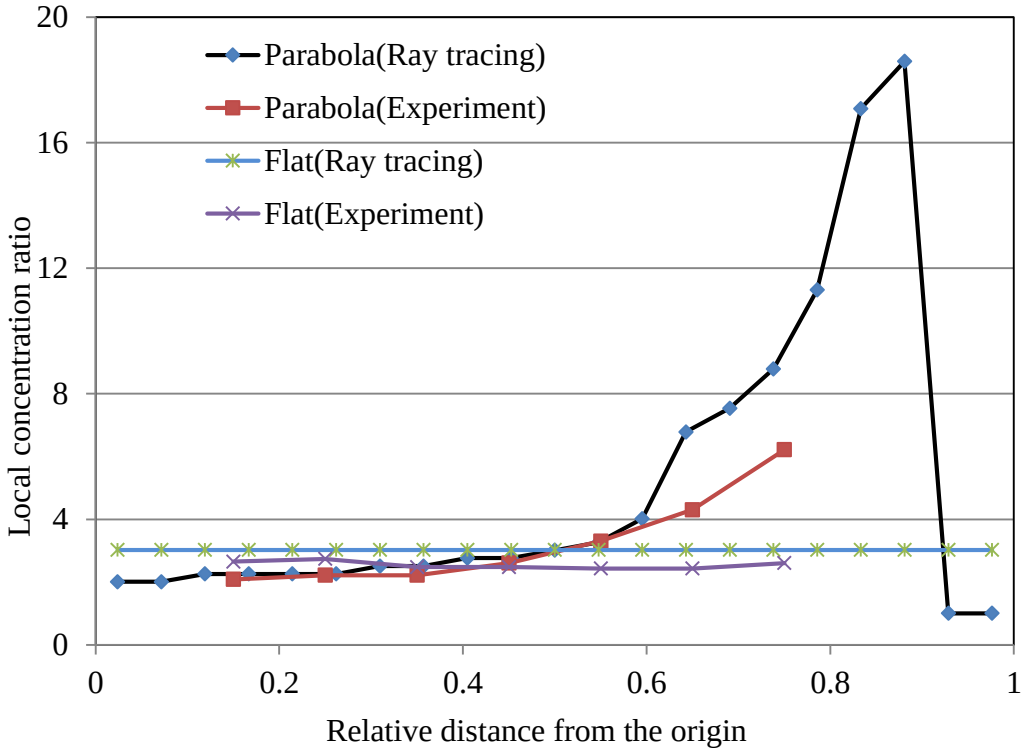

Figure 19 Local concentration ratios across the absorber at 30 degree elevation angle

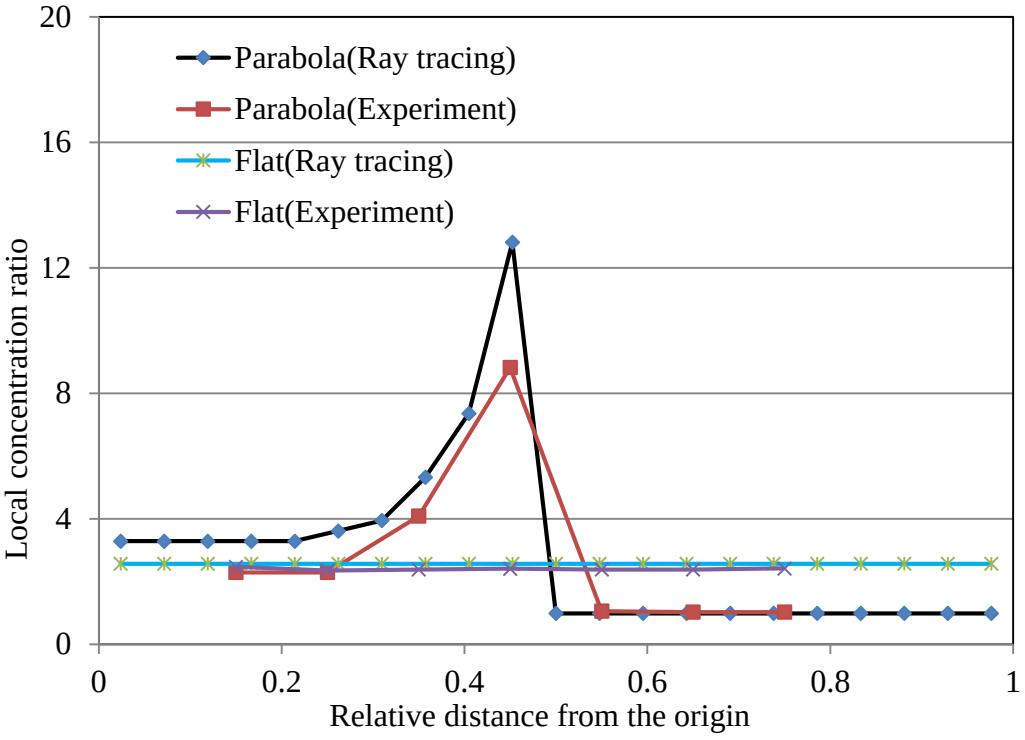

Figure 20 Local concentration ratios across the absorber at 45 degree elevation angle

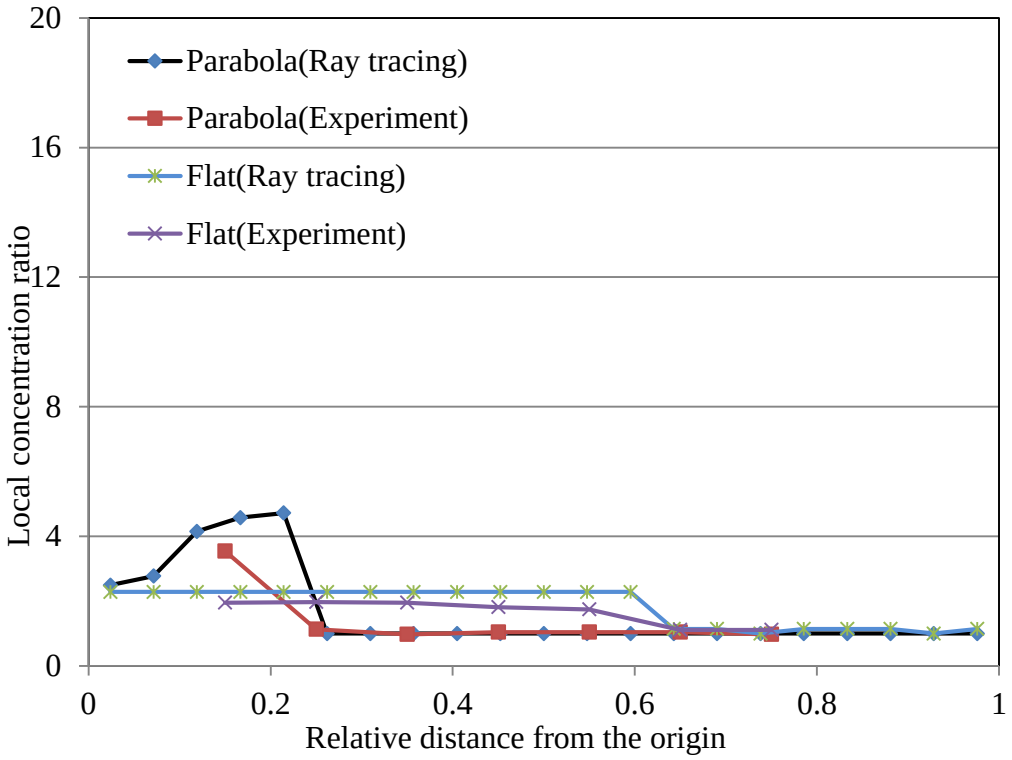

Figure 21 Local concentration ratios across the absorber at 60 degree elevation angle

From the ray tracing, at a 30° elevation angle, the peak of the local concentration ratio was achieved at the edge of the absorber. The experimental value also follows the trend of the ray tracing output, as shown in Figure 19. Similarly, at an elevation angle of 45°, it can again be observed that both ray tracing and the experimental values follow the same pattern. There is a slight difference in concentration values between the experiment and the ray tracing that is attributable to some limitations in the experiment. In particular, ray tracing allows a finer resolution of data to be achieved, whereas the experiments are only able to get discrete measurements.

From the experiments the average concentration ratio obtained from the larger cells under the parabolic reflector at 45 degrees was 2.90 while the average concentration

ratio under the flat plate reflector was 2.54. This value corresponds to the value obtained from the ray tracing, as shown in Figure 14. This implies that the usage of parabolic reflectors will deliver higher concentration ratios without considering the local concentration distribution and its consequences along the absorber.

On the whole though, it can be seen that the flat plate reflector gives a uniform local concentration ratio across the absorber for all conditions. Hence, the electric current produced at any point on a cell under a flat plate reflector will be similar. This reduces the cross currents that cause the hotspot across the cell and so would appear to be an appropriate compromise for BIPVT concentrator systems.

2.6 Remarks

From these results, it is possible to draw the conclusion that parabolic reflectors can deliver high concentration ratios. However, they are perhaps better suited to thermal applications where non-uniform illumination of an absorber surface is less problematic.

If one were to utilize a parabolic reflector for a BIPVT application, the non-uniform illumination would cause high ohmic losses and would also produce internal current flow, even when it is open circuited as mentioned earlier. Hence, if the parabolic reflector is used as a concentrating device for photovoltaic concentration it may not improve the performance of the module due to the cross currents forming hotspots in lower irradiated cells. In turn this may lead to permanent defects or premature failure of cells (Yang et al. 1991). As such, it reinforces the benefits of flat reflectors for BIPVT systems.

Chapter 3: Development of the collector geometry

In Chapter 2, it was shown that a flat reflector offers less variation in the local concentration ratio to that observed with a parabolic reflector, thus providing a more uniform illumination profile on the absorber surface. In the case of a BIPVT module, this would eliminate the problems associated with cross currents and accelerated degradation of the solar cells caused by the non-uniform nature of illumination provided by a parabolic reflector (Royne, Dey and Mills 2005). Hence flat reflectors appear to be a potential substitute for the parabolic reflector module for the purpose of making durable façade integrated low concentration ratio solar collectors.

3.1 Ray tracing and concentration ratio

Now, in order to verify a suitable geometry for a building integrated concentrator with a flat reflector it is important to understand the effect of the absorber and reflector tilt angle on the optical performance of the collector. As such the FRED ray tracing software package was used to analyse the effect of the parameters such as reflector tilt (θ_r), absorber tilt (θ_a) and solar elevation angle (α) on the optical performance of a collector, as shown in Figure 22 (Collector is assumed to be north facing). In order to trace the beam radiation, it was decided to use a collimated source as an approximation of beam component of solar radiation.

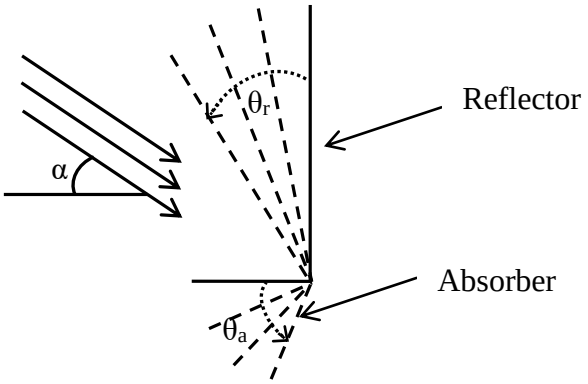

Figure 22 Angle of rotation of reflector and the absorber combination

To explore the angular relationship between the absorber and the reflector, it was decided to vary the tilt angle of the absorber and the reflector over a range of conditions and combinations. Subsequently, the relative number of rays received by the absorber was determined against the elevation angle of the source.

As shown in Figures 23, 24, 25 and 26 increasing the inclination angle of the reflectors decreases the ability of the absorber to receive more radiation at higher elevation angles. Furthermore, as shown in Figure 25 at an absorber angle of 20° to the horizontal, the total number of rays received by the absorber over the range of elevation angles is high without becoming shaded by the reflector at higher elevation angles.

The reason for this being that if the reflector tilt is increased, the reflector starts to shade the absorber at higher solar elevation angles, while when the absorber angle is increased the proportion of the rays missing the absorber increases at lower elevation angles. To keep the aperture of the collector significantly high, and gather a significant portion of the radiation at moderate elevation angles without losing much radiation at high and low elevation angles, a reflector-absorber combination with approximately 20° tilt angle would seem appropriate. This will also eliminate

the shading effect of the reflector on the absorber plate at high elevation angles during the summer.

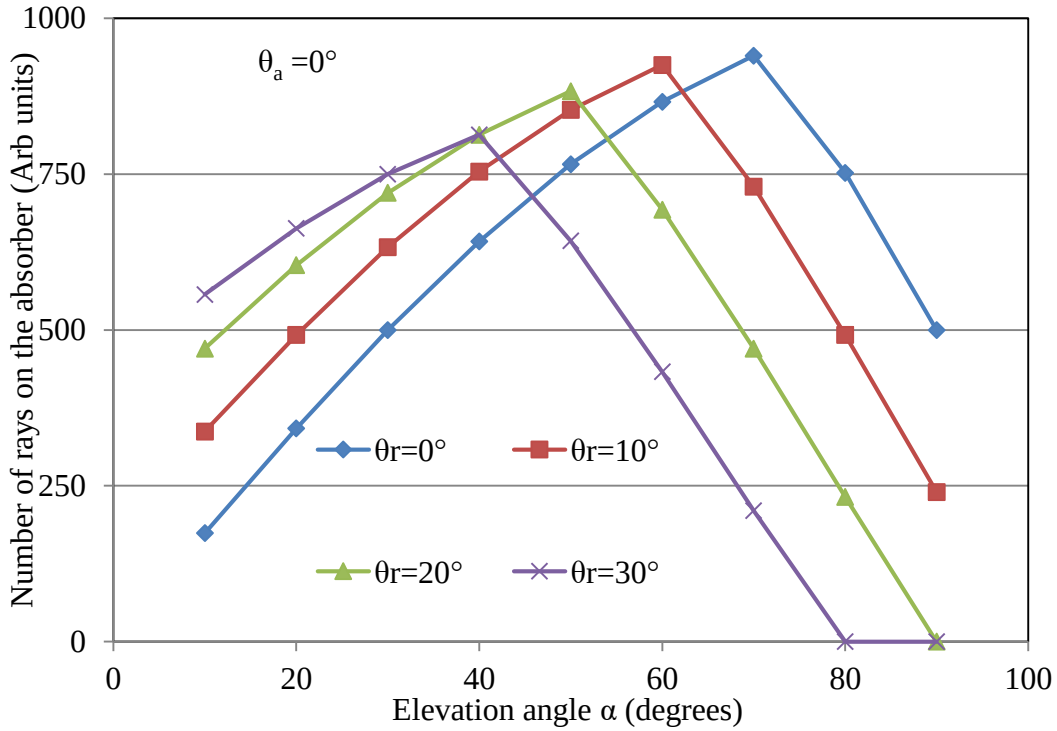

Figure 23 Number of rays received by the absorber at different elevation and reflector angles when the absorber is fixed at 0°

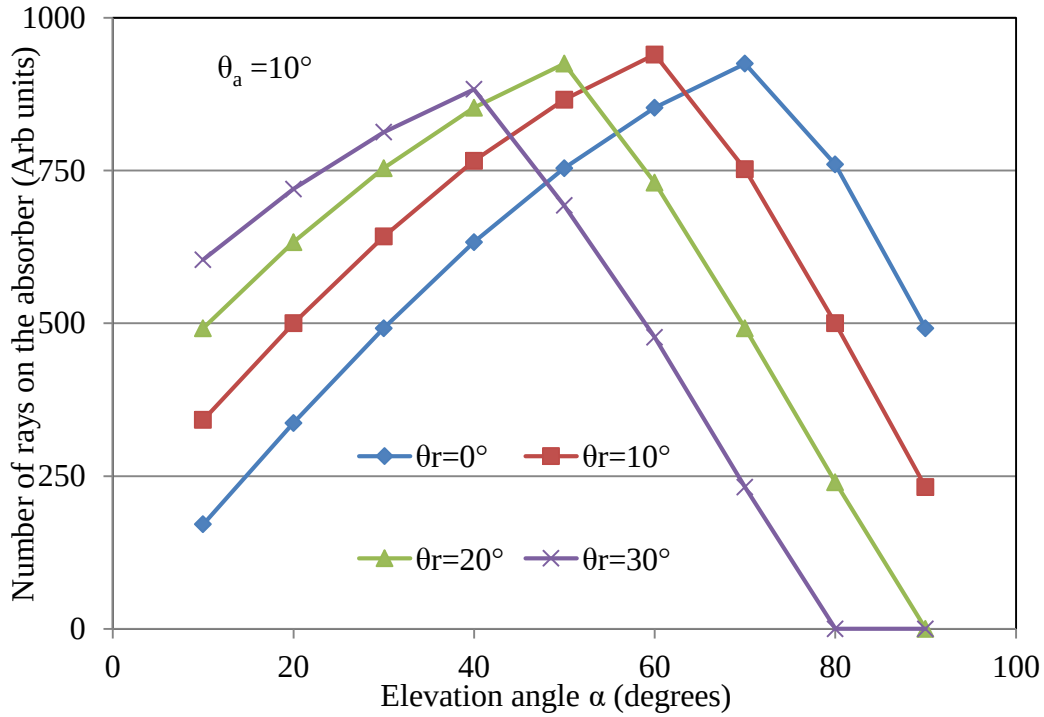

Figure 24 Number of rays received by the absorber at different elevation and reflector angles when the absorber is fixed angle at 10°

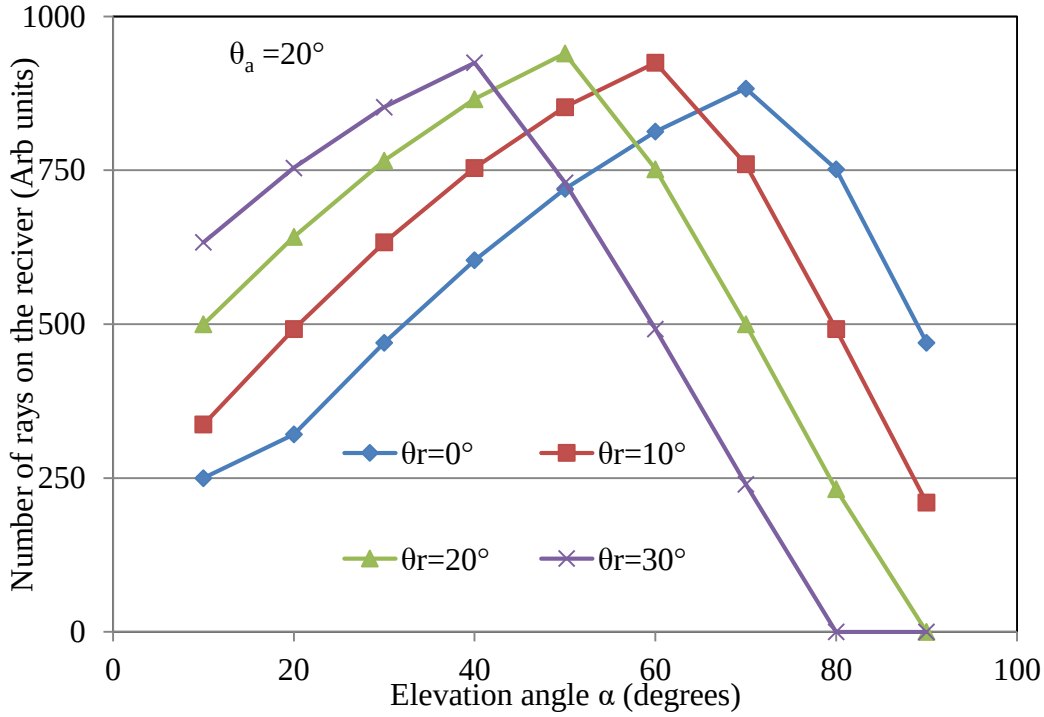

Figure 25 Number of rays received by the absorber at different elevation and reflector angles when the absorber is fixed angle at 20°

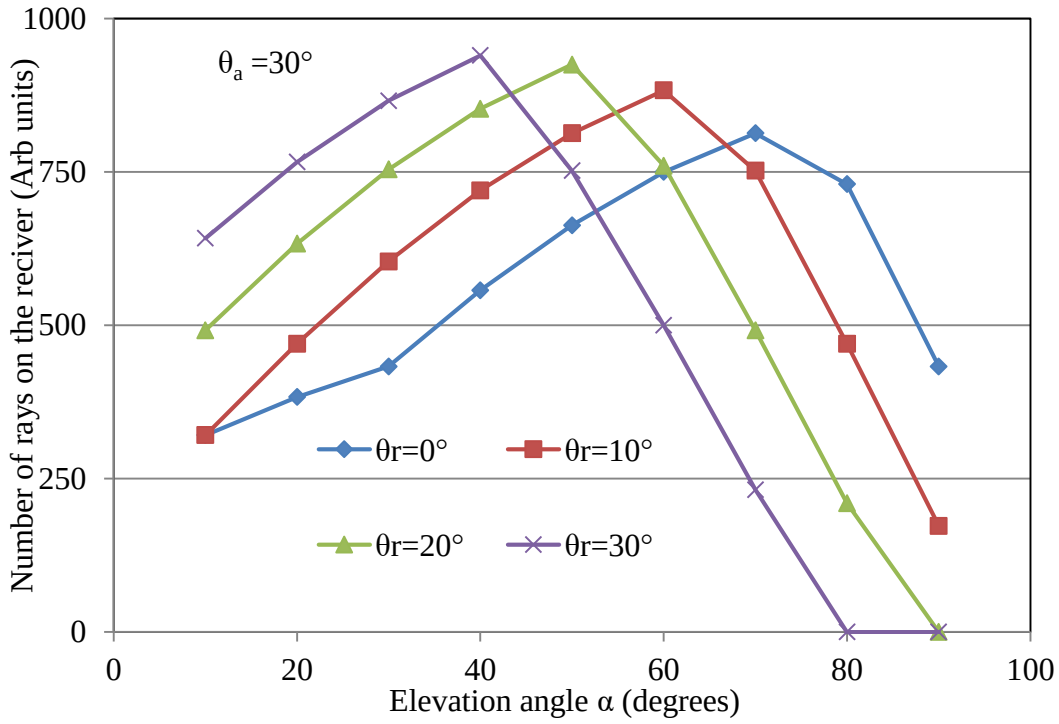

Figure 26 Number of rays received by the absorber at different elevation and reflector angles when the absorber is fixed angle at 30°

3.2 Mathematical expression for concentration ratio at different elevation angles.

Now, although ray tracing was able to provide insight into potential geometric configurations of the concentrator, these results are not particularly generalizable. Hence, to investigate the concentration ratio of the particular combination, it was decided to develop a geometric relationship in terms of the principle angles.

Although the geometrical concentration ratio is defined by the ratio of area of the aperture and the absorber, the concentration ratio defined by Kostic, et al. (2010) is a more practical expression of concentration ratio *C*, as given in Equation 2,

$$C = \frac{G_{tot}}{G_{net}} \tag{2}$$

Here the G_{tot} is the total radiation received by the absorber plate under reflector while the G_{net} is the total radiation received by a horizontal absorber without any reflector. Given that the beam radiation on a horizontal surface can be easily determined, the total radiation on to the absorber plate can be estimated if the appropriate geometrical relationship is established in terms of direct (G_{dir}) and reflected (G_{ref}) radiation. Here, the ground reflection was discounted as it was found to be less than 5% of the global radiation.

As a significant portion of the radiation falling on the absorber comes from the reflector, it is essential to include the reflectance of the reflector to precisely calculate the radiation on the absorber.

By incorporating the reflectance ρ_{Al} of the reflector, C can be expressed as in Equation 3.

$$C = \frac{G_{dir} + \rho_{Al} G_{ref}}{G_{net}} \tag{3}$$

Considering Figure 27 , When the elevation angle $\alpha < (90\text{-}2\beta)$, some of the rays hitting the reflector will not be incident on the absorber surface as shown in Figure 28(i).

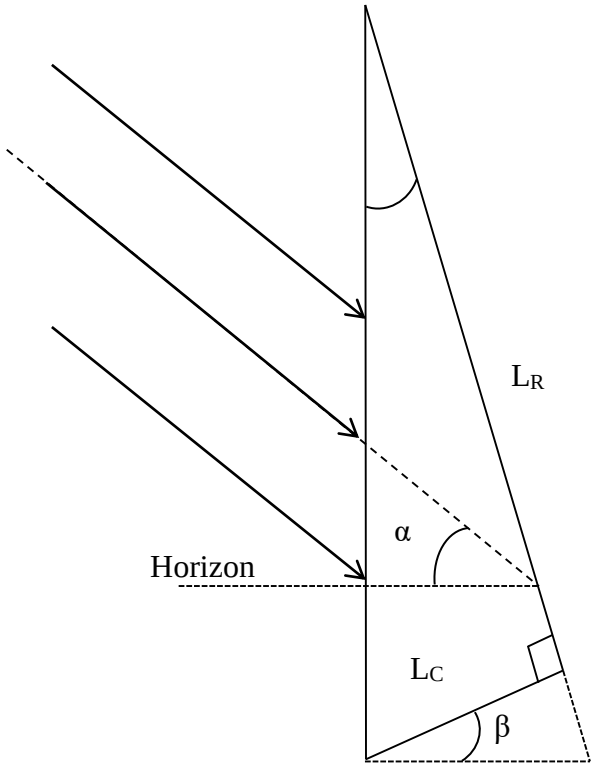

Figure 27 Geometrical representation of the collector

Furthermore, when the elevation angle α is between (90-2β) < α < (90-β), the reflector will receive the sum of all the rays coming from the reflector and rays directly falling on the absorber, as shown in Figure 28(ii). However, when the elevation angle is above 90-β, the reflector will shade the absorber therefore the number of rays directly falling on the absorber will reduce as shown in Figure 28 (iii).

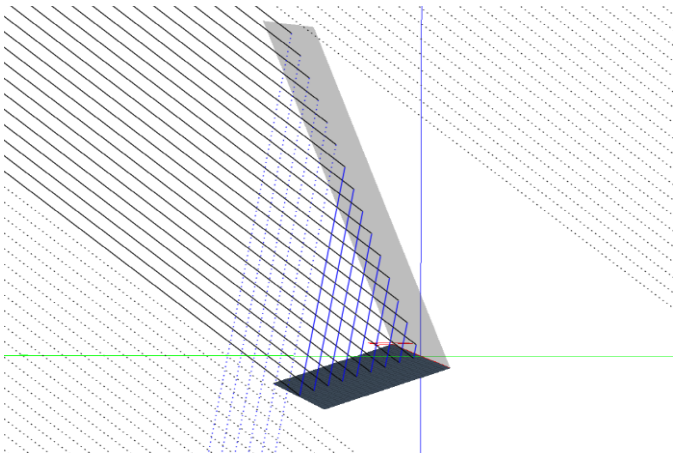

(i) $\alpha < (90-2\beta)$

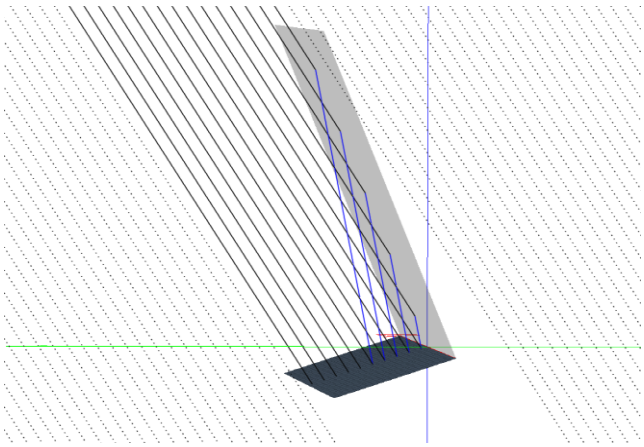

(ii) $(90-2\beta) < \alpha < (90-\beta)$

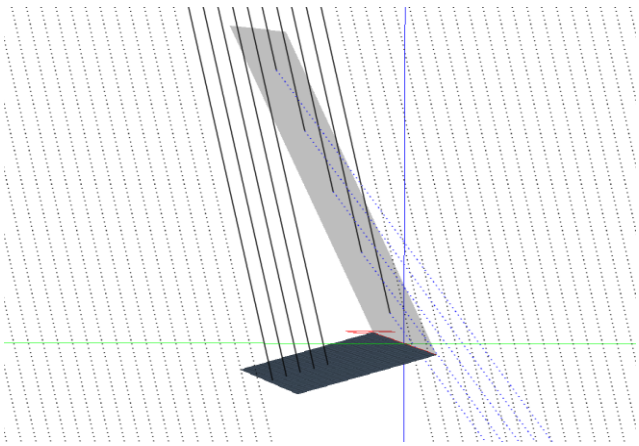

(i) $(90-2\beta) < \alpha$

Figure 28 Optical ray tracing at different elevation angles

Based on this, using fundamental geometry, an expression for the concentration ratio *C* can be given by Equation 4.

$$C = \begin{cases} \left[\frac{\text{Cos}\,(\alpha+\beta)\,(\tan\,(\alpha+\beta)+\tan\beta\,)}{Sin\,\alpha}\right]\rho_{Al}+\frac{1}{\cos\,\beta} & \alpha < (90-2\beta) \\ \left[\frac{\text{Cos}\,(\alpha+\beta)\,(3+\tan\beta\,)}{Sin\,\alpha}\right]\rho_{Al}+\frac{1}{\cos\,\beta} & (90-2\beta)<\alpha<(90-\beta) \\ \frac{Sin\,\alpha\;\;(1-tan(90-\beta))\,(tan\,(\alpha-(90-\beta)))}{\sin\,(\beta+\alpha)} & (90-\beta)<\alpha<90 \end{cases} \quad (4)$$

3.3 Sun-Earth geometric relationship

Now, to examine the influence of these optical characteristics across a year, there is a need to understand the variation in the sun's position across the year. Hence, to combine the concentration ratio with the solar elevation angle α, the Sun Earth geometric relationship is used for a north facing surface. The solar elevation angle α can be expressed in terms of latitude *(L)*, declination (δ_s) and the hour angle (h_s) as given by Equation 5 (Goswami et al. 2000).

$$\alpha = sin^{-1}(\sin L \sin\delta_s + \cos L\, cos\,\delta_s cosh_s) \quad (5)$$

Here solar declination angle δ_s can be estimated by Equation 6

$$\delta_s = 23.45 \sin\left(\frac{360(284+n)}{365}\right) \quad (6)$$

Where n is the Julian day number.

The hour angle (h_s) can be expressed in terms of the local solar time (*LST*) as given in Equation 7.

$$h_s = 15(LST - 12) \quad (7)$$

Local solar time *LST* can be found in terms of local time *(LT)* and the time correction factor (*TC*) as given in Equation 8.

$$LST = LT + \frac{TC}{60} \tag{8}$$

In Equation 8 the time correlation factor *TC* in minutes can be given by Equation 9.

$$TC = 4\,(longitude - 15(LT - GMT) + ET \tag{9}$$

Here, the Greenwich Mean Time is denoted by *GMT* and *ET* is a correction factor given in minutes that accounts for the irregularity of the speed of earth's motion around the sun that can be expressed by Equation 10.

$$ET = 9.87 \sin 2b - 7.53 \cos b - 1.5 \sin b \tag{10}$$

b is defined by Equation 11.

$$b = \frac{360\ (n - 81)}{364} \tag{11}$$

Finally, by combining Equation 4 and 5 the concentration ratio of the collector at any time on a particular day can be calculated. Here, to avoid the end effect, the collector was assumed to be infinitely long, hence elevation angle was taken as a proxy to the azimuth angle.

3.4 Experimental validation

In order to validate the mathematical model and findings it is necessary to compare the outcome with an experiment. For the experiment, the absorber plate was assembled by placing standard silicon solar cells (156mm x 156mm) under a static reflector. The reflector was affixed to a supporting frame with an inclination of approximately 20° to the vertical while the photovoltaic cells were placed at an angle of 20° to the horizontal. Subsequently, a Delta-T SPN1 sunshine pyranometer was mounted adjacent to the concentrator to measure the beam and diffuse radiation. The voltage generated by the photovoltaic absorber was measured simultaneously with the current, measured across a 1mΩ shunt resistor, in order to determine the power produced by the concentrator. A schematic representation of the experiment that was developed is shown in Figure 29.

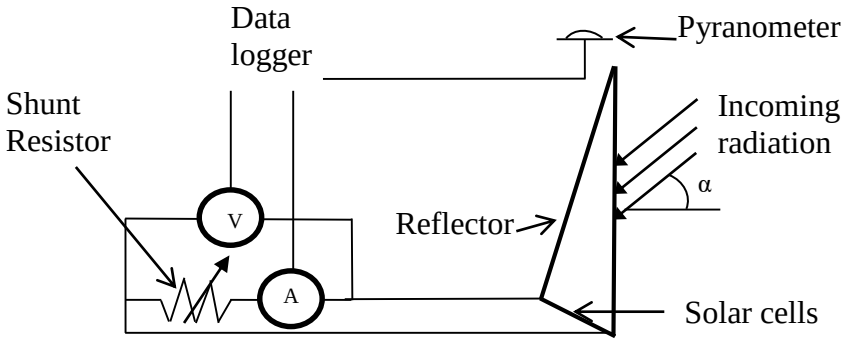

Figure 29 Schematic diagram of the test rig

Now, when radiation falls on a solar cell, it produces a current proportional to the radiation falling on it, so to determine the concentration ratio, the current produced by the concentrator was compared with the current produced by a reference cell mounted adjacent to the concentrator. By finding the ratio between the short circuit

current measured across the absorber and across the reference cell, the relative concentration ratio *C* could be estimated. To validate the optical model several sets of readings were taken from the test rig at various solar elevation angles. In order to do so, the readings were taken on different days over the year, when the sun was near solar noon to reduce the effect of shading due to the design of the mounting enclosure. Furthermore, to minimise the effect of diffuse radiation, the experiment was done under clear sky.

As shown in Figure 30 the geometrical model of the optical concentration ratio including the solar elevation angle is capable of predicting the concentration ratio with good accuracy, further illustrated by the uncertainty analysis in Appendix A.

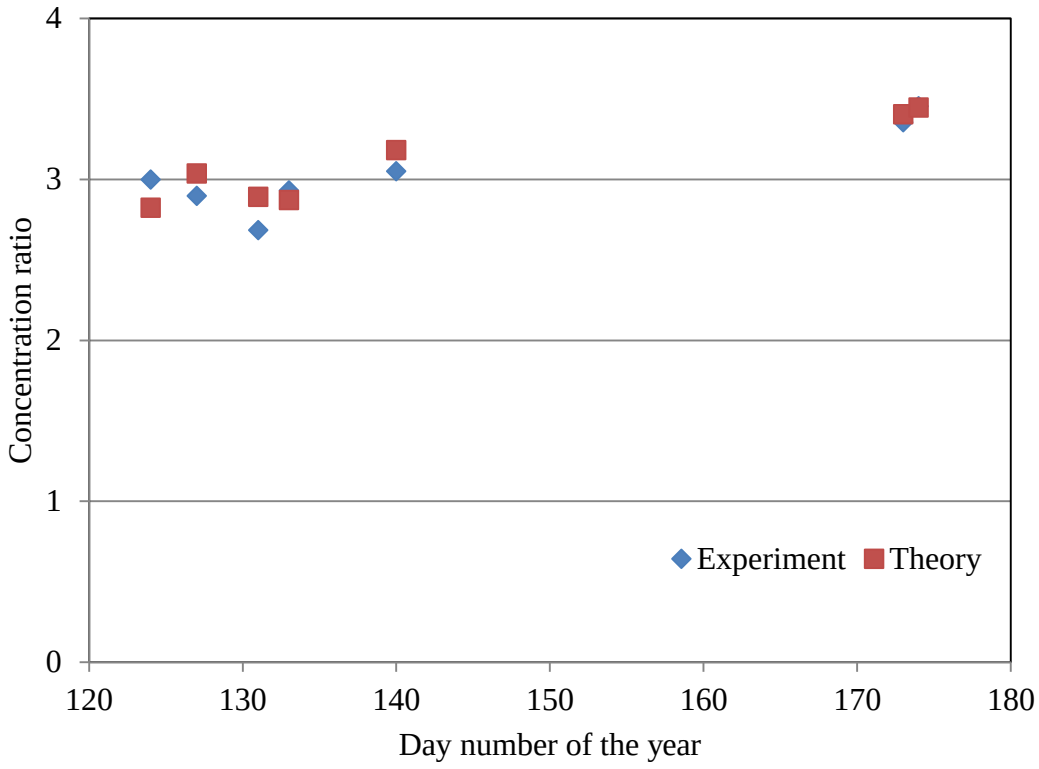

Figure 30 Experimental concentration ratio and calculated concentration ratio

3.5 Modelling results and analysis

Having shown experimentally that the geometric model can be used to evaluate the performance of the collector, it was decided to examine its capabilities on any given day and time of the year. When the annual concentration ratio variation is calculated, as shown in Figure 31, the optical concentration ratio is higher during winter days with low solar elevation angles (for example day numbers 120-210) than during the summer period (for example day numbers 330-60) with a higher solar elevation angle. Similarly, for a given day, the concentration ratios in the morning and evening are again high due to low elevation angle of the sun while as noon approaches, the concentration ratio decreases.

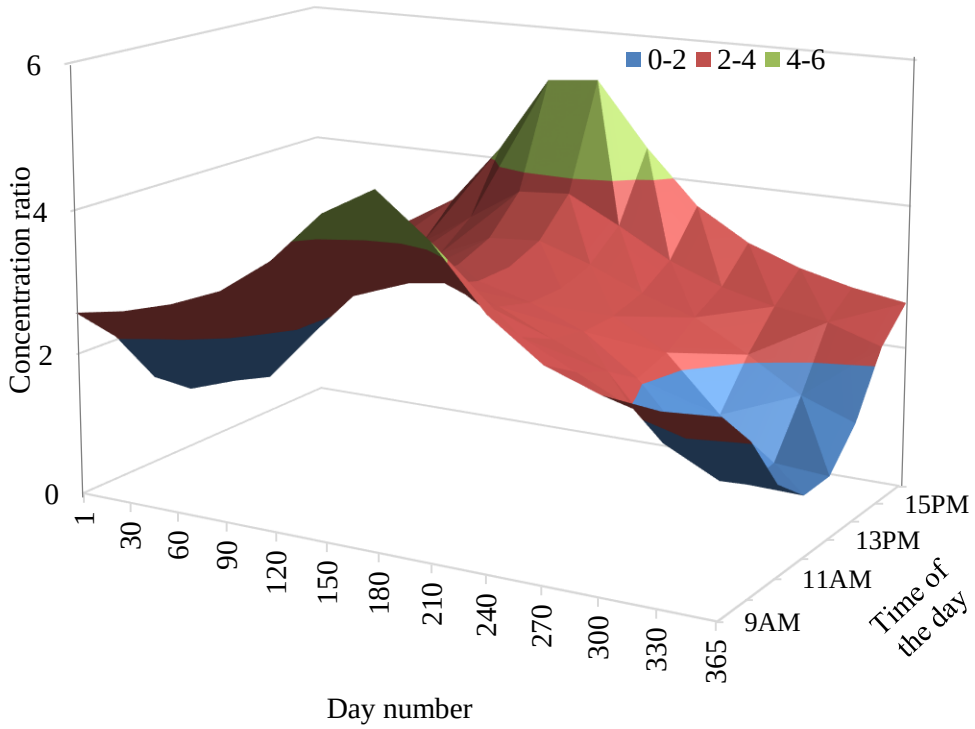

Figure 31 Concentration ratios over the year

To illustrate this point, the total radiation reaching the absorber on a typical clear summer day (January 9 in Kaitaia, NZ) calculated from the mathematical model is shown in Figure 32. Here the total radiation falling on the absorber is high in the morning and the afternoon and the collector responds with higher concentrations, as the solar elevation angle is lower than that at midday. However, as the elevation angle of the sun approaches 75° during the middle of the day, the reflector shades the absorber and reduces the radiation falling on it.

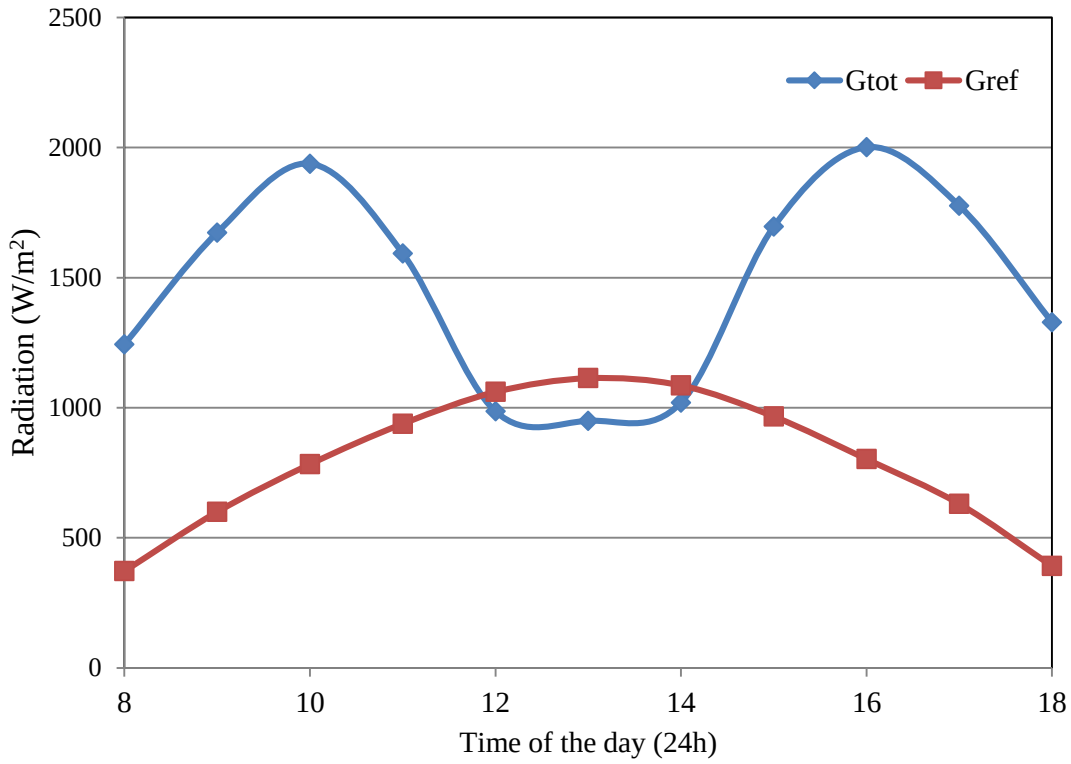

Figure 32 Change in radiation on absorber on 9th of January

Notably though, as shown in Figure 33, the radiation falling on the absorber on a typical clear winter day (June 30 in Kaitaia NZ) does not encounter shading from the reflector, as the sun elevation angle at solar noon is only 34°. Furthermore, it is important to note that, the reflector has increased the radiation falling on the

absorber by at least 3 times throughout this winter day, and this highlights one of the major benefits of the flat reflector.

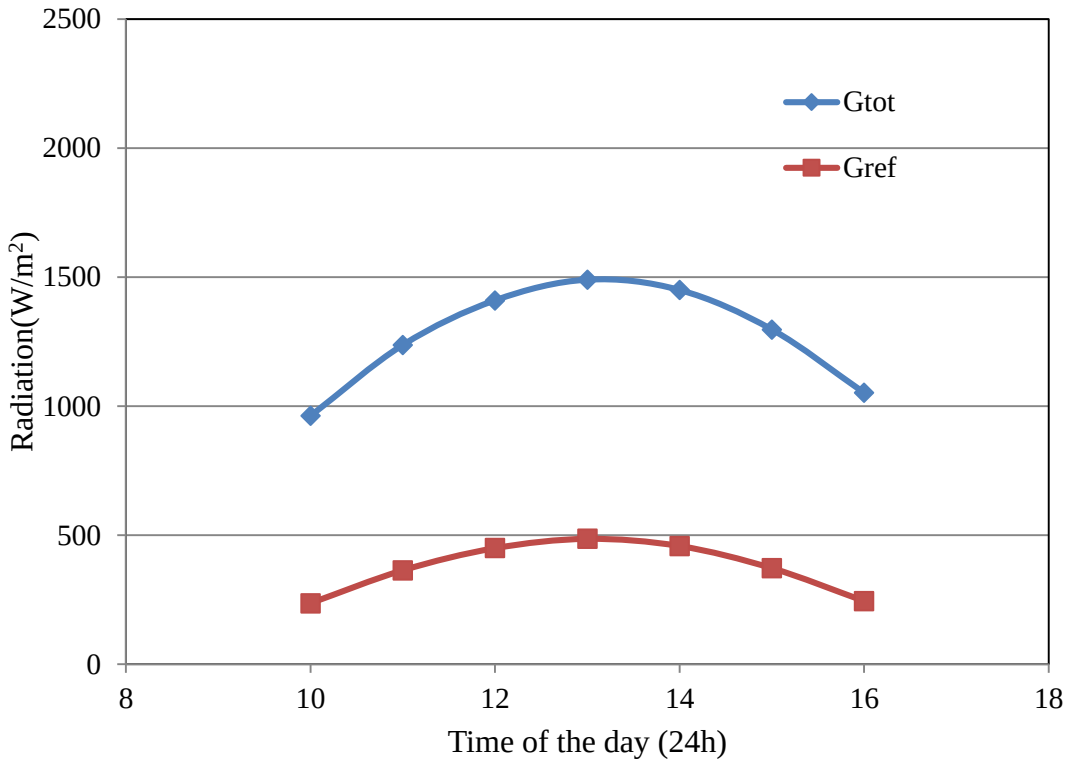

Figure 33 Change in radiation on absorber on 30th of June

3.6 Remarks

From the results, it was shown that the optical model incorporated with the Sun-Earth geometrical relationship presented in this chapter was able to calculate the total radiation falling on the absorber plate. Further from weather data, it was found that collector performance can be significantly improved during the winter days with lower elevation angle than the summer days.

It is important to note that, reflectors dramatically improve the concentration ratio at lower elevation angles. This can potentially increase the performance of the

collector significantly especially during the winter, spring and autumn seasons possibly the period when energy is needed the most.

Furthermore, this increases the potential of a combination of roof top PVT collectors, which produces significantly higher energy during the summer season, with low concentrating façade integrated solar collectors, and this may well be a next step towards zero energy buildings.

Chapter 4: Determination of thermal losses

In Chapter 2 and 3 ways of improving the capture of radiation on the absorber surface were discussed. In an ideal scenario the majority of the energy that reaches the photovoltaic collector should be absorbed and utilised. One promising way of achieving this is by using hybrid photovoltaic/thermal absorbers that deliver both thermal and electrical energy simultaneously. Here the thermal energy can be carried away by a transport medium as useful energy; however, thermal losses from the collector to the environment are inevitable. Interestingly, though two of the studies discussed earlier (Brogren and Karlsson 2002);(Gajbert 2008) used water to cool the photovoltaic absorber in order to improve their electrical performance, neither study took steps to determine the heat balance of the absorber module explained as shown in Figure 34. Hence there is a need to develop a mathematical model that determines the heat gain or loss from the absorber, in particular the natural convection heat transfer between absorber and glass.

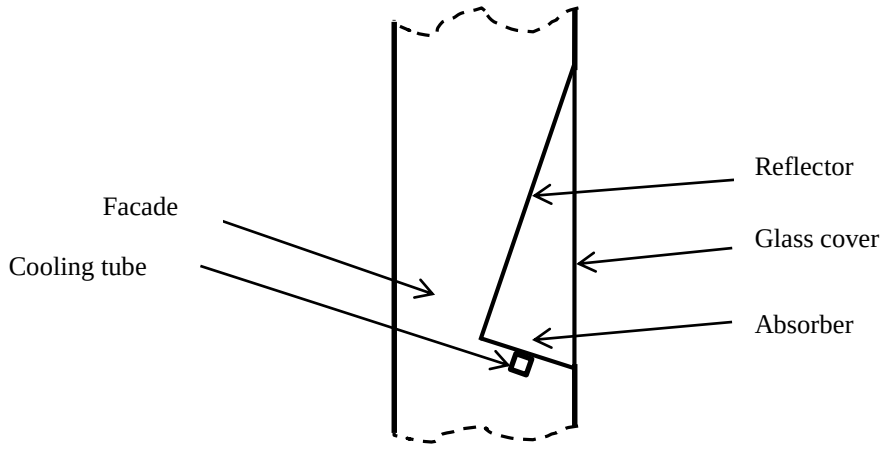

Figure 34 Façade integrated solar concentrator

4.1 Introduction

In considering the natural convection heat transfer in such an enclosure, a large number of computational studies have been performed ((Asan and Namli 2001); (Holtzman, Hill and Ball 2000); (Saha 2011); (Salmun 1995); (Varol, Oztop and Yilmaz 2007)). However, the majority of the studies are related to horizontal right or isosceles triangular spaces (attic shaped enclosures) with one heated and one cooled side or enclosures heated from below ((Flack 1980); (Holtzman et al. 2000)) and amongst these studies there is a lack of generalised correlations to predict the heat transfer in triangular enclosures that are applicable to the proposed solar concentrator.

That said, there have been a number of studies that examine natural convective heat transfer in concentrating solar collectors. Anderson (2009a) developed a relationship to describe the natural convection heat transfer in an enclosed V-trough solar concentrator, essentially a two reflector version of the proposed system. Furthermore, a study by (Singh and Eames 2011) reviewed the significance of the shape, aspect ratio, and the orientation of the solar concentrator enclosures in terms of their effect on convective heat transfer coefficients and thermal performances.

Despite the numerous studies on static solar concentrating systems, and the heat transfer from concentrating cavity enclosures, there are no existing relationships that can confidently be used to describe the natural convection heat transfer between the absorber and glazing for an enclosure formed by a façade integrated solar concentrator as shown in Figure 34, or any other façade integrated truncated parabolic reflector enclosures similar to that of (Brogren 2004). In light of this lack of relationships, this study evaluates the convection heat transfer coefficient in the

proposed collector, and other possible variations, in order to facilitate accurate prediction of façade integrated solar concentrator performance.

4.2 Computational fluid dynamics analysis

In order to develop a correlation that describes the natural convection heat transfer in the enclosures formed by a façade integrated solar concentrator it was decided to undertake a computational fluid dynamics analysis of the system without radiative heat transfer. Therefore, several models were created and analysed using Solidworks Flow Simulation, a commercial computational fluid dynamics (CFD) solver based on the finite volume method. The Solidworks Flow Simulation solver is capable of analysing both laminar flow and turbulent flows using the Reynolds averaged Navier-Stokes equations. In doing this, it uses the same transport equations for both laminar and turbulent flow which gives the flexibility to use them in transitional flows as well (Solidworks 2014). The turbulence in the flow is treated using the turbulent kinetic energy (k) and turbulence dissipation rate (ε) using a standard k- ε turbulence model. In doing this, the standard values for the constants in the transport equations are used, those being $C_m = 0.09$, $C_{e1} = 1.44$, $C_{e2} = 1.92$, $\sigma_e = 1.3$ and $\sigma_k = 1$ (Versteeg and Malalasekera 2007). Despite the inability to modify these coefficients, Anderson et al (2009) showed that this did not unduly affect the solvers ability to accurately model natural convection heat transfer in an enclosure.

In order to reduce the complexity and computational time for the simulations, the geometry and simulation were performed using a two-dimensional simulation. This assumption was made on the basis that the enclosure for such a system would be

relatively long and thus the majority of the buoyancy driven flow would be two-dimensional in nature. In defining the boundary conditions for the simulation it was assumed that the inclined wall (the reflector) was an adiabatic surface and the absorber was kept at a constant high temperature (T_h), while the vertical glazing (cold wall) was set at a lower constant temperature (T_c). In order to change the Rayleigh number, the cold wall was kept at a constant temperature while the temperature of the absorber was changed in order to achieve ΔT values in the range of 20-60K. This corresponded to the Rayleigh numbers between $1x10^8$ and $1x10^9$.

Additionally, three triangular enclosures were tested with angles between the reflector and absorber ranging from 90 - 120 degrees, as shown in Figure 35 (i-iii). This was achieved by changing the length of the adiabatic wall without changing the length of either the hot or cold wall. This was done in order to determine the change in heat transfer for various potential absorber-reflector configurations. This variation is subsequently presented as the aspect ratio, which for this study was defined as the ratio of the length of the absorber (A) and the length of the reflector (H). Hence, the variation of aspect ratio ranged from 0.324-0.381. Furthermore, as previous studies had utilised parabolic rather than flat reflectors a fourth enclosure was modelled, where the flat reflector was replaced by a truncated parabola as shown in Figure 35 (iv). This was done in order to examine the possibility of using the deduced correlation to predict the value of heat transfer coefficients in enclosures where a truncated parabolic reflector might be utilised.

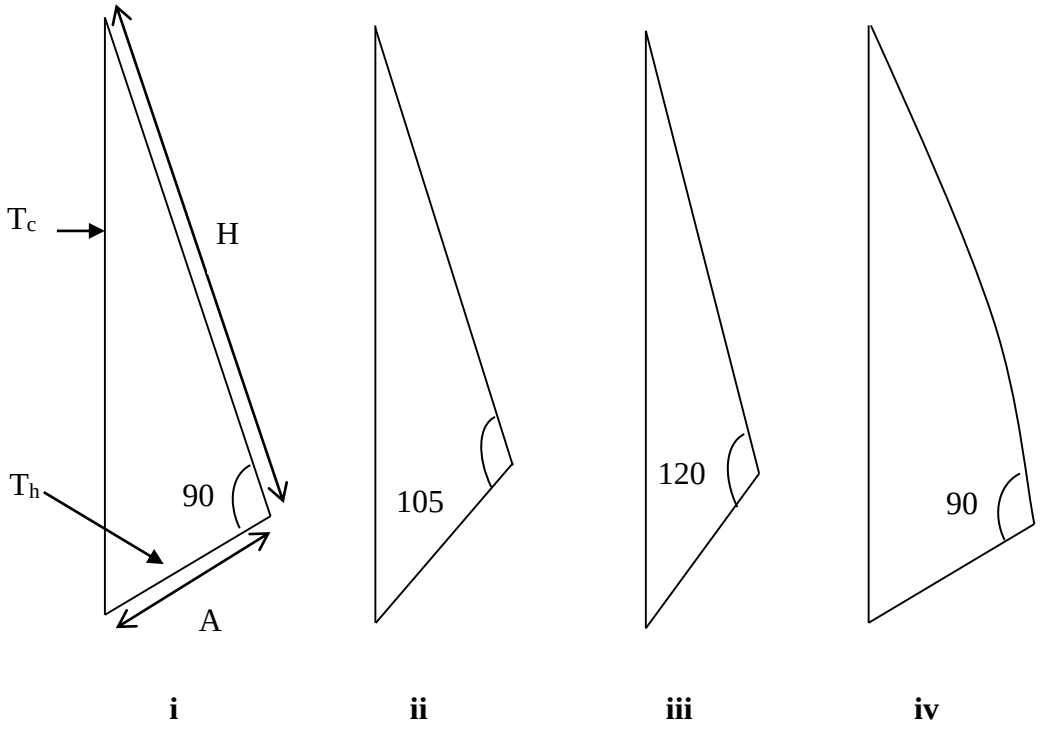

Figure 35 Enclosures modelled in CFD

4.3 Experimental validation method

In order to validate the results of the computational fluid dynamics analysis an analogue of the collector shown in Figure 35 i, with a 90 degree angle, was fabricated. In constructing this analogue, a heating element was used to replicate the photovoltaic absorber plate in the proposed collector and a 1.2 m long enclosure with cross sectional dimensions shown in Figure 36 was built.

To achieve a temperature gradient between the cold plate and the hot plate, the hot plate was made by bonding a flexible resistance heater to a 2 mm thick 1200 mm x 200 mm polished aluminium plate. Aluminium plate was used to ensure a uniform temperature along the length of the enclosure thus providing an isothermal surface and also for its low emissivity, to reduce radiation heat transfer.

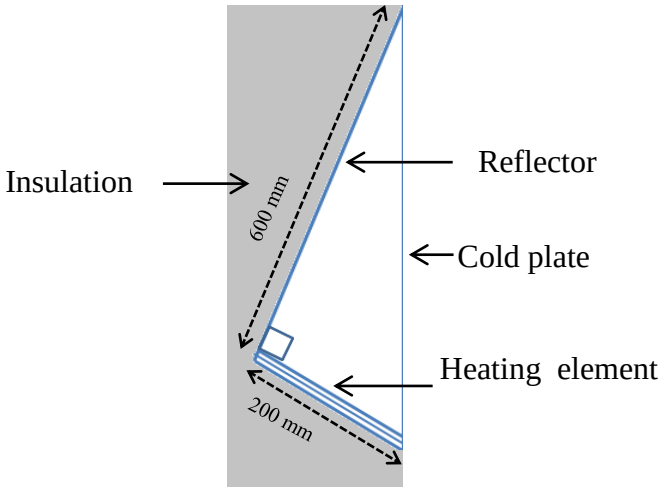

Figure 36 Module to be used for the heat transfer experiment

In an effort to minimize the heat losses through the rear and sides of the heater, the rear side of the heater and the reflector plate were insulated with 100 mm thick (or more) mineral wool fibre with a nominal R-value of 2.8 and enclosed by 18mm plywood, while the ends of the enclosure were fabricated from 18 mm plywood. The inclined "reflector" surface was also constructed of 2 mm thick polished aluminium plate, with a low emissivity, to minimize radiation heat transfer between it and the other surfaces in the enclosure. In addition, the vertical "glazing" (cold plate) consisted of a polished 2 mm thick aluminium sheet in order to keep the temperature uniform over the entire area. Furthermore, the external surface of the "glazing" was cooled by two fans to ensure the majority of the heat from the enclosures was taken away through this surface. Finally, all the edges and joints of the enclosure were sealed with high temperature aluminium duct tape to reduce any undesirable heat losses by air leakage.

In order to vary the Rayleigh number, either the temperature difference between the plates or the characteristic length has to be varied. To vary the temperature difference, the power supplied to the electrical heater was varied by a variable

transformer (Variac) and the amount of power supplied was measured by a single-phase MS6115 power meter.

The mean temperature of the hotplate was measured by six T-type thermocouples attached uniformly along the length of the hotplate. Nine more T-type thermocouples were used over the surface of the cold plate to measure its mean temperature. The ambient temperature was measured by another T-type thermocouple. Subsequently all of these thermocouples were connected to two Picolog TC-08 data loggers connected to a computer through a USB interface. A schematic of the experimental configuration is shown in Figure 37.

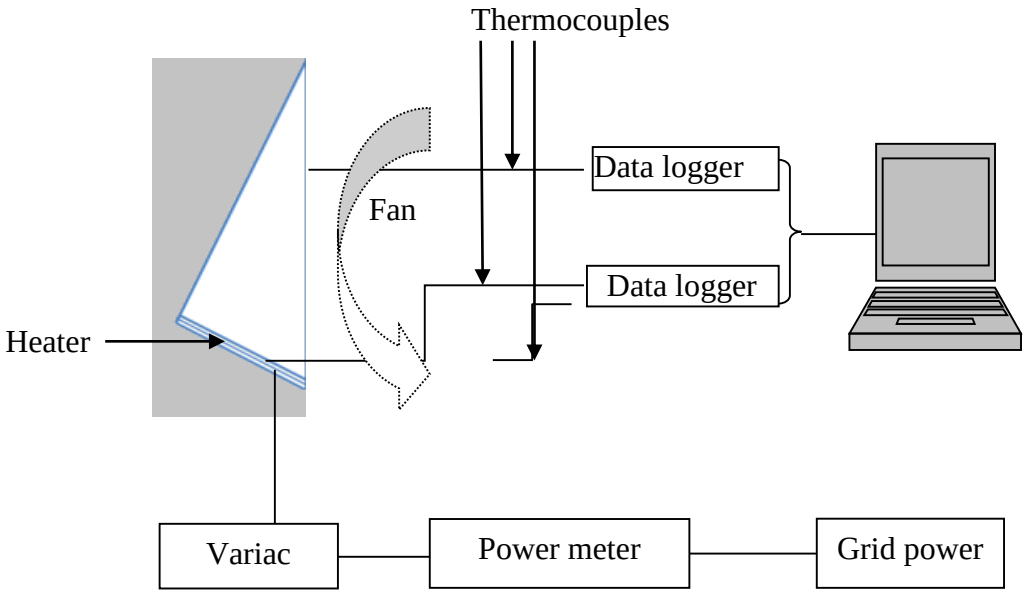

Figure 37 Schematic of the experimental setup

The difference between the hot and cold plate temperatures (ΔT) was calculated using the mean hot and cold plate temperatures. The experiment was allowed to run until it reached steady state, where the thermocouple readings were used to identify the region of steady state. Here the steady state condition was determined by taking

the region where the difference between the mean temperature of the heater and the cooled surface did not vary by more than 0.6K over a 30 minute time period.

4.4 Experimental analysis

From the experimental results, the overall heat transfer coefficient (U) can be derived from Newton's cooling law. Here the heat transfer coefficient under steady state conditions is given as a function of the input electrical power (Q_T), the temperature difference between the plates (ΔT) and the area of the hotplate (A_h) as shown in Equation 12.

$$U = Q_T / (A_h \, \Delta T) \tag{12}$$

However, this provides only an approximate indication of the convective heat transfer coefficient inside the enclosure. In order to obtain the heat that is being transferred by the convection ($Q_{convection}$) a complete heat balance should be undertaken, as given by Equation 13. Thus, the $Q_{convection}$ can be expressed in terms of total electrical energy input and the other means of heat losses.

$$Q_T = Q_{convection} + Q_{conduction} + Q_{radiation} \tag{13}$$

Where, $Q_{conduction}$ is the sum of rear, base and end conduction losses while the $Q_{radiation}$ is the amount of heat loss by radiation.

The rear, bottom and end heat losses by conduction ($Q_{conduction}$) can be calculated by applying Fourier's law over the areas of interest (A_i) across the thickness (L)

where (k) is the thermal conductivity of the wall and temperature difference across the wall is (T_i-T_a) as given in Equation 14. In this equation T_a is the ambient air temperature. In the case of rear and bottom heat losses T_i was the temperature of the hot plate, while the end loss was calculated using the bulk temperature of the air inside the enclosure as the value of T_i.

$$Q_{conduction} = \frac{kA_i\ (T_i - T_a)}{L} \tag{14}$$

Now, the radiation heat transfer between the hot and cold plate ($Q_{radiation}$) is another portion of the thermal losses from the hotplate. However, as the inclined reflector surface of the enclosure was heavily insulated, it can be assumed to be an adiabatic surface under steady state conditions, and the radiation losses can be discounted. Similarly, given that both hot and cold plates were fabricated using low emissivity aluminium plate ($\varepsilon_p \approx 0.06$); one could assume that radiation between these surfaces is also negligible.

To confirm the decision to discount the radiation from the heat balance calculation, the enclosure was assumed to be a two-surface enclosure with the aluminium heater as one of the surfaces. Hence the expression of the $Q_{radiation}$ can be written in terms of area of the hotplate (A_h), area of the cold plate (A_c), both made up of aluminium with the emissivity of ε_p and the view factor (F) (Cengel 2007), as given by Equation 15.

$$Q_{radiation} = \frac{\sigma\ (T_h^4 - T_c^4)}{\left(\frac{1-\varepsilon_p}{\varepsilon_p}\right)\left(\frac{1}{A_h} + \frac{1}{A_c}\right) + \frac{1}{A_h F}} \tag{15}$$

Here T_h and T_c are hot and cold plate temperatures.

The analysis found that $Q_{radiation}$ accounted for less than 4% of the heat transferred by convection; hence it is reasonable to assume it to be negligible. Based on this assumption, Equation 13 can be reduced to Equation 16 without the radiation component.

$$Q_{convection} = Q_T - Q_{conduction} \tag{16}$$

By using Equation 16, the convection heat transfer coefficient (h_c) can be expressed in terms of $Q_{convection}$, area of the hotplate (A_h) and the temperature difference (ΔT) between the hot and cold plate as given by Equation 17.

$$h_c = (Q_T - Q_{conduction}) / (A_h \Delta T) \tag{17}$$

4.5 Results

4.5.1 CFD results

In order to determine the natural convection heat transfer coefficient of the proposed enclosures, the temperature of the isothermal heater was varied to achieve a 26, 46 and 63K temperature difference between the heater and the isothermal cold wall.

As expected, Figure 38 shows that there is an increase in the heat transfer coefficient as the temperature difference increases. This is because as the temperature difference increases the degree of turbulence in the fluid increases, and hence there is increased heat transfer from the heater (Cengel 2007). Furthermore, the increase

in aspect ratio defined as a ratio between the length of the absorber plate (A) and reflector plate (H) from 0.324-0.381, achieved by varying the angle between the reflector and absorber, also increased the heat transfer coefficient at a particular temperature difference. This suggests that the heat transfer coefficient is also a function of the aspect ratio.

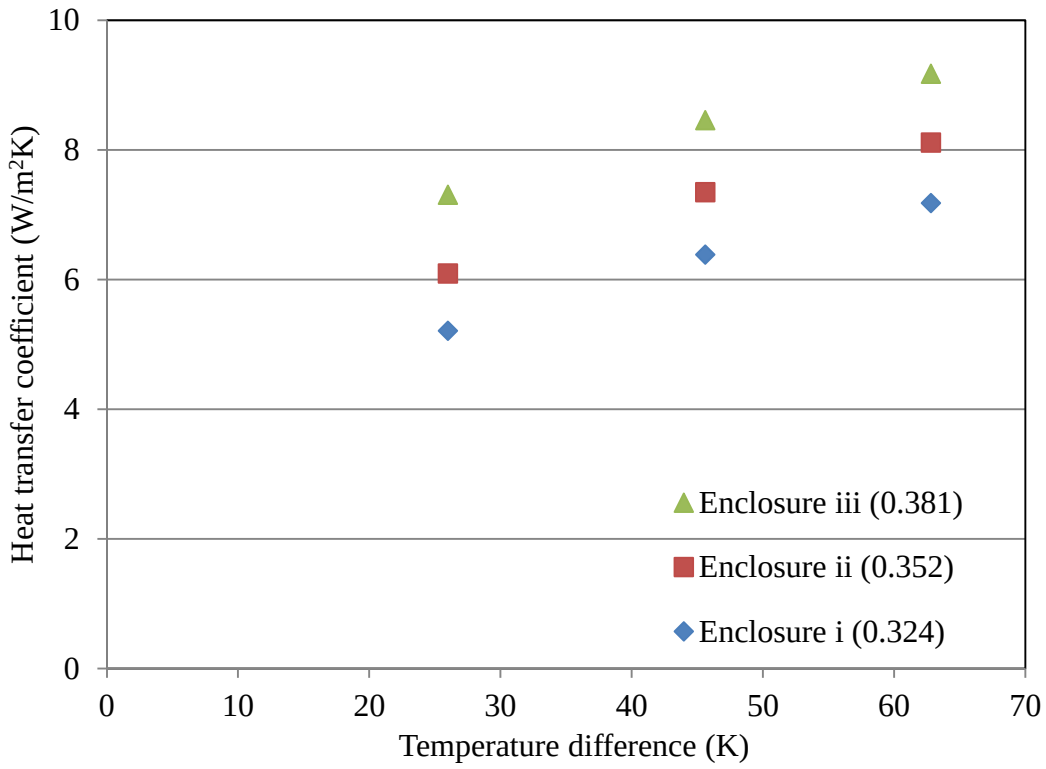

Figure 38 Natural convection heat transfer coefficient vs Temperature difference for enclosures with varying aspect ratios

Although the results given in Figure 38 relate the temperature gradient to the heat transfer coefficient, they cannot be used directly to find the heat transfer coefficient in different sized enclosures with different angles. As such, Figure 39 shows the relationship between Nusselt number and Rayleigh number for enclosures of varying aspect ratios. From these it is possible to develop a generalised relationship

between these parameters that can be used to obtain the heat transfer coefficient of geometrically similar enclosures of various sizes.

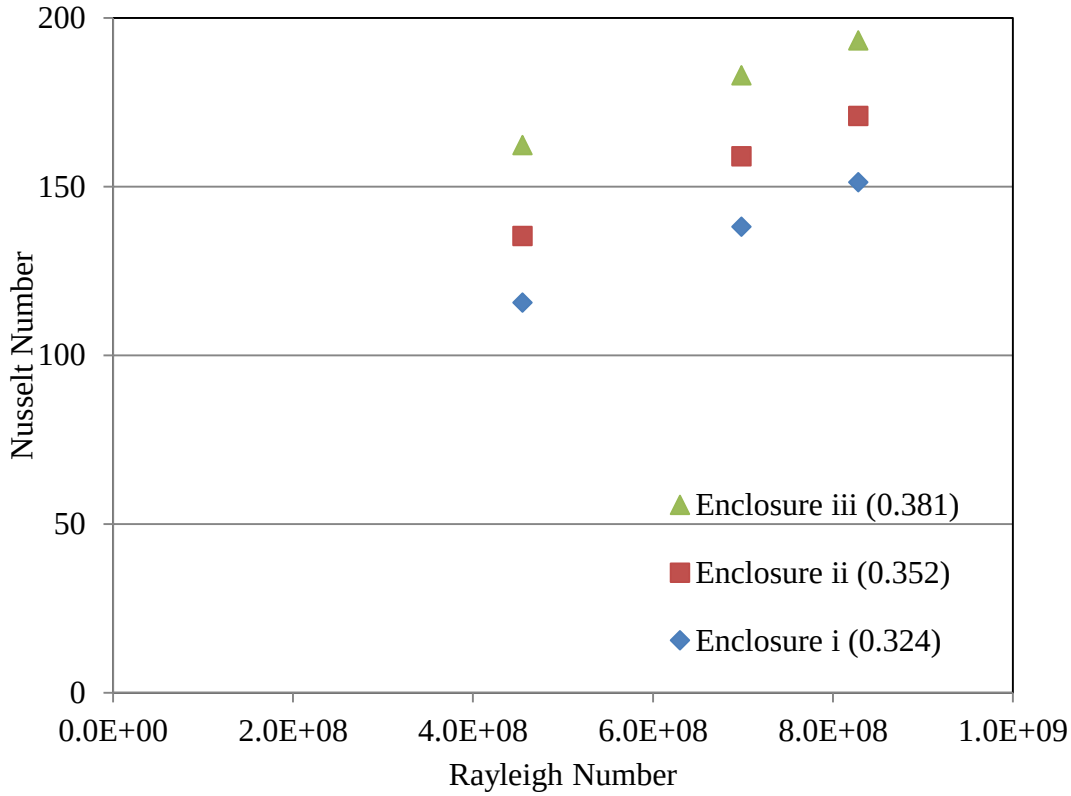

Figure 39 Nusselt vs Rayleigh number for enclosures with varying aspect ratios

In achieving this, the air in the enclosure was assumed to be a real fluid and its thermo-physical properties were calculated at the bulk temperature (the average temperature of hot and cold plate) of the enclosure and the Rayleigh and Nusselt number were calculated on this basis. This corresponded to Rayleigh numbers from 5×10^8 to 1×10^9, taking the characteristic length to be the height of the cold plate.

Now, in Figure 38 and Figure 39, the heat transfer characteristics of triangular enclosures (enclosures i-iii) were examined, however an enclosure with a parabolic reflector was also modelled (enclosure iv). Therefore, the natural convection heat

transfer coefficients in this enclosure, under the same conditions as the three triangular enclosures, were also determined.

In Figure 40, it can be seen that the natural convection heat transfer coefficients in the parabolic enclosure, under the same conditions, are essentially the same as those of enclosure i, and varied only by having a flat rather than curved reflector. On this basis it is apparent then, that a single relationship could be developed that describes the natural convection heat transfer coefficient for enclosures with flat and parabolic reflectors.

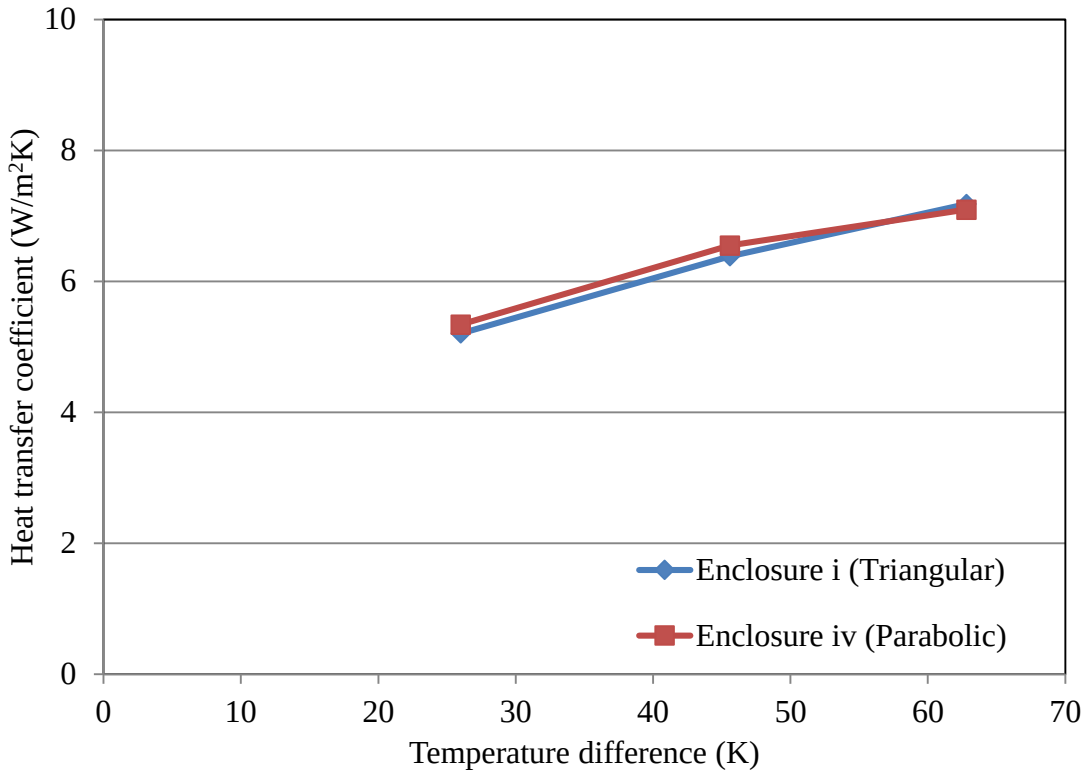

Figure 40 Natural convection heat transfer coefficient vs Temperature difference in enclosures i and iv

As shown in Figures 38 and 39, all four enclosures follow the same trend of increased Nusselt number with Rayleigh number, and clearly indicate that Nusselt number also strongly depends on the aspect ratio. Therefore, a relationship was

determined from the computational analysis that expressed the natural convection heat transfer in terms of both the Rayleigh number and the cavity aspect ratio as given by Equation 18.

$$Nu = 0.67Ra^{0.36} \left(A/H\right)^{1.75} \tag{18}$$

4.5.2 Experimental results

In order to validate the CFD results, the natural convection heat transfer coefficient of the proposed enclosure was calculated by varying the heat supplied to the hotplate. By changing the heater power, the mean temperature of the hotplate was varied from 48°C to 112°C. Using the recorded temperature difference and the amount of heat supplied, it was possible to calculate the convection heat transfer coefficient from Equation 18. At each temperature difference under steady state, the Nusselt numbers were plotted against the Rayleigh number.

As shown in Figure 41 the experimental results closely match the previous CFD results for the enclosure of the same geometry (a full uncertainty analysis is given in Appendix A). As such, the experiments validate both the results of the computational analysis and also the correlation developed from this analysis to describe the natural convection heat transfer coefficient for an enclosed solar concentrator with a static reflector.

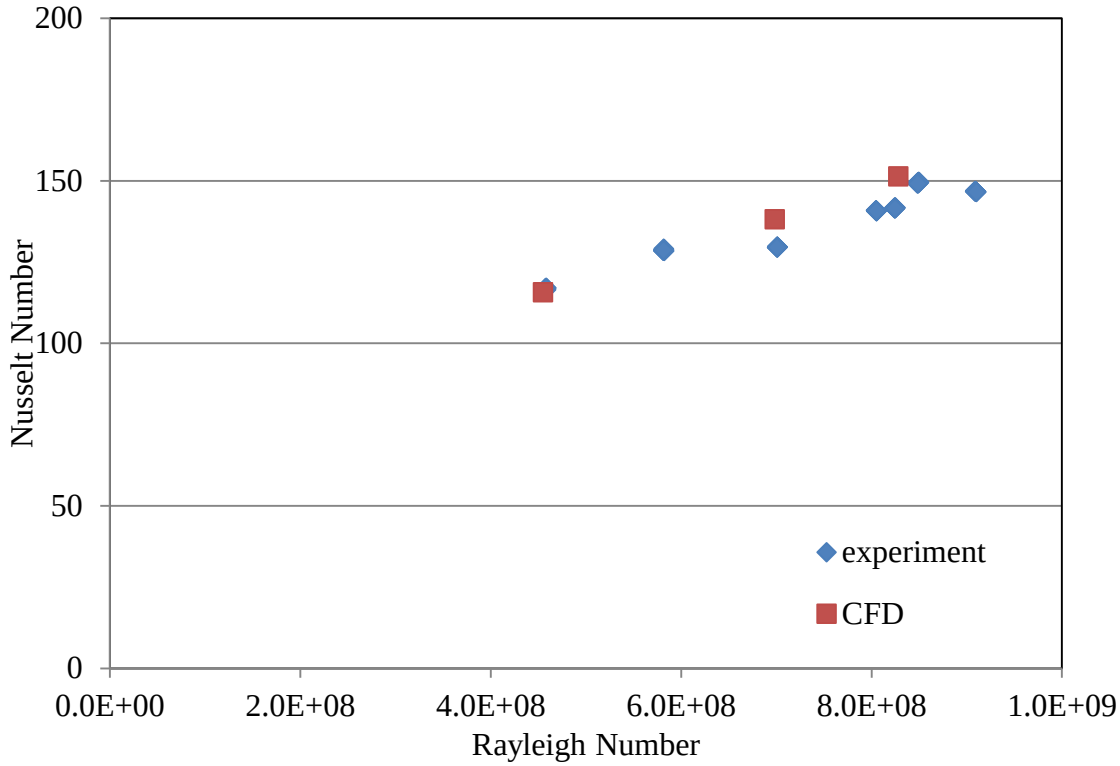

Figure 41 Nusselt vs Rayleigh number for experimental and CFD analysis

4.6 Empirical relationship

In light of the lack of correlations relating the natural convection heat transfer coefficient for the solar collector geometries, this study found that the natural convection heat loss could be predicted by the relationship $Nu = 0.67Ra^{0.36}\ (^{A}/_{H})^{1.75}$ for Rayleigh numbers in the range of 1 x 10^8 to 1 x 10^9. The experimental results suggest that this relationship is capable of determining the natural convection heat transfer coefficient in enclosed solar concentrators with flat reflectors. Furthermore, the inclusion of the aspect ratio term allows this relationship to be used in enclosures with different concentration ratios. As such, this correlation can be applied for geometrically similar enclosures with different dimensions, assuming that the Rayleigh number is within the range of the tested values.

Finally, there is close agreement between the natural convection heat transfer coefficient in enclosures with flat reflectors and the enclosure with the parabolic reflector. This shows that the relationship can be used in the determination of the natural convection heat transfer coefficient in enclosures with parabolic reflectors that may also be used in façade applications, as discussed in Chapter 2 and 3.

Chapter 5: Determination of appropriate heat transfer media

In Chapter 4 the heat loss from a BIPVT was discussed. However, another means of improving the removal of heat from the absorber as noted previously by Anderson (2009) is increasing the thermal heat transfer capabilities of the working fluid. This will improve the heat removal efficiency and ultimately improve the overall efficiency of the collector. On this basis, in 2012 (Yousefi et al.) studied flat plate thermal collectors using multiwall carbon nanotube (MWCNT) nano-fluids as a working fluid and reported an efficiency improvement of up to 30%. With this conclusion, MWCNT nano-fluids may open the possibility of proposed façade collector achieving a higher efficiency within the given space by an improved value of the convection heat transfer coefficient of the working fluid. Hence it was decided to examine the suitability of this nano-fluid in the proposed collector.

5.1 Overview

Introducing small particles into heat transfer fluids in order to increase the thermal performance of the fluid is not a new idea. More than a century ago Maxwell (1881) published a theoretical work that showed the effective thermal properties of fluids could be improved by the addition of highly thermally conductive particles dispersed in a base fluid. However, until recently these studies were limited to solid particles at millimetre or micrometre scale dispersed in a liquid media, the stability of such fluids is very poor and the particles tend to coagulate. However, in recent years, modern technologies have facilitated the manufacture of the particles down to nanometre scale. As such it is possible make nanoparticle dispersions in a base fluid that exhibit increased dispersion quality and stability (Haddad et al. 2014). In this regard, the term nanofluid was coined in the mid-1990's to describe a solid-

liquid two phase mixture consisting of engineered nanometre-sized metallic, non-metallic or oxide particles suspended in a base liquid (Choi and Eastman 1995).

In an early study Choi et al (1995) presented a theoretical analysis of copper metallic particle based nanofluids and concluded that it increased the effective thermal conductivity of the solutions significantly. Furthermore, during the past two decades numerous research works have examined the thermal properties of these nanofluids in the hope of improving the thermal characteristics of cooling liquids. Many of them concluded in showing the thermal conductivity of a base liquid increased by adding small particles in suspension (Li et al. 2009).

However, limited work has been undertaken on forced convection heat transfer using nanofluids (Godson et al. 2010). Pak et al (Pak and Cho 1998) studied the forced heat convection heat transfer coefficient of nanofluids containing Al_2O_3 and TiO_2 nanoparticles under turbulent flow. They found that Nusselt number increased with an increase in the volume fraction of nanoparticles and Reynolds number. Subsequently Eastman et al (1999) reported an improvement in heat transfer coefficients with a CuO based nanofluid. In 2008 Williams et al (2008) observed a considerable increase in heat transfer coefficient when ZrO_2 based nanoparticle were used.

Additionally, many experimental studies have reported a very high thermal conductivity for carbon nanotubes (CNT) (Berber, Kwon and Tomanek 2000, Maruyama 2002), therefore one might expect that a fluid suspension consisting of CNT would deliver better thermal properties than conventional liquids. In this respect, (Yousefi et al. 2012) applied a multi-walled carbon nanotube (MWCNT)

based nanofluid to enhance the efficiency of a flat plate solar collector. However, there is very limited work on forced convection heat transfer of MWCNT based nanofluids in turbulent flow (Rashmi et al. 2013). Moreover, the improvements reported by Choi et al (Choi et al. 2001) could not be reproduced by subsequent studies on MWCNT based nanofluids (Xie 2012).

In summary, there are a number of studies that have reported inconsistent results (Chein and Chuang 2007, Ding et al. 2007, Lee and Mudawar 2007, Nelson, Banerjee and Ponnappan 2009, Pak and Cho 1998) and also some studies showing a decrease in heat transfer coefficient after adding nanoparticles to the base fluids (Ding et al. 2007, Yang et al. 2005). As such, where previous studies concentrated on laminar flow or various formulations of nanofluids, for this study, it was decided to investigate the forced convection heat transfer of a MWCNT nanofluid under turbulent flow conditions that might be encountered with the BIPVT concentrator.

5.2. Experiment and the validation of the test rig

5.2.1 Method

To determine the convective heat transfer from the MWCNT nanofluid, a copper tube-in-tube heat exchanger was built with an inner and outer tube diameter of 1/4" and 1" respectively, as shown in Figure 42. An entrance length of approximately 20 diameters of the inner tube was left outside the outer shell of the heat exchanger, to ensure fully developed turbulent flow through the inner pipe. Saturated steam, at approximately 4-bar, was condensed in the outer tube to provide a constant wall temperature to the nanofluid circulating through the smaller inner tube. A control

valve at the pump was used to control the flow rate of the fluid by allowing fluid to be recirculated into the supply tank. Additionally, the temperature of the steam and the inlet and outlet temperatures of the heated inner tube were measured using T-type thermocouples (±0.3°C). The flow rate was measured by recording the time taken for a measured mass to be accumulated in a collection container.

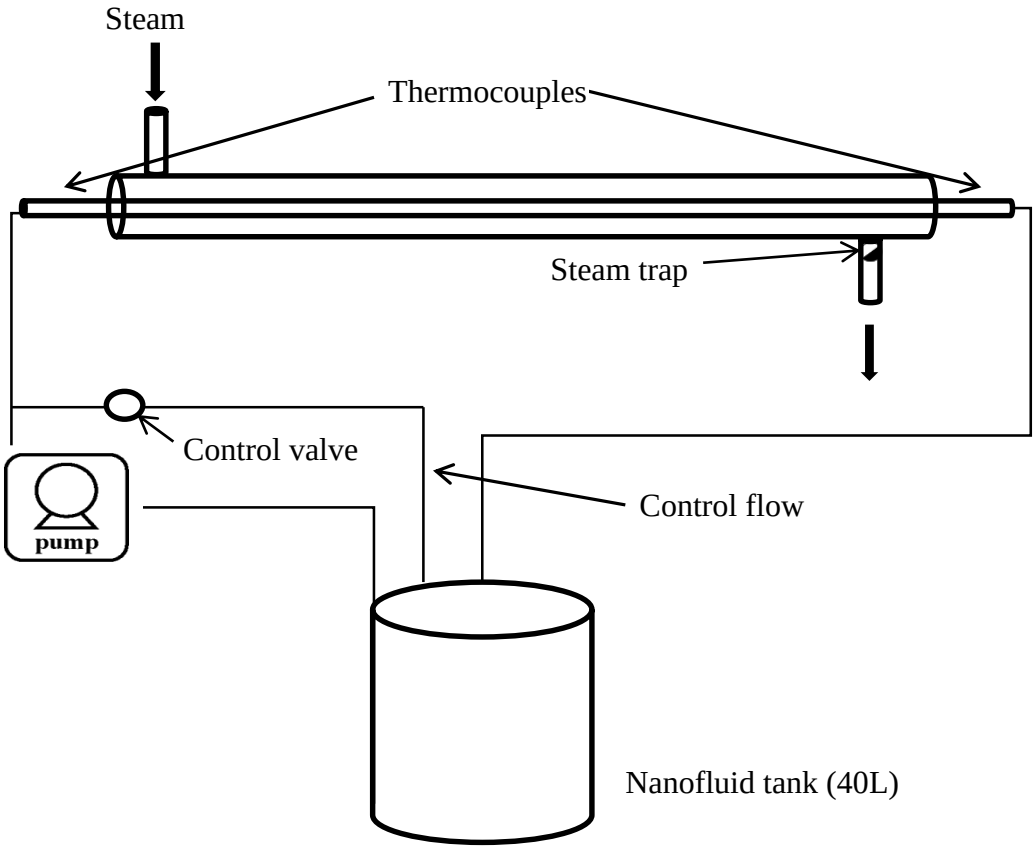

Figure 42 Test rig to measure the heat transfer coefficient of the fluid under constant temperature

5.2.2 Validation of experimental apparatus

In order to ensure that the experimental setup was able to accurately determine the convective heat transfer coefficients for turbulent flow in a tube, a preliminary experiment was conducted in which water was used as the heat transfer medium. From the inlet and outlet fluid temperature readings, as well as knowledge of the

mass flow rate and specific heat of water, the heat transferred from the steam to the fluid (Q) can be calculated. Now because the wall resistance of the copper inner tube is relatively small it was assumed to be negligible, hence the overall forced convection heat transfer coefficient, (h_{fc}) can be calculated according to Newton's law of cooling as given in Equation 19.

$$h_{fc} = \frac{Q}{(A * \Delta T_{ln})} \tag{19}$$

Here ΔT_{ln} is the Log-Mean Temperature Difference.

Fifteen sets of readings were taken under steady state conditions for each flow condition, and the mean fluid temperature value was used to determine the physical properties of the heat transfer fluid for each flow condition. Here, the steady state condition was determined by taking the region where the difference between the mean temperature of the heater and the cold surface was not varying more than 0.6K over a 60 minute time period. This allowed the Nusselt number and Reynolds number values to be determined for the experiment.

Now to validate the experimental apparatus, the experimental values of Nusselt number were compared to those predicted by the Gnielinski empirical correlation (Gnielinski 1976) shown in Equation 20.

$$Nu = \frac{\frac{f}{8}(Re - 1000) * Pr}{1 + 12.7\sqrt{\frac{f}{8}}\,(Pr^{2/3} - 1)} \tag{20}$$

For $0.7<Pr<2000$ and $3000<Re<5*10^6$

Where the friction factor (f) is given by Petukhov's correlation (Cengel 2007), as shown in Equation 21.

$$f = \frac{1}{\left(1.8 log_{10} \frac{Re}{6.9}\right)^2} \tag{21}$$

In Figure 43, it can be seen that the Nusselt numbers obtained from the experiment compare favourably with those computed by Gnielinski's empirical correlation. As such, the experimental apparatus should be able to accurately determine the heat transfer characteristics of the nanofluid.

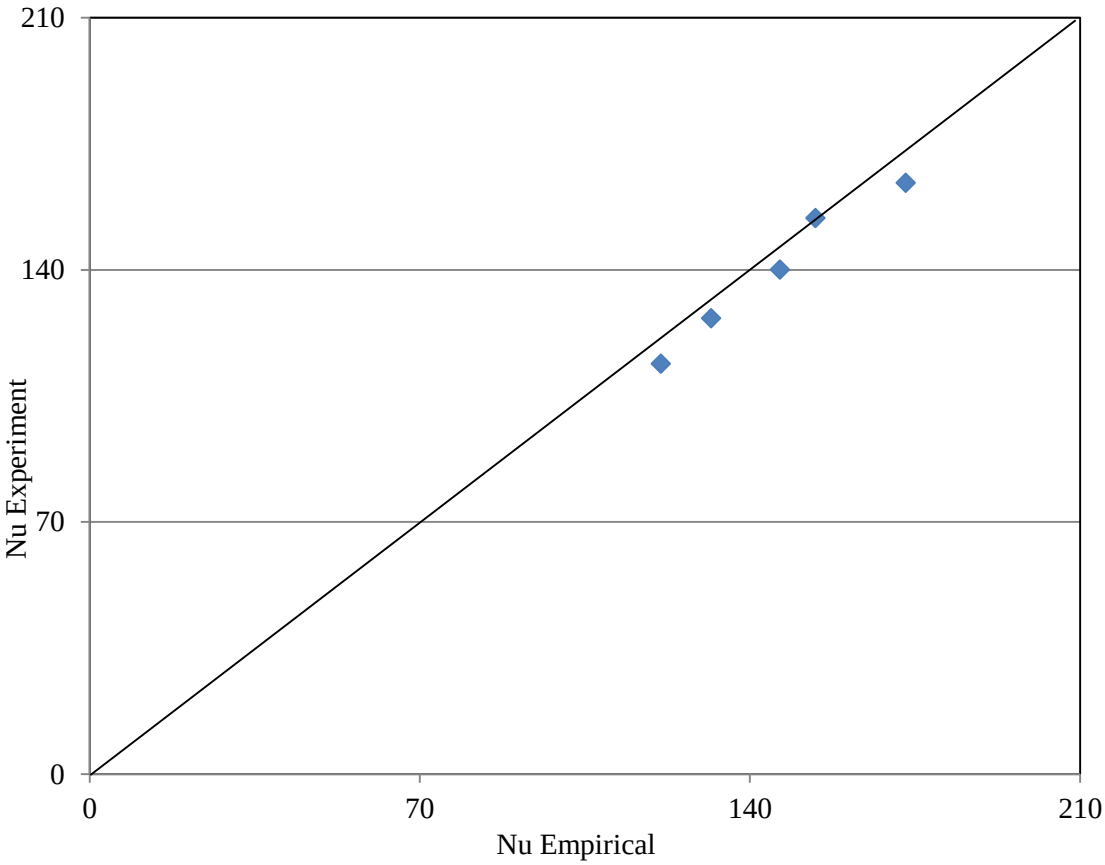

Figure 43 Experimental vs empirical Nusselt number values

5.3 Nanofluid preparation

5.3.1 Pre-preparation

Nanofluids are not simply liquid-solid mixtures, but have special requirements. In this regard stability, homogenous suspension, durability of the suspensions and agglomeration effects should be considered while making such fluids.

As MWCNT particles are hydrophobic in nature their dispersability in water is expected to be poor. However, adding a surfactant that has hydrophobic and hydrophilic functional groups may improve the stability of the liquid (Rastogi et al. 2008). Hence, it was decided to investigate the stability and the dispersion of the

MWCNT nanoparticles in the water using a surfactant. Rastogi et al (2008) compared the dispersion of MWCNT particles in water using four different surfactants: Triton X-100, Tween 20, Tween 80 and Sodium dodecyl sulphate, and found that Triton X-100 had the greatest ability to disperse MWCNT nanoparticles. In addition to that, sonication of the mixture appears to improve the dispersion ability of the particle in the fluid (Liu et al. 1998, Li, Zhu and Wang 2007).

In order to minimize the agglomeration of nanoparticles and to study the stability of the MWCNT nanofluid, it was decided to use Triton X-100 surfactant in conjunction with sonication to prepare the MWCNT nanofluid. In undertaking this analysis different compositions, as shown in Table 1, and different sonication times were tested.

Table 1 Composition of the sample experiments

Experiment number	Amount of surfactant in 1L solution	MWCNT Concentration g/L
Ex 1	5 mL	1
Ex 2	2.5 mL	1
Ex 3	1 mL	1
Ex 4	0 mL	1
Ex 5	2.5 ml	2

Four portions of each sample (MWCNT with an average diameter: 10-40 nm, length: 1-25μm, purity by weight: 93% min, specific surface area: 150-250 m^2/g) (Playwithcarbon.com) were sonicated for 10, 20, 30 and 40 minutes in a 2L, 100W

ultrasonic bath. Samples were stored in stoppered test tubes to be observed for a few days, to assess their stability over time. As can be seen in Figure 44 the samples of the fourth experimental set, without any surfactant, MWCNT's precipitated regardless of the sonication time. This is understandable due to the hydrophobic nature of the MWCNT, which implies particle dispersion will be poor.

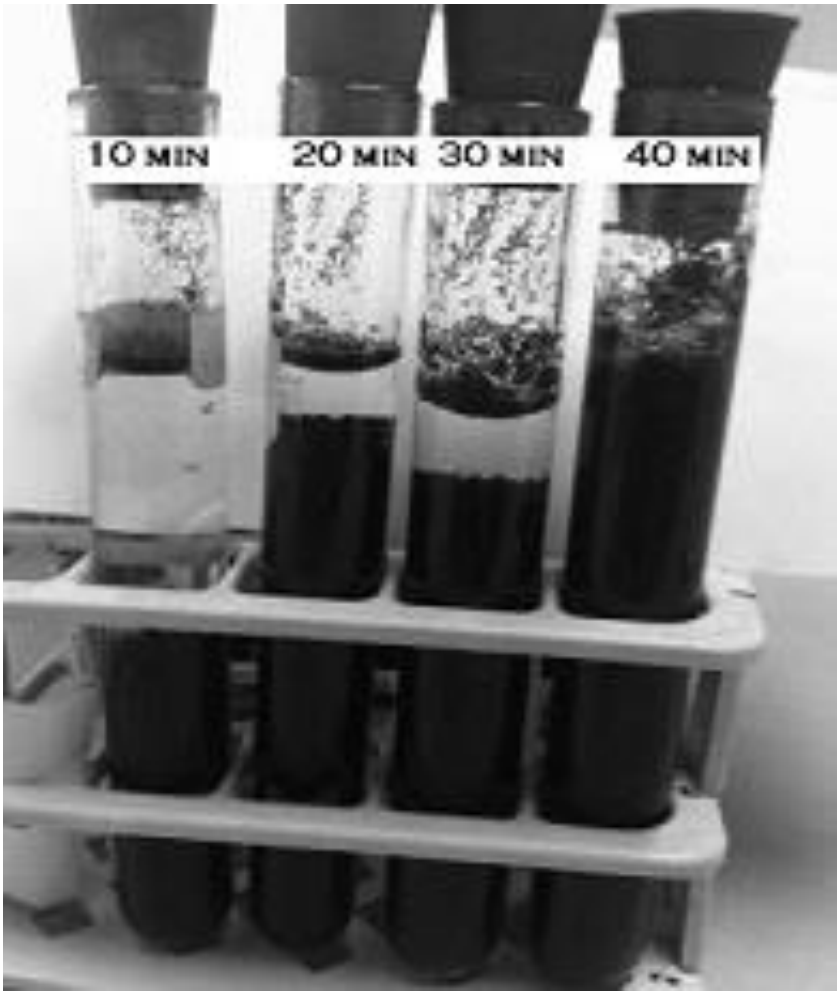

Figure 44 Samples without surfactant with different sonication time

Additionally, the MWCNT particles precipitated more rapidly under 10 minutes sonication compared to the samples sonicated for longer periods. This illustrates the effect of the sonication time on producing a homogenous nanofluid. Furthermore, if we consider the effect of surfactant on the dispersion, as shown in

Figure 45, samples of fluid sonicated for 30 minutes with a lower surfactant to MWCNT ratio (Ex 3 and Ex 5) showed some agglomeration whilst samples of condition Ex 1 and Ex 2 were more homogenous.

Figure 45 Sonicated samples with surfactant as shown in table 1

To understand the properties of the nanofluid better dried samples of untreated and surfactant treated MWCNT particles were examined with a scanning electron microscope (SEM). In Figure 46 it can be seen that the MWCNT nanoparticles appear to be coated with what we believe to be, surfactant and are slightly less tangled in comparison to the untreated sample shown in Figure 47. Finally, a

magnified image, Figure 48, was used to confirm the diameter of the nanotubes as specified by the supplier.

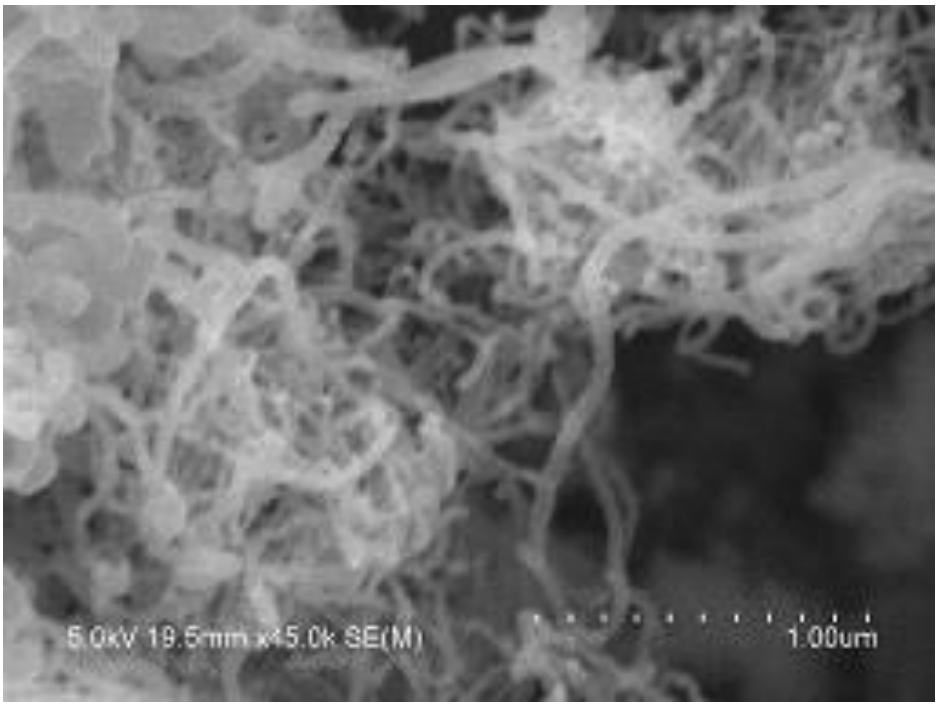

Figure 46 Surfactant treated MWCNT sample

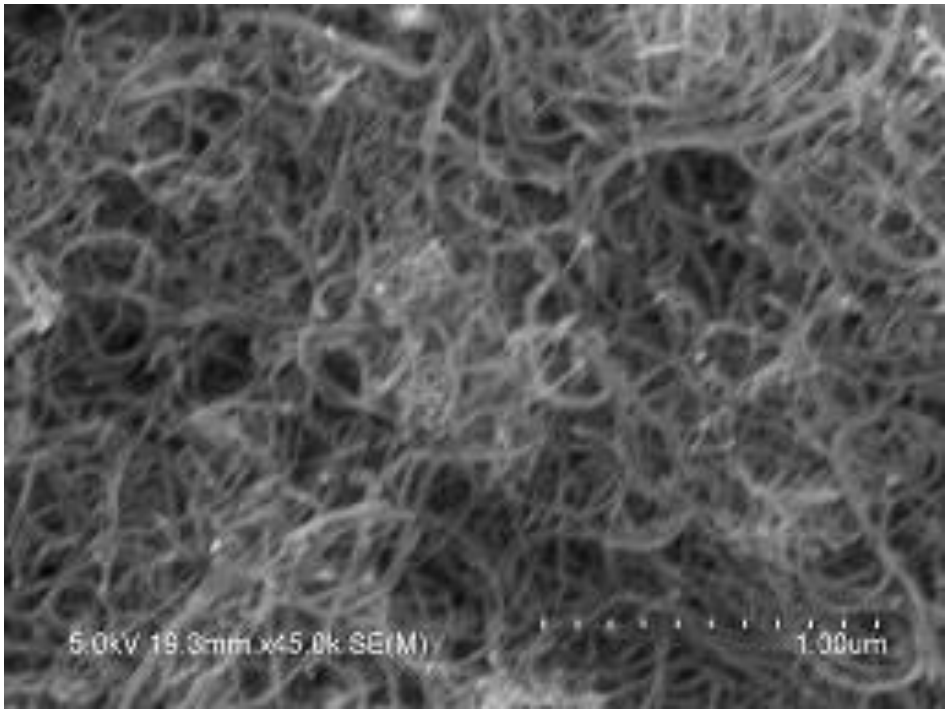

Figure 47 Untreated MWCNT sample

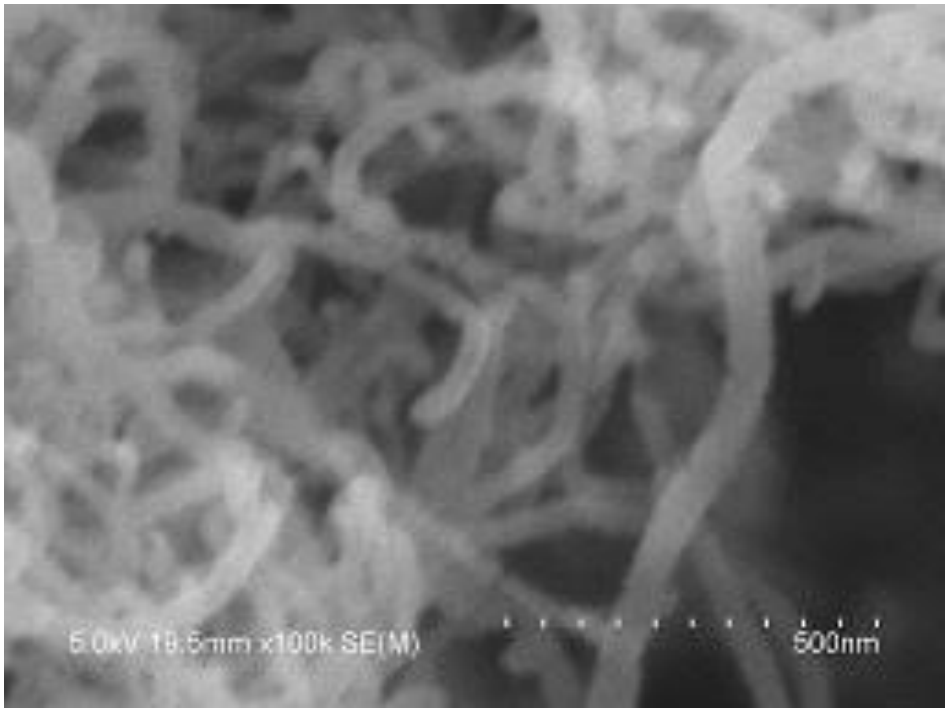

Figure 48 Magnified view of surfactant treated MWCNT sample

5.3.2 Bulk nanofluid preparation

Based on the above stability experiment, it was decided to use 30 minutes of ultrasonic mixing to form a stable mixture. Although both the first and second sample solutions were stable enough to conduct the experiment, the first run of the second sample fluid (1 g of MWCNT and 2.5 mL surfactant in 1 L of water) through the test rig resulted in excessive loading on the pump and some agglomeration after pumping. Hence, it was decided to lower the nanoparticle loading while keeping a similar or higher surfactant to MWCNT volume ratio, by doing this one would expect the nanofluid to be more homogenous.

In order to prepare this solution, 0.24 g of MWCNT and 10 mL Triton X-100 were mixed with 990 ml of water for 30 minutes in the ultrasonic bath. Hence the volume ratio of the MWCNT to surfactant was kept at 1:90 while the MWCNT volume fraction in the final solution was 0.011% (True density of the nanoparticle is 2.16g/cm^3). This process was repeated until 40 litres of nanofluid was prepared for use in the system. Subsequently, the same experimental testing and measurement procedure used in the water experiments was performed.

5.4 Analysis of nanofluid and results

In order to find the corresponding Nusselt numbers of the nanofluid at various flow rates, it is essential to calculate the thermo-physical properties of the nanofluid. For this work, the bulk properties of the nanofluid were calculated assuming they were a homogeneous liquid.

The heat capacity of the nanofluid can be found by calculating the heat capacity of the water-surfactant mixture, then using that value to calculate heat capacity of the

MWCNT nanofluid by a simple mixing model. However, as there is no available data on the specific heat capacity of the surfactant, and the amount of surfactant used is small compared to the mass of water, the effect of surfactant on the heat capacity is assumed to be equal to water, so that the heat capacity of the nanofluid can be calculated using Equation 22 (Xuan and Roetzel 2000).

$$\rho_{nf} * C_{pnf} = (1 - ø)C_{p\,f} * \rho_f + ø * \rho_p C_{pp} \tag{22}$$

Where the density of the nanofluid ρ_{nf} can be calculated using a mixing model as shown in Equation 23 (Yousefi et al. 2012) and C_{pnf} is the heat capacity of the nanofluid while C_{pf} and C_{pp} are the heat capacities of water and nanoparticles respectively.

$$\rho_{nf} = (1 - ø)\rho_f + ø\rho_p \tag{23}$$

Where ρ_n is the density of the nanoparticle (taken to be 2.16g/cm^3) (Kanagaraj et al. 2007) while the density of the water is ρ_f is based on the bulk temperature and ϕ is the volume fraction of nanoparticles.

The dynamic viscosity of the fluid can be calculated using the correlation for non-spherical particles suggested by Brenner et al (Brenner and Condiff 1974), considering the shape effects, as shown in Equation 24.

$$\mu_{nf} = \mu_f\,(1 + \eta ø) \tag{24}$$

where $\eta = \frac{0.312r}{ln2r-1.5} + 2 - \frac{0.5}{ln2r-1.5} - \frac{1.872}{r}$

And μ_f is the viscosity of the base fluid and r is the aspect ratio of the particle, assumed to be 100 based on the supplier's data and the SEM images.

The relative viscosity of the base fluid was assumed to be the same as water, although there was surfactant dissolved in the water, the amount was not sufficient enough to change the viscosity of the resultant solution significantly (Qiao 1996). Therefore the Reynolds number for the nanofluid can be determined from Equation 25.

$$Re = \frac{\rho_{nf} * v * D_H}{\mu_{nf}} \quad (25)$$

Where D_H is the diameter of the pipe; and v is the velocity of the fluid along the pipe, found from the mass flow rate. As such Newton's law of cooling allows the forced convection heat transfer coefficient to be determined as described previously.

To non-dimensionalise the results, and express them in terms of the Nusselt number, the thermal conductivity can be calculated using Hamilton and Crosser's modified Maxwell's model (Hamilton and Crosser 1962) for the effective thermal conductivity of spherical and non-spherical particles by using a shape factor as given in Equation 26. The function consists of thermal conductivities of both solid and liquid phases, volume fraction and the shape of the dispersed particles.

$$\lambda_{nf} = \lambda_f \left[\frac{\lambda_p + (n-1)\lambda_f - (n-1)\phi_p (\lambda_f - \lambda_p)}{\lambda_p + (n-1)\lambda_f + \phi_p (\lambda_f - \lambda_p)} \right] \quad (26)$$

Where n=6 for cylindrical particles,

ϕ_p is the particle volume fraction

λ_f is the thermal conductivity of water

λ_p is the thermal conductivity of the nanoparticle

and λ_{nf} is the thermal conductivity of the nanofluid

The thermal conductivity of the MWCNT nanoparticles is in the range of 2000W/mK (Nieto de Castro et al. 2012) while the thermal conductivity of the water was determined based on the bulk temperature.

By comparing the dimensionless parameters of water and the MWCNT nanofluid, the suitability of the nanofluid for forced convection heat transfer can be examined. From Figure 49 we can see that the Nusselt number and corresponding Reynolds number for the nanofluid are significantly lower than those of water at the same flow condition under steady state.

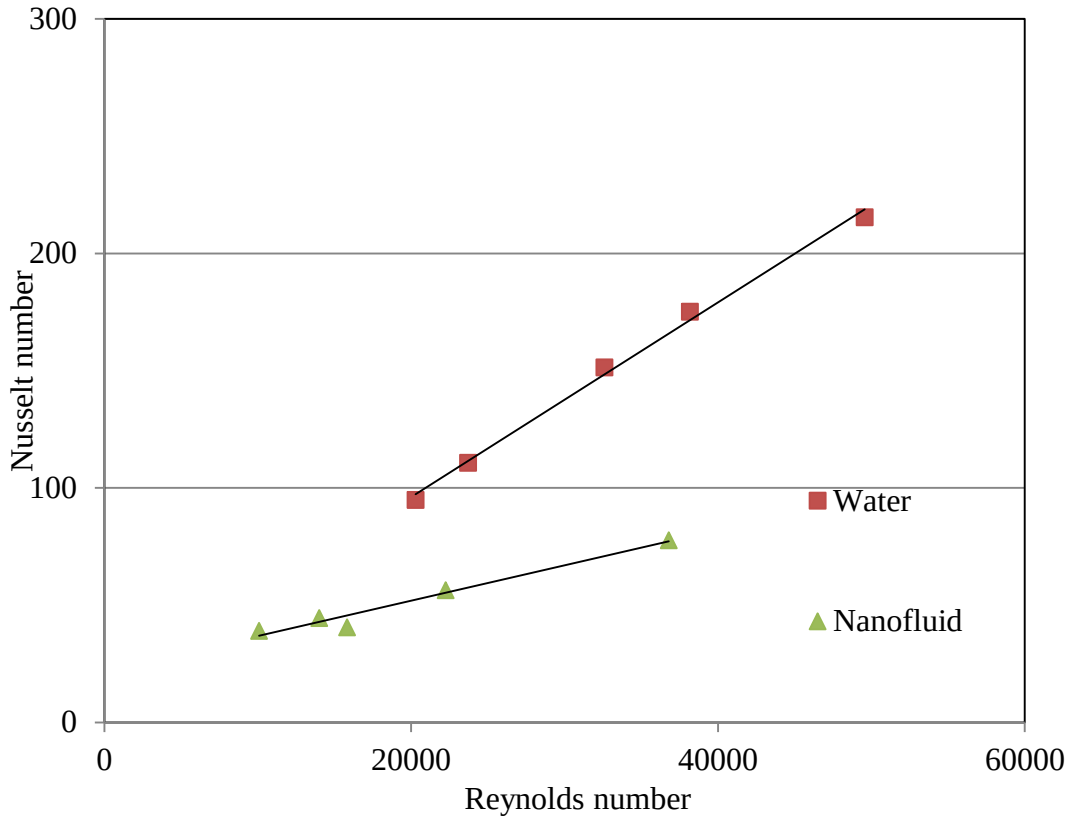

Figure 49 Comparison of water and nanofluid heat transfer characteristics

Furthermore, it was observed that the nanofluid imparted a high loading on the pump, meaning that the pumping power to achieve a similar Reynolds number was significantly higher with a nanofluid than that of water. This is a significant observation in terms of using the nanofluid as a heat transfer fluid such as this may demand additional energy input not needed if water is used.

5.5 Remarks

In this work, the forced convection heat transfer coefficient of a MWCNT nanofluid under fully developed turbulent flow was experimentally examined for its possible use as a heat transfer media for the BIPVT concentrator. By analysing both water and MWCNT nanofluid on the same equipment, it was found that operational

conditions (such as pumping power) and thermo-physical characteristics of the fluid vary significantly from the base fluid, water. However, the MWCNT based nanofluid did not improve the heat transfer characteristics; instead there was a significant drop in heat transfer capabilities. This suggests that MWCNT nanofluids in turbulent flows will actually impair heat transfer rather than improve it and so may not be an appropriate heat transfer media in forced turbulent flows that would likely be encountered in BIPVT collectors.

Chapter 6: Development of a combined analytical PVT system model

6.1 Overview

In the previous chapters, a number of factors that impact BIPVT concentrator systems have been discussed. Despite the work showing the benefits of using reflectors with PVT absorbers, there are few studies that have investigated systems with a static reflector combined with a hybrid absorber plate for façade applications. A study by (Gajbert et al. 2007) found that low concentration ratio PVT modules have advantages over traditional modules and proposed a PVT collector with a parabolic reflector. However, there appears to be few active attempts to utilise concentrating BIPVT systems, and a lack of detail in describing their combined thermal/electrical performances.

In one of his studies (Anderson 2009) investigated the performance of a building integrated PVT collector that could be integrated in to a roof, in this a mathematical model was developed and validated with an experimental set up. In a similar study Kunnemeyer et al (2014) developed a mathematical model of an unglazed V-trough photovoltaic thermal concentrator and stated that further improvement of the collector performance could be made by reducing the convective heat losses.

In light of this, this chapter will develop a model to analyse the performance of a façade integrated solar collector that incorporates the flat reflective element described earlier and PVT absorber plate, as shown in Figure 50.

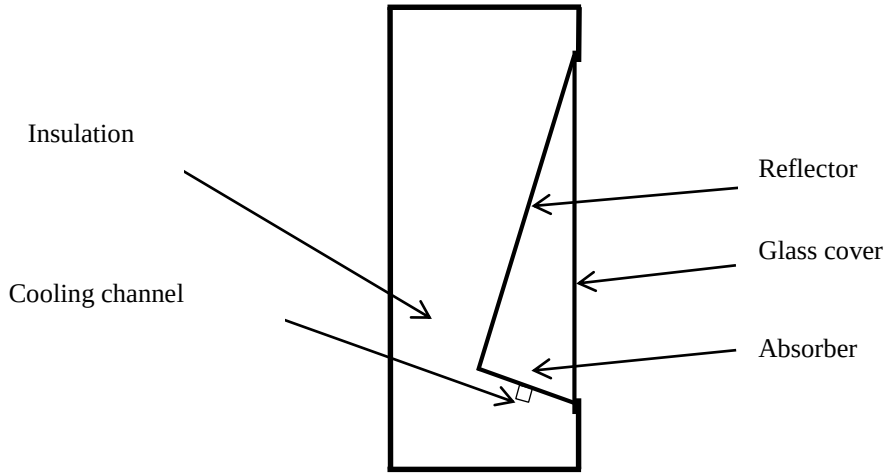

Figure 50 Façade integrated concentrator

6.2 Mathematical model

When the absorber receives solar radiation, in an ideal scenario all of the energy should be absorbed by the transport medium to be carried away as a useful energy. However, the thermal losses from the collector to the environment via various modes of heat transfer are inevitable. Minimizing the thermal losses and knowing the parameters governing the heat losses will help to understand the operation of the collector at its design phase. In order analyse the performance of the proposed façade integrated collector, a one dimensional steady state thermal model was developed based on Figure 51. In doing so a simplified thermal resistance network as shown in Figure 52 was used to undertake a heat balance of the absorber plate.

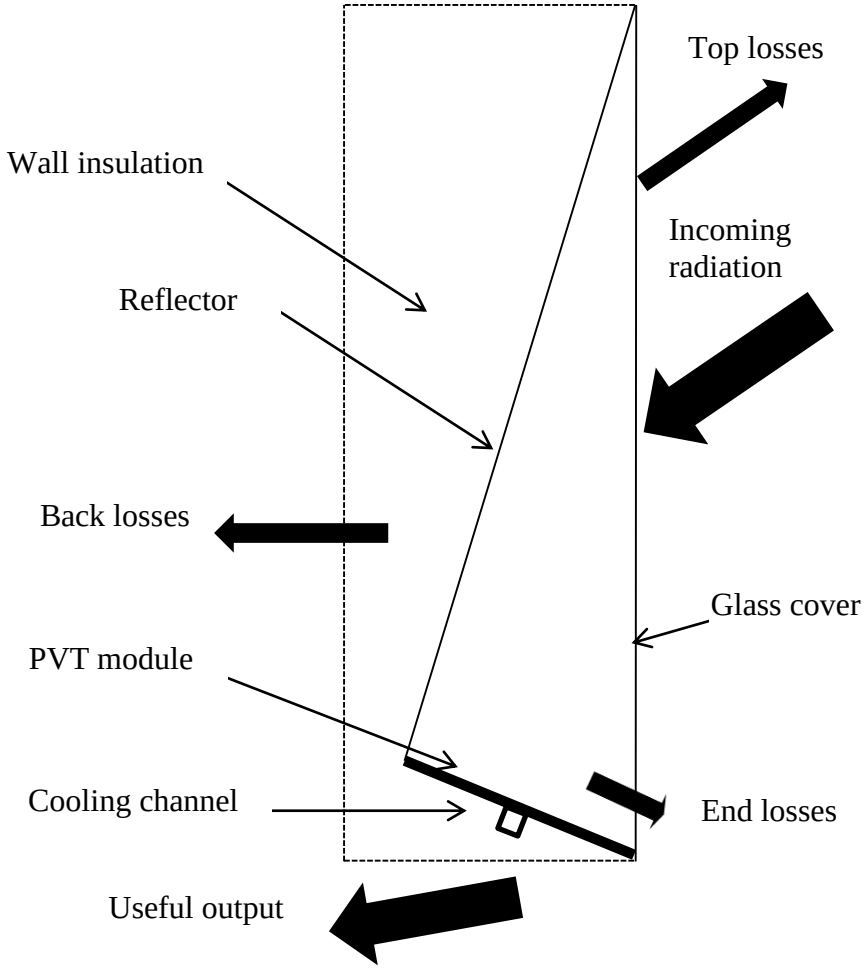

Figure 51 Schematic arrangement of the collector and the thermal energy balance

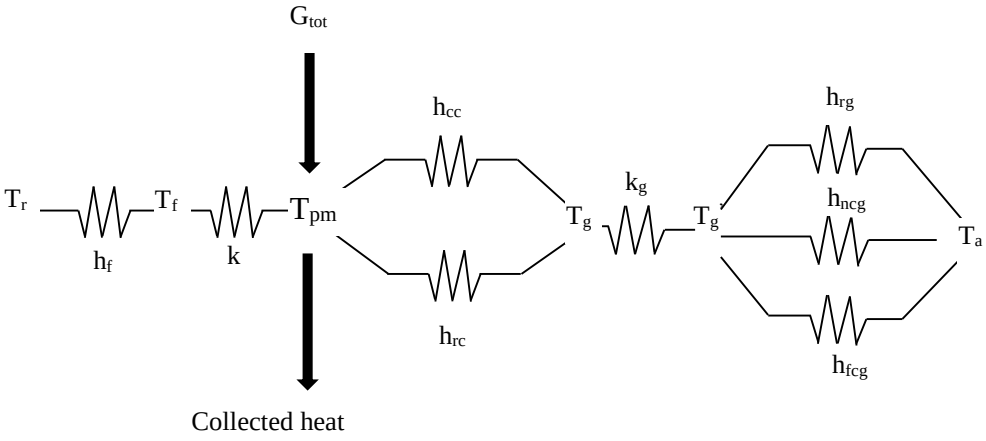

Figure 52 Simple thermal network of the proposed module

For a typical solar thermal collector, the useful thermal energy gain *Q* can be determined from Equation 27

$$Q = AF_R[(\tau\alpha)_{PV}G - U_L(T_i - T_a)] \quad (27)$$

This equation can be further modified, as shown in Equation 28, to incorporate the concentration ratio *C* of the proposed low concentration collector.

$$Q = AF_R[(\tau\alpha)_{PV}G.C - U_L(T_i - T_a)] \quad (28)$$

Here Q is given by a function of absorber area (A), heat removal factor (F_r), the transmittance-absorptance product for the photovoltaic absorber ($(\tau\alpha)_{pv}$), the solar radiation on horizontal plane (G), the concentration ratio (C), the overall heat loss coefficient (U_L) and the temperature difference between inlet (T_i) and the ambient (T_a) temperature.

In practice it is not possible to cover the whole absorber module with photovoltaic cells; hence Equation 28 can be further modified to include a packing factor (S) and the transmittance-absorptance product of the thermal absorber and the PV material ($(\tau\alpha)_{pv}$), as shown in Equation 29.

$$Q = S\left[AF_R[(\tau\alpha)_{PV}G.C - U_L(T_i - T_a)]\right] + (1 - S)\left[AF_R[(\tau\alpha)_T G.C - U_L(T_i - T_a)]\right] \quad (29)$$

The ratio of the heat collected against the irradiation falling on the absorber plate gives the thermal efficiency of the collector as shown in Equation 30.

$$\eta_{thermal} = F_R[S(\tau\alpha)_{PV} + (1-S)(\tau\alpha)_T] - F_R U_L \frac{(T_i - T_a)}{GC} \quad (30)$$

Here, the previously derived average concentration ratio in terms of principle angles described earlier (Equation 4) can be used in place of *C*.

Furthermore, the collector heat removal efficiency factor (F_R) can be expressed in terms of heat loss coefficient (U_L), mass flow rate (m) and the collector efficiency factor (F') as given by Equation 31.

$$F_R = \frac{mC_p}{AU_L}\left[1 - exp^{-\frac{AU_L F'}{mC_p}}\right] \quad (31)$$

The collector efficiency factor (F') can be calculated using Equation 32 in terms of its fin efficiency factor F, tube hydraulic diameter (d) spacing (w).

$$F' = \frac{1/U_L}{\left[\frac{1}{U_L[d + (w-d)F]} + \frac{1}{wh_{PVA}} + \frac{1}{\pi d h_{fl}}\right]} \quad (32)$$

Here h_{PVA} accounts for the bond resistance between the *PV* cell and the absorber plate as shown by (Zondag et al. 2002). The forced convection heat transfer coefficient (h_{fl}) in the cooling tube can be determined from Equation 33.

$$h_{fl} = \frac{Nu * k_{fl}}{d} \quad (33)$$

Where k_{fl} is the conductivity of the fluid at the mean temperature and Nu is the Nusselt number that can be determined from any number of relationships for forced convective heat transfer in a tube, in this study the Gnielinski (Cengel 2007) correlation interms of friction factor (f), Reynolds number (Re) and Prendlt number (Pr) as given in Equation 34 was used.

$$Nu = \frac{\left(f/8\right)(Re - 1000)Pr}{1 + 12.7\left(f/8\right)^{0.5}\left(Pr^{2/3} - 1\right)} \tag{34}$$

In order to calculate the fin efficiency factor F, it is necessary to calculate the coefficient (M) that accounts for the overall thermal conductivity and the thickness of the PV/T absorber plate as given by Equation 35 in terms of overall thermal loss coefficient U_L.

$$M = \sqrt{\frac{U_L}{K_{abs}L_{abs} + K_{PV}L_{PV}}} \tag{35}$$

As such, the modified fin efficiency F can be calculated using Equation 36, where w is the tube spacing and d is the hydraulic diameter of the tube.

$$F = \frac{tanh\left[\frac{M\,(w-d)}{2}\right]}{\frac{M\,(w-d)}{2}} \tag{36}$$

In the determination of M in Equation 35, the overall thermal loss coefficient U_L is the sum of the heat losses via top, rear and edge of the collector as given by Equation 37.

$$U_L = U_{top} + U_{rear} + U_{edge} \tag{37}$$

As the rear heat loss and edge losses are mainly through the insulation, the rear loss coefficient (U_{rear}) and the edge loss coefficient (U_{edge}) can be determined from Fouriers Law.

To determine the losses through the top (glazed face) radiation heat the radiation heat transfer coefficient inside the concentrator enclosure (h_{rc}) was assumed to be a two-surface enclosure consisting of the absorber plate and the glazing by assuming the reflector is adiabatic. Hence the expression of (h_{rc}) can be written in terms of area of the absorber plate (A), area of the glazing (A_g), the view factor (F_{cg}) from the absorber to the glazing, and the emittance of absorber plate and the glazing (ε_p) and (ε_g) as expressed in Equation 38.

$$h_{rc} = \frac{\sigma\,(T_{pm}^4 - T_g^4)}{\left(\frac{1-\varepsilon_c}{A\varepsilon_c}\right) + \left(\frac{1}{AF_{cg}}\right) + \left(\frac{1-\varepsilon_g}{A_g\varepsilon_g}\right)} \tag{38}$$

Where (T_{pm}) and (T_g) are the mean plate temperature and the internal glazing temperature of the collector respectively.

The view factor (F_{cg}) can be deduced from Equation 39 in terms of enclosure dimensions absorber width b, height of the glazing h and inclination angle β.

$$F_{cg} = \frac{2b}{b\left(1 + \frac{1}{sin\,\beta}\right) - h} \tag{39}$$

As noted earlier in Chapter 4, in light of the absence of convection heat transfer coefficients in the literature, the empirical relationship to determine the convection heat transfer coefficient (h_{cc}) found by Piratheepan and Anderson (2015) based on Equation 18 has been used, as shown in Equation 40.

$$h_{cc} = \left(\frac{k}{b}\right) 0.67 Ra^{0.36} \left({}^{b}/_{h}\right)^{1.75} \tag{40}$$

Subsequently, the heat loss through the glass cover can be calculated using the heat transfer coefficient of the glass k_g internal glazing temperature T_g and external glazing temperature T_g'.

Now, the external heat loss from the glazed cover is the sum of the radiation, natural and the forced convection heat losses. As the majority of the collector faces the ambient environment, it was assumed that the glass cover radiated heat to the surroundings with an ambient temperature T_a. Hence, the radiation heat transfer coefficient from the glazing $h_{rcg,}$ can be expressed in terms of external glazing temperature T_g' and the ambient temperature T_a as shown in Equation 41.

$$h_{rcg} = \sigma \varepsilon_g \left(T_g'^2 + T_a^2\right)\left(T_g' + T_a\right) \tag{41}$$

Furthermore, the losses due to natural and forced convection also must be taken in to account. The forced convection heat transfer coefficient (h_{fcg}) will be a function of velocity of the wind, an approximation of which can be expressed by Equation 42, where V is the wind velocity (Eicker 2006).

$$h_{fcg} = 4.214 + 3.575V \tag{42}$$

The natural heat transfer coefficient h_{ncg} can be expressed by Equation 43 (Eicker 2006).

$$h_{ncg} = 1.78\,(T'_g - T_a)^{1/3} \tag{43}$$

Using this approximation it is possible to calculate the overall convection heat transfer coefficient (h_c) by integrating both forced and natural heat transfer coefficient using Equation 44 (Eicker 2006).

$$h_c = \left(h_{fcg}^3 + h_{ncg}^3\right)^{1/3} \tag{44}$$

In summary; the combination of heat losses and the total useful energy extracted, considering the energy balance of the collector, mean the thermal efficiency of the façade integrated collector can be established.

Now in examining the electrical performance of the system, one trade-off of using silicon solar cells under concentrated radiation is that their efficiency degrades with

the temperature increase. Hence it is essential to express the electrical efficiency in terms of the temperature of the absorber plate.

The electrical efficiency of the solar cell can be determined by firstly determining the power generated by the cell at its maximum power point, as given by Equation 45.

$$P = I_{mp} V_{mp} \tag{45}$$

This can also be expressed in terms of fill factor (*FF*) and the open circuit voltage (V_{oc}) and short circuit current I_{oc} as shown in Equation 46.

$$P = FF\ I_{sc} V_{oc} \tag{46}$$

However, V_{oc} and *FF* decrease significantly with increased temperature, while short circuit current increases marginally with the temperature (Zondag 2008). Taking this into account using Equation 47 (Dubey et al. 2013), gives a good approximation of the electrical efficiency of a photovoltaic cells under various temperatures, given that the nominal operating cell temperature (*NOCT*). The efficiency of the cell at *NOCT* conditions are known from the manufacturer's data.

$$\eta_e = \eta_{NOCT}\ (1 - \beta\ (T_{pm} - NOCT)) \tag{47}$$

And for typical crystalline silicon modules β can be assumed to be 0.004 (Notton et al. 2005).

When the packing factor S is taken in to account, the electrical efficiency of the collector on a relative area basis (η_{elect}) can be expressed by Equation 48

$$\eta_{elect} = \eta_{NOCT}\left(1 - \beta\left(T_{pm} - NOCT\right)\right) * S \tag{48}$$

By combining Equations 30 and 48 the combined efficiency (η_{tot}) of the collector can be calculated from Equation 49.

$$\eta_{tot} = \eta_{thermal} + \eta_{elect} \tag{49}$$

6.3 Development of a prototype collector and the model validation

In order to validate the complete mathematical model and findings derived from its use, it is necessary to compare the outcome with an experimental model. As there is no standard method for testing photovoltaic/thermal hybrid modules it was decided use a standard steady state test method similar to the one describing the thermal performance of glazed liquid heating collectors given in AS/NZS 2535.1 (AS/NZS 2007). As such, an experimental testing system was constructed on the roof of Auckland University of Technology's School of Engineering building, facing true north (36.8° S Latitude and 174.8° Longitude).

In doing this, T-type thermocouples were used to measure the inlet and the outlet of the coolant as well as the ambient temperature. Flow rate was measured using a

Parker variable area liquid flow meter and a Grundfos vortex flow sensor. A cup anemometer and a wind vane were mounted adjacent to the collector to measure the wind speed and direction. Finally, a Delta-T SPN1 type sunshine pyranometer was used to measure the beam and global radiation. For the electrical power output, the voltage and current were measured simultaneously while keeping the system loaded at its maximum power point using a dynamic load. These readings were taken when the sun was near solar noon, such that the effect of shading due to the design of mounting enclosures was minimised.

Now, fabrication of the façade collector involves three main parts; the PV/T absorber, the reflector and the insulation elements including the glass cover. For this work the finned tube absorber plate was fabricated from a 1.2 m length of 2 mm aluminium painted matte black, with two absorbers mounted in series. A single 10 mm square aluminium tube was attached to the back of each absorber to act as a cooling channel using an adhesive (two-part epoxy resin ADR 240TG was sourced from Adhesive Technologies NZ LTD) filled with aluminium micro particles to improve its conductivity. Square tube was used as it provides a larger contact surface between the absorber plate and the cooling tube, thus improving the fin efficiency.

Each absorber plate was then fitted with a custom made string of seven 156 mm monocrystalline solar cells connected in series and bonded to the absorber using a silicone conformal coating. This thin layer of clear conformal coating protects the cells under extreme environmental and climatic condition and insulates the rear wiring of the solar cells when the absorber is exposed to the concentrated radiation.

The reflector was prepared by attaching a silver metalized film (3M Solar Mirror Film 1100) with 94% reflectance to an aluminium sheet.

Due to the practical issues associated with integrating the façade integrated collector into an actual building façade, two vertical “wall” sections as shown in Figure 53 were fabricated to mount the concentrators.

Figure 53 Façade integrated PVT collector outdoor test rig

Each wall was packed with mineral wool insulation (R value 2.8) to insulate the rear of the concentrator, and replicate a building façade, while the front surface was glazed using a low-iron glass cover. Water was drawn from a 1000L tank by a small electrical water pump, while an instantaneous electrical water heater was used to heat the inlet water to the desired temperature. A schematic representation of the combined collector test system is shown in Figure 54.

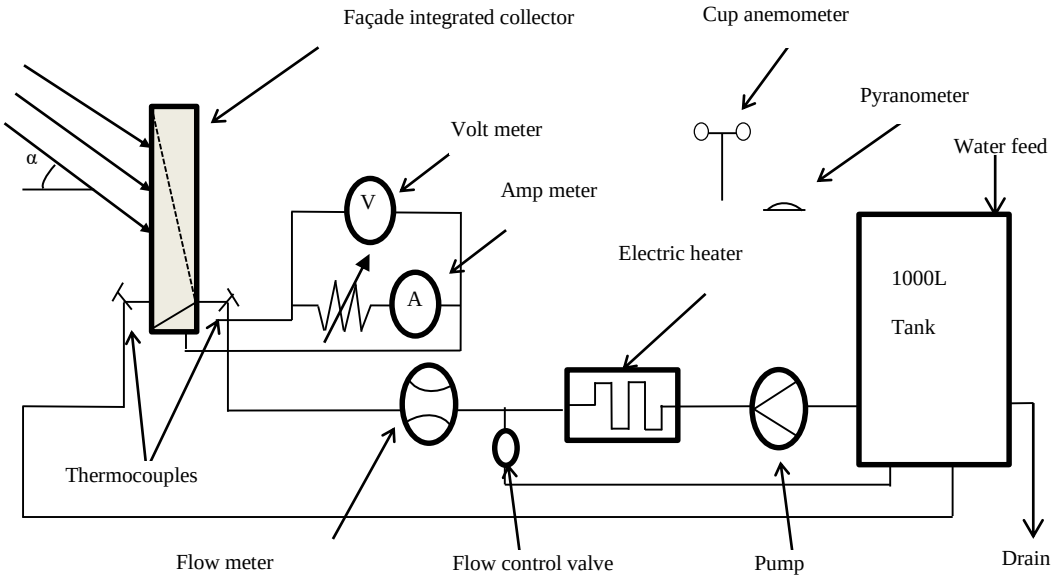

Figure 54 Experimental test rig and the circuit diagram for electrical measurements

All the measurements were recorded at 10 second intervals by a 20 channel data logger connected to an indoor data acquisition system.

To simplify the collector dimensions, although the test rig contains two sets of façade block connected in series, for modelling purposes it was treated as a single block. As such, the design parameters of the prototype collector tested here are given in Table 2.

Table 2 Physical characteristics of experimental prototype

Parameter	Symbol	Value	Unit
System flow rate	m	0.8	L/min
Absorber length	L	2.4	m
Absorber width	b	0.2	m
Reflector height	h	0.6	m
Collector area	A	0.48	m^2
PV Transmit/apsorpt	$\tau\alpha_{PV}$	0.82 ((Anderson et al. 2009b))	-
Thermal Transm/apsorpt	$\tau\alpha_{T}$	0.925 (Anderson et al. 2009b)	-
Absorber thickness	L_{abs}	0.002	m
PV thickness	L_{PV}	0.0004	m
PV conductivity	K_{PV}	130	W/mK
Tube hydraulic diameter	d	0.0088	m
Tube spacing	w	0.2	m
Cell-absorber Quasi heat transfer coefficient	h_{PVA}	45	W/m^2K
Insulation conductance	k_{ins}	0.045	W/mK
Back insulation thickness	L_{ins}	0.1	m
Edge insulation thickness	L_{edge}	0.025	m
Absorber conductivity	K_{abs}	130	W/mK
Packing factor	S	0.7	-
Conductance of glass	k_g	0.9	W/mK
Reflectance of silver metalized film	ρ_{Al}	0.9	-

By combing the electrical and thermal output relative to the incident radiation, the combined efficiency was calculated. To generalise the mathematical model, any effects on the efficiency due to the reflectance from the neighbouring surfaces were ignored.

As shown Figure 55 the mathematical model incorporating with the heat transfer relationships for the concentrator, as well as the concentration ratio, is capable of predicting the performance with good accuracy, the uncertainty of which is detailed in Appendix A.

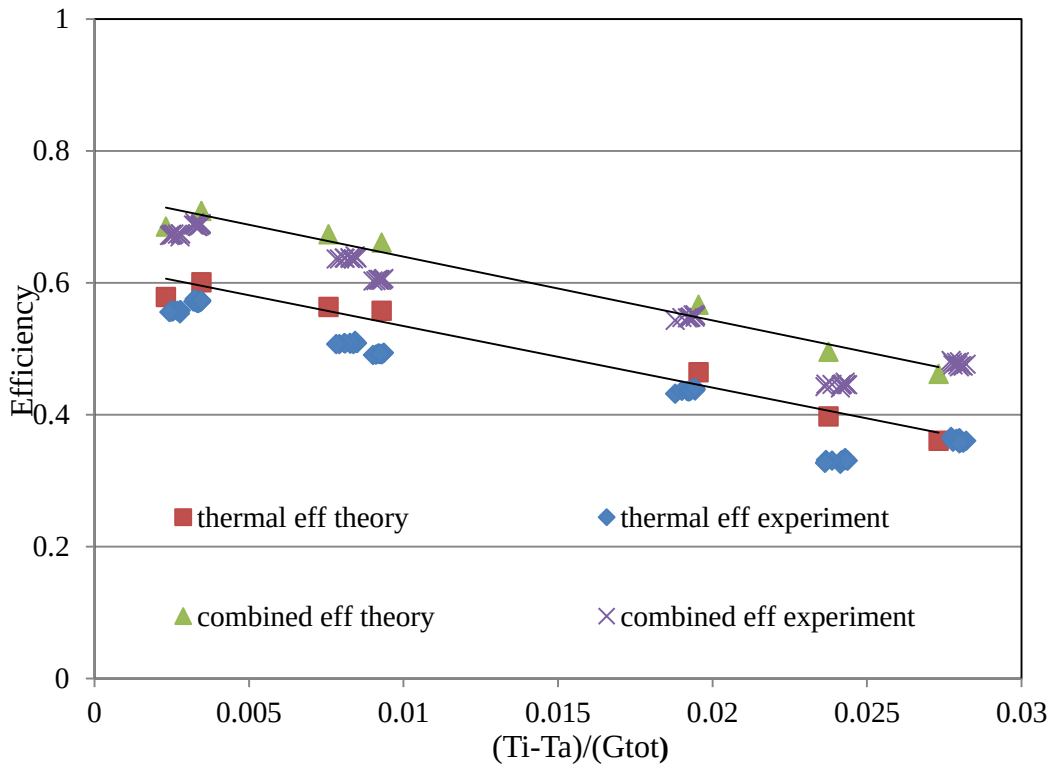

Figure 55 Experimental and theoretical efficiencies of façade integrated collector

As such, the developed model can be used to optimize the key parameters of the collector in order to achieve high efficiencies. As suggested earlier, this global

model can be used to predict the performance of the collector at different locations as this includes the Sun-Earth relationship in terms of principle angles as well.

Furthermore, inclusion of ambient temperature, wind speed and the input water temperature in the model enables it to predict the performance of the collector at different environmental conditions.

6.4 Model results

Having validated the mathematical model of the collector, in order to learn and assess the possible performance improvements of the collector, a sensitivity analysis was performed by changing the design variables. Only one design variable was varied at a time while the environmental parameters were kept at the same values as shown in Table 3. Hence, the effect of that particular parameter on the efficiency can be observed to determine the design variables that are critical in terms of efficiency of the system.

Table 3: Parameters used for the sensitivity analysis

Parameter	**Symbol**	**Value**	**Unit**
Emittance of the absorber plate	ε_p	0.95	-
Emittance of the cover	ε_p	0.88	-
System flow rate	m	0.8	L/min
Absorber length	L	2.4	m
Absorber breath	b	0.2	m
Reflector height	h	0.6	m
Collector area	A	0.48	m^2
PV Transmit/apsorpt	$\tau\alpha_{PV}$	0.82	-

Thermal Transm/apsorpt	$\tau\alpha_T$	0.925	-
Absorber thickness	L_{abs}	0.002	m
PV thickness	L_{PV}	0.0004	m
PV conductivity	K_{PV}	130	W/mK
Tube hydraulic diameter	d	0.0088	m
Tube spacing	w	0.2	m
Cell-absorber heat transfer coefficient	h_{PVA}	45	W/m^2K
Insulation conductance	k_{ins}	0.045	W/mK
Back insulation thickness	L_{ins}	0.1	m
Edge insulation thickness	L_{edge}	0.025	m
Absorber conductivity	K_{abs}	130	W/mK
Packing factor	S	0.7	-
Ambient temperature	T_a	289	K
Wind speed	V	5	m/s
Incoming radiation	G	600	W/m^2
Sun elevation angle	α	37	Degrees
Conductance of glass	k_g	0.9	W/mK

From Equation 32, as the collector fin efficiency factor depends on the design parameters, for all design purposes it can be treated as a design parameter (Goswami et al. 2000). It is desirable to have this factor with a maximum value in order to improve the performance of the collector. To achieve this, improving the factors

such as the forced convection heat transfer coefficient of the fluid and reducing the bond resistance between the PV cells and the absorber plate may be instrumental.

6.4.1 Effect of design variables

In the concentrator it is likely that high temperatures will be achieved, hence there is a need for improved cooling. Heat transfer in the cooling channel is a function of Reynold's number and thus varying the flow rate may have the effect on the overall efficiency of the collector. However as shown on Figure 56, given that flow rate is well above the stagnation point, the efficiency of the collector does not significantly improve with the increased fluid flow rate. The slight increase in efficiency can be attributed to an increase in the turbulence in the system increasing the heat transfer marginally. Furthermore, a reduction in temperature will increase the electrical efficiency marginally though the pumping power required to achieve this may offset any gains by doing this.

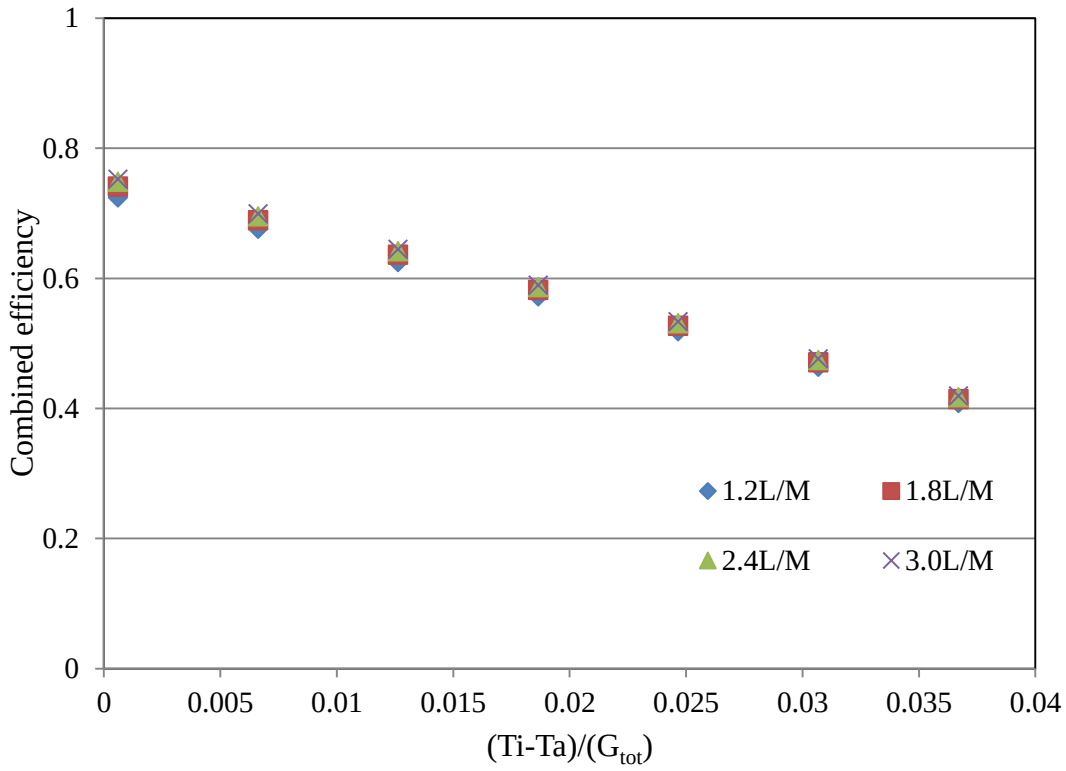

Figure 56 Combined efficiency by varying flow rate

Recently (Yousefi et al. 2012) conducted an experiment investigating the effect of MWCNT-H_2O nanofluid on the efficiency of flat-plate solar and concluded that MWCNT/H_2O nanofluids increase the performance of the collector substantially. As shown in Chapter 5, it was found that operational conditions (such as pumping power) and thermos-physical characteristics of the fluid vary significantly from the base fluid, water and so the MWCNT based nanofluid did not improve the heat transfer characteristics; instead there was a significant drop in heat transfer capabilities. This suggests that MWCNT nanofluids in turbulent flows will actually impair heat transfer rather than improve it and so may not be an appropriate heat transfer media in forced turbulent flows.

Another means of improving the efficiency could be to reduce the width of the absorber for a single tube, or by decreasing the spacing between adjacent tubes in

systems with multiple cooling tubes. As shown in Figure 57, this will increase the efficiency significantly. This can be explained by the fact that an increase in the number of tubes across the absorber plate improves the fin efficiency and thus increases the performance of the collector. However, it can be seen that, at higher $(Ti-Ta)/G_{tot}$ values they tend to converge. This suggests that although decreasing the tube spacing increases the efficiency initially, there are other factors which will decrease the efficiency at higher $(Ti-Ta)/G_{tot}$.

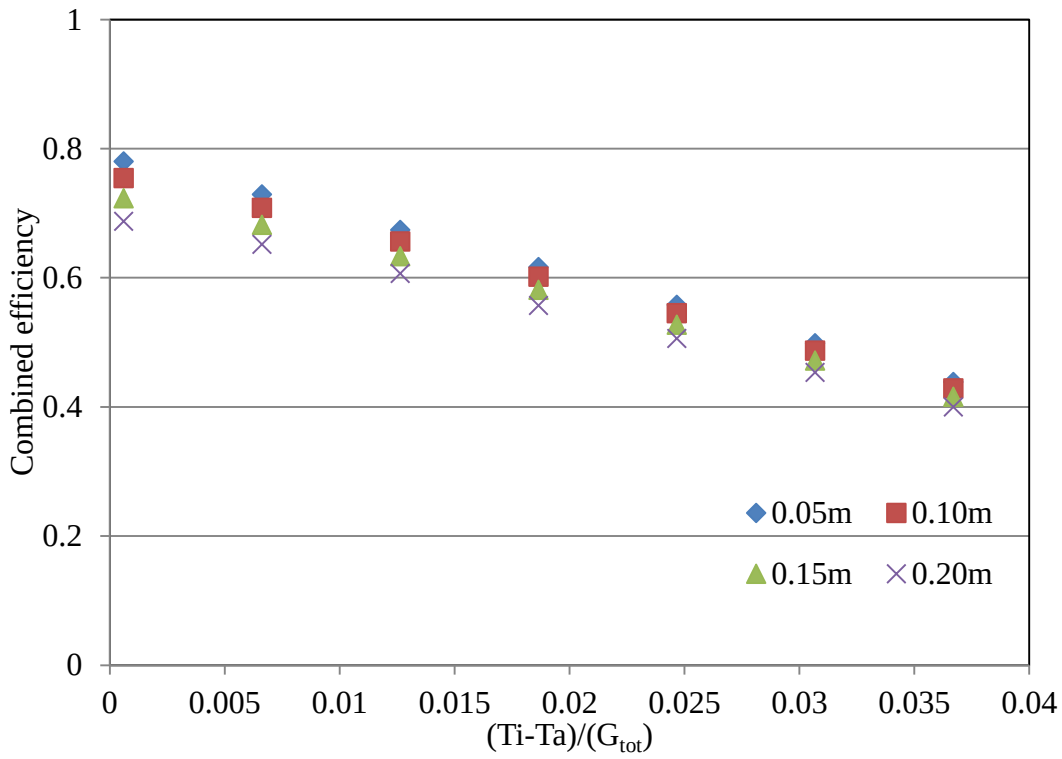

Figure 57 Combined efficiency by varying tube spacing

Further, the combined efficiency of the collector could be also improved by improving the heat transfer coefficient between the solar cells and the thermal absorber. Unlike a thermal collector that has a bond resistance between the tube and absorber (Duffie and Beckman 2006), a "quasi" heat transfer coefficient, with a

value of 45W/m^{2}K, between the PV cells and the absorber plate is used (Zondag et al. 2002). Based on these Anderson et al (2009) stated that this thermal conductance might be improved by means introducing a thermally conductive adhesive. Following on from this recommendation, it can be seen in Figure 58, that when the heat transfer coefficient is doubled from 30W/m^{2}K to 60W/m^{2}K the efficiency is improved by approximately 10%.

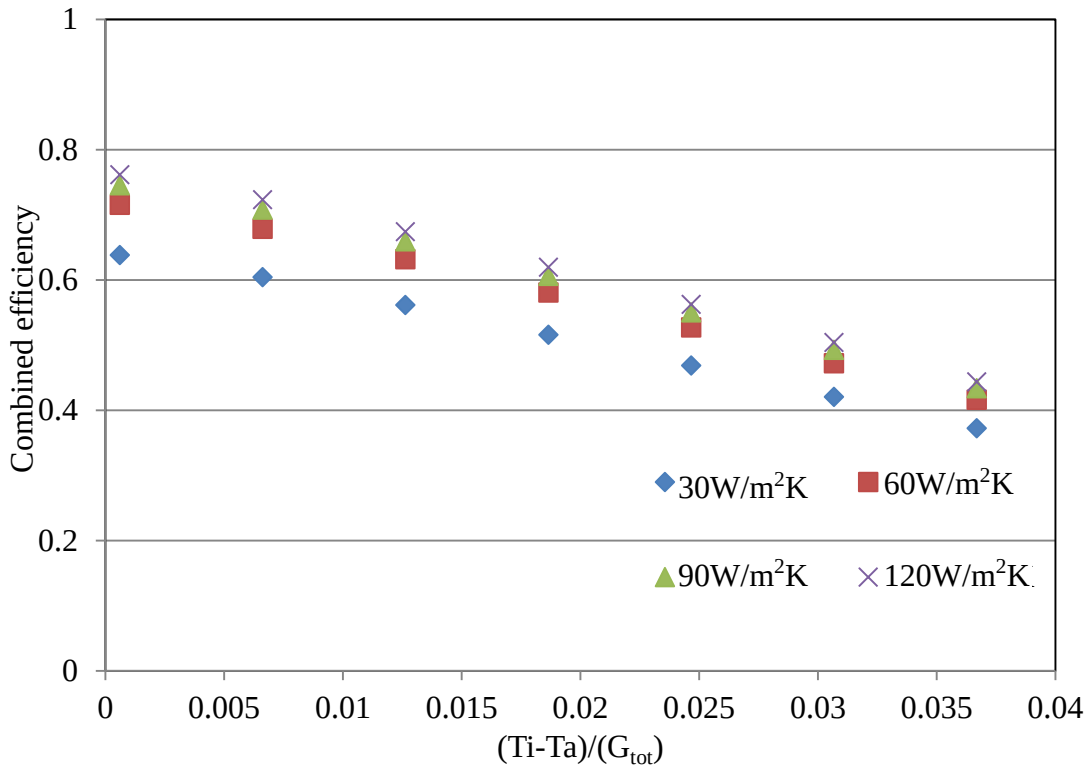

Figure 58 Combined efficiency by varying cell to absorber heat transfer coefficient

It is also important to see how, the packing factor of the solar collector (accounts for the ratio of the area covered by PV solar cells out of total area of the absorber) influence its efficiency due to the low $\tau\alpha$ of the silicon cells. As shown on Figure 59, the thermal efficiency of the collector decreases with the PV cell coverage. However as shown in Figure 60, although the thermal efficiency of the collector

decreases significantly with the packing factor, the overall efficiency of the collector increased marginally. This shows that covering the thermal absorber with the PV cells will increase the overall efficiency by compensating for the thermal efficiency reduction.

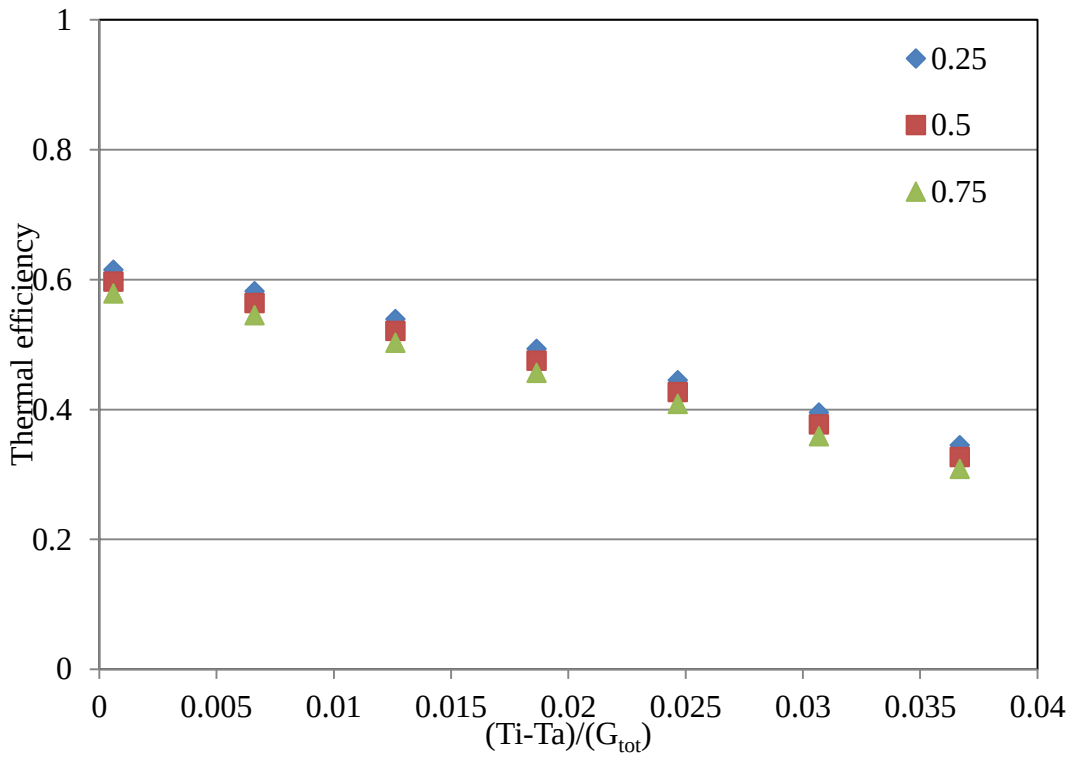

Figure 59 Thermal efficiency varying packing factor

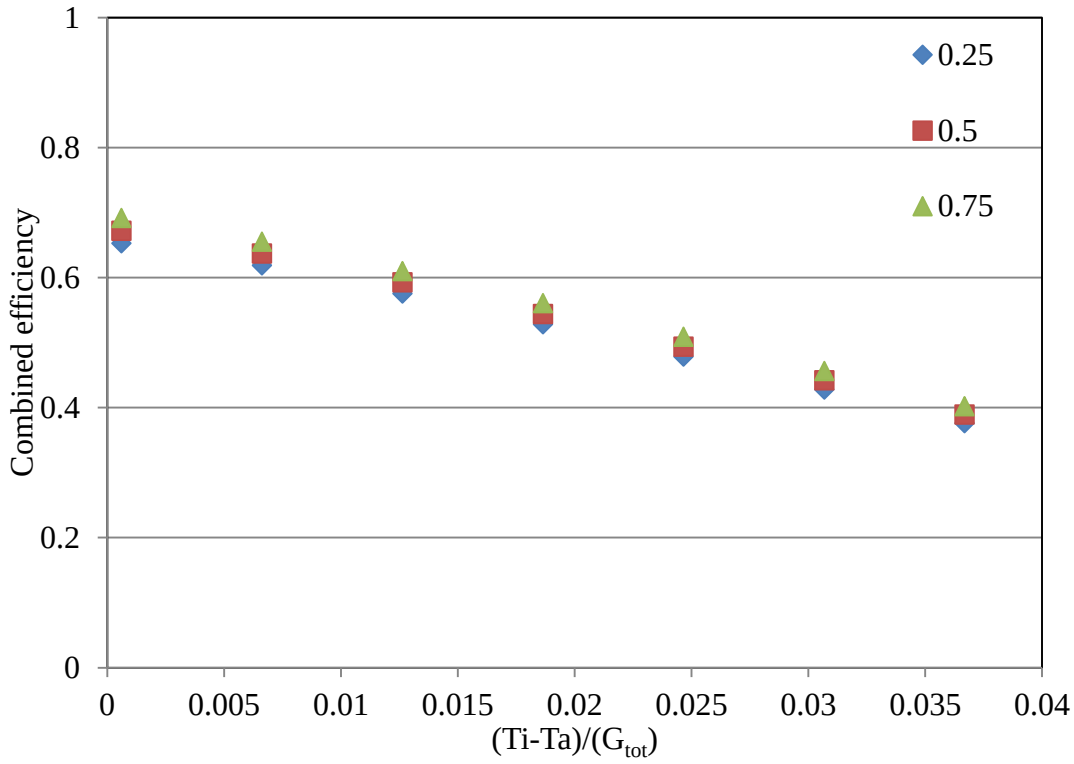

Figure 60 Combined efficiency varying packing factor

To understand the effect of reflector reflectance for different scenarios, the performance of the collector was modelled for a sunny day using data for Kaitaia, New Zealand. The model was simulated with the reflectance varied from 0.3 to 0.9 and the output was observed. As shown in Figure 61 the performance of the collector increases with the reflector reflectance.

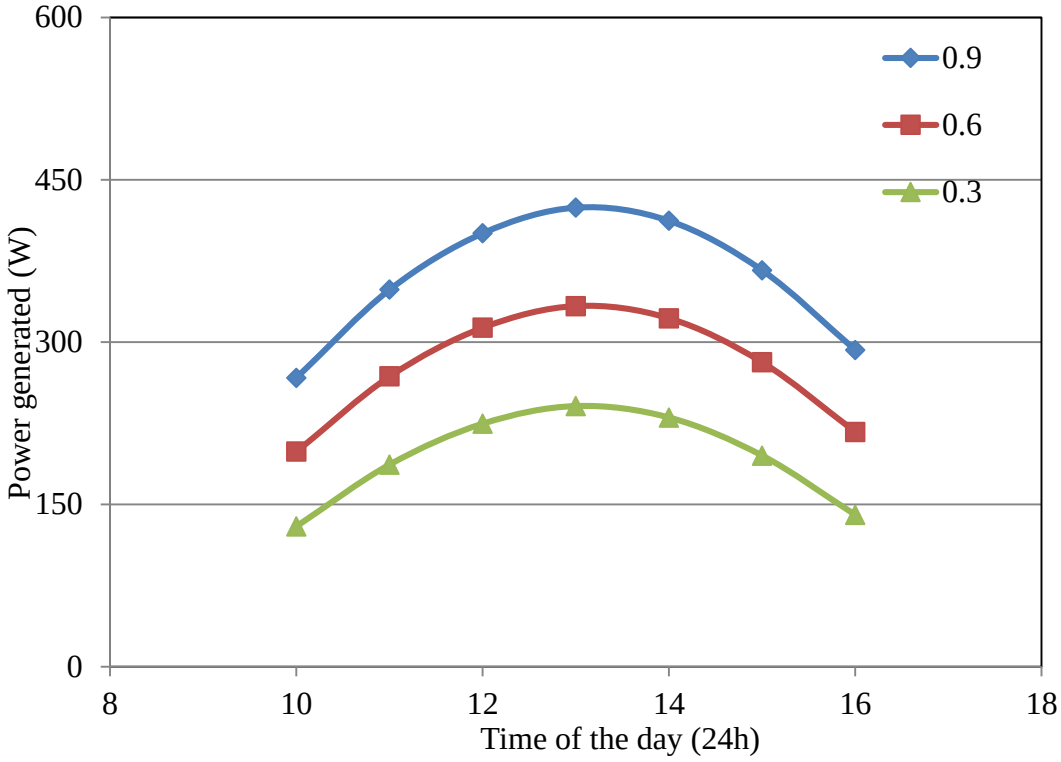

Figure 61 Performance of the collector varying the reflectance of the reflector

It is important to note that, the performance of the collector strongly depends on the reflector reflectance and reduction in reflectance will reduce the performance of the collector dramatically.

6.4.2 Performance of collector under various weather conditions

Now this model can also be used to predict the performance of the proposed collector under various weather conditions such as various wind speed and solar elevation angles.

Although the absorber is fairly isolated from the atmosphere, the efficiency of the collector decreases with the wind speed particularly at high absorber temperatures as shown in Figure 62. Compared to the efficiency variation of the unglazed collector with the wind speed reported by Anderson (2009), this is marginal.

However, unlike a typical collector, the glazing exposed to the wind is relatively large compared to the area of the absorber plate. Therefore, one possible reason for the notable variation could be due to higher thermal losses via the exposed glazing.

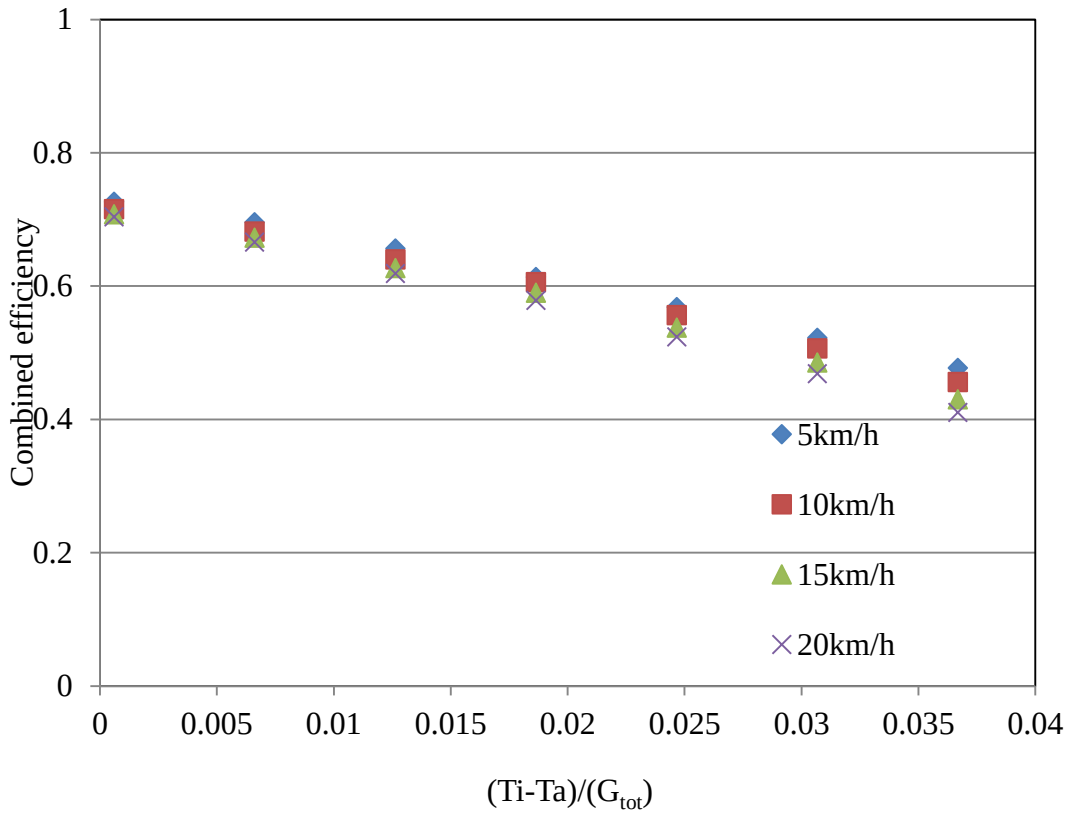

Figure 62 Combined efficiency varying wind speed

The performance of the collector was analysed under a typical sunny summer and a winter day using the real data collected in Kaitaia, NZ. As shown in Figure 63, the performance of the collector is improved before 12 pm and after 2 pm, peaking at 10 am and 4 pm compare to the absorber without the concentrating element. During the summer the collector will produce more power at lower elevation angles, coincidently that is the time a typical house may have more power demand.

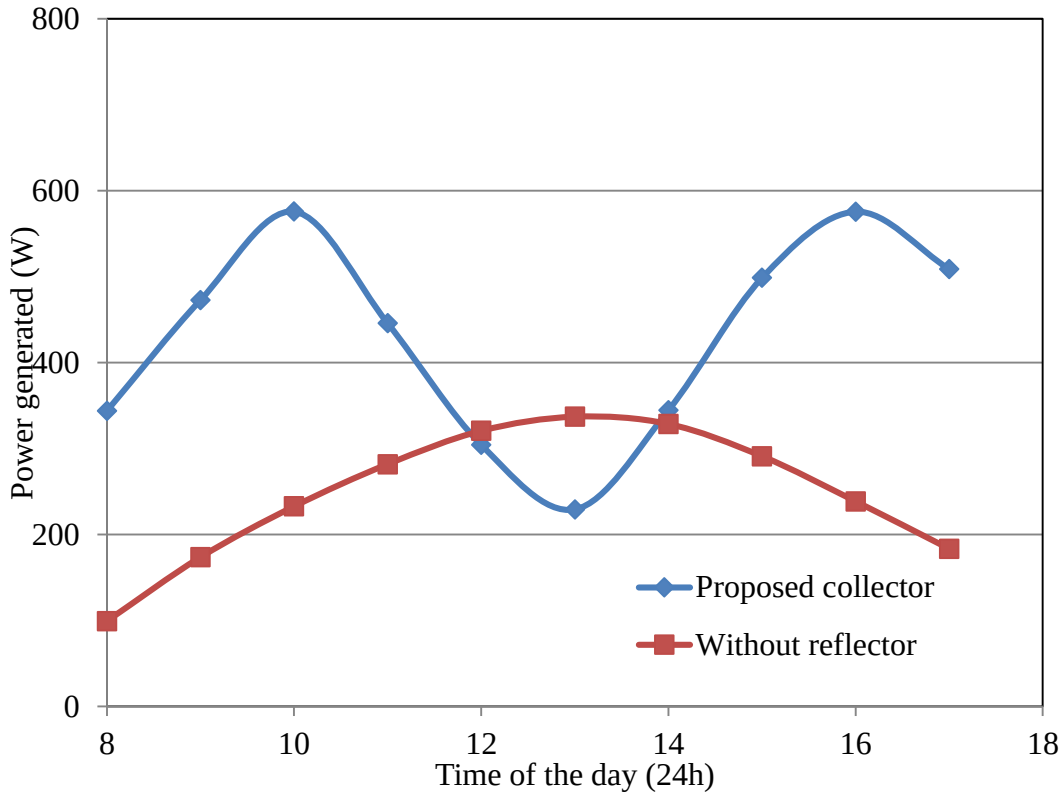

Figure 63 Performance of the collector on 9th of January

Likewise, in winter, the performance of the collector compared to the absorber without the concentrating element, improved dramatically up to 5 times early in the morning and evening and was continuously improved throughout the day, as shown in Figure 64.

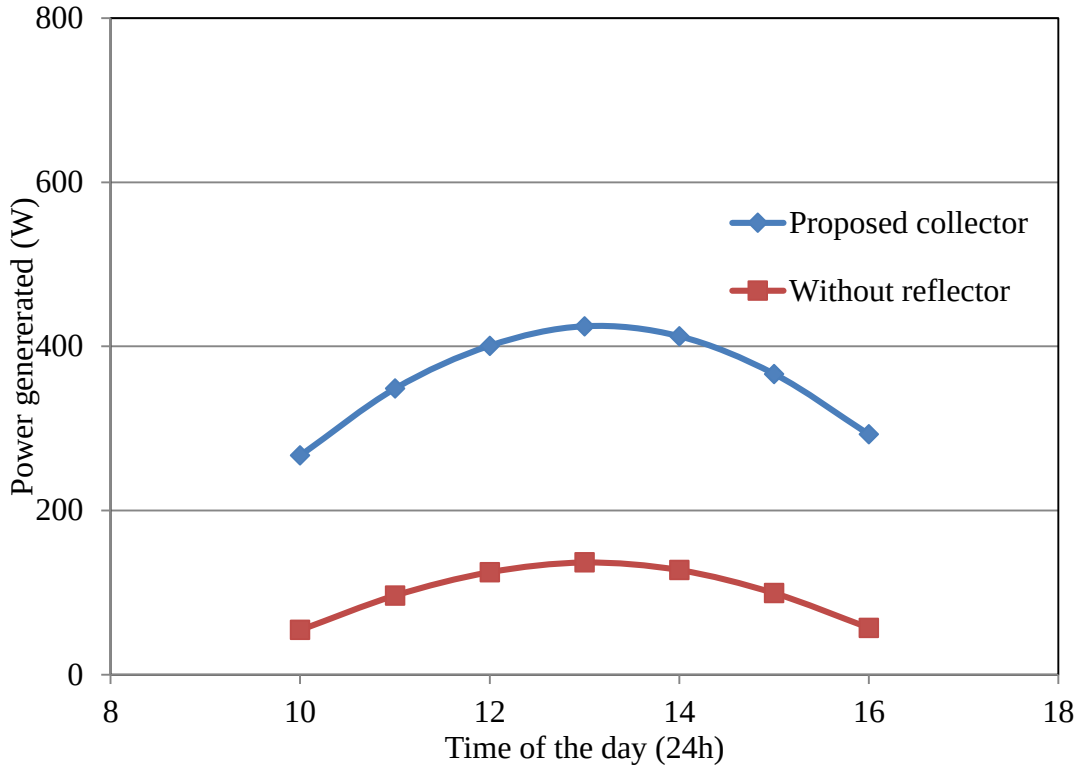

Figure 64 Performance of the collector on 30th of June

6.5 Remarks

From the sensitivity analysis, there are number of conclusions that can be drawn. Firstly, increasing the flowrate in the cooling tubes appears to offer little benefit with respect to increasing the efficiency of the collector.

However, the combined efficiency of the collector can be improved by increasing the number of cooling channels across the absorber plate, though this may not be economical. Hence increasing the number tubes has to be considered as a trade-off between the efficiency and the cost of the collector.

Furthermore, improved thermal contact between the solar cells and the thermal absorber will increase the efficiency dramatically and appears to offer significant

potential in improving the performance of the façade integrated BIPVT solar concentrator system.

The output of the collector appears to be heavily dependent on the reflectance of the reflector. Hence it is important to have a quality reflector that can keep its reflectance throughout the lifetime of the collector. Finally, as also noted in Chapter 3 and above, the collector performs well under moderate and low elevation angles throughout the winter, autumn and spring.

Chapter 7: Conclusions and recommendations for future work

7.1 Conclusions

In the wake of recent drastic climate changes and global warming, there is a growing demand to consider the alternative cost effective ways to harness the renewables. It is virtually impossible to build a sustainable environment without considering the use of solar energy, as the largest possible energy source available for the world.

In the recent past, PV electricity generation has become increasingly affordable and has gained a strong foothold in the global energy mix. Meanwhile according to the IEA (2012), 47% of the global energy consumption is used to produce heat. This justifies the use of PVT collectors which can produce both thermal and electrical energy. Despite the rapid growth in the PV industry, collectors combing PV with thermal absorbers are not widely available yet. In an attempt to reduce the cost of the collector, the use of low concentration ratio concentrating elements will increase the intensity of the radiation on the absorber module. Furthermore, extending them to be used in a built environment as building integrated collectors, not only reduces the transmission of heat to the building but also takes away part of the material cost.

The work presented in this study concerns the optical, electrical and thermal performance of a set of façade integrated collectors that can be fabricated from off the shelf materials. In particular, it was shown that a flat plate reflector is a suitable alternative to low concentrating over edge parabolic façade collectors. Notably, the uniform illumination profile on the absorber under flat reflectors ensures that traditional silicon solar cells can be used instead of CIGS. Furthermore, it also

demonstrates the significance of the tilt angle of the reflector and the absorber plate using the ray tracing technique.

The analyses conducted on the collector showed that this façade integrated collector performs well under low elevation angles while performing moderately under higher elevation angles. However, this can be adjusted to a certain extent by adjusting the tilt angle of the module and the reflector. The parameters for a particular design must therefore be estimated from considerations of the energy demand and other auxiliary system.

An empirical correlation describing the convection heat losses in the enclosed air gap between the absorber and the glazing was found in order to describe the mathematical model of the whole collector. Furthermore, it was shown that the empirical correlation is generic enough to be applicable for enclosures with parabolic over edge reflectors as well.

From the literature it was suggested that improving the heat transfer capabilities of the heat transfer media particularly by using nanofluids, may improve the efficiency of the collector. However, the forced convection heat transfer coefficient of MWCNT based nanofluid studied here was impaired when tested under turbulent flow conditions compared to water, depicting the scenario in the solar thermal collector pumping power.

For photovoltaic cells accepting concentrated irradiation the temperature of the cells is an important parameter as it decreases the electrical efficiency. However, in terms of thermal energy recovery it is preferable to keep it as high as possible. From the sensitivity analysis on the validated model a number of significant design

parameters which greatly influence the overall efficiency of the collector were found. In particular, the thermal connection (bond conductance) between the PV cells and the thermal absorber was found to be a vital contributor to improving the efficiency of the collector. This can possibly be improved by using highly conductive adhesives. Improving the convection heat transfer capability of the coolant by changing the flow rate or using a different fluid may improve the performance of the collector. Although increasing the flowrate marginally improves the efficiency of the collector this may require more pumping power, hence may not be cost effective. It was also demonstrated that the mathematical model presented in this work is robust enough to optimise the size of the similar suitable façade integrated modules at different locations for different applications.

Finally, according to the demand of the form of energy, the design can be manipulated to match the requirements of the building by changing the flow rate of the water to some extent. Good thermal contact between the thermal absorber and the solar cells however will give greater control towards such selectivity.

7.2 Future recommendations

Besides the work done regarding the design of façade integrated collector, there are a number of possible opportunities that could be explored to improve these collectors for them to be truly integrated in the facade. In particular, the proposed model was predominantly designed for north facing collector in order to maximize the output. However, in real life, buildings may not have a façade facing true north or may be shaded from the true north. Hence it is essential to examine the performance of the proposed collector mounted in other directions as well, in order to improve the chances of use for different scenarios.

It is worthy to note that the proposed collector is modelled in a way that the size of the collector can be manipulated according to the particular requirements. However, changing the dimensions of the collector is not necessarily proportional to the cost of the system, as the cost associated with the collector depends on the building materials as well. Hence it will be interesting to see how the cost analysis of a building with the façade integrated collectors made up of different size façade integrated collectors pans out.

It was shown that the façade integrated collector performed well under low elevation angles while roof mounted solar collectors are known to work well under higher elevation angles. Hence, the combination of façade integrated collector with roof mounted collectors may help produce more uniform output, and produce energy for longer periods during a day. The performance of combined roof and façade integrated collectors has to be further explored in terms of supplying a consistent amount of energy to the building in different seasons across the year.

As a building integrated collector, the proposed collector may have some additional constraints to be addressed such as the durability and the manufacturing techniques. It was noted that, the thermal contact between the silicon cells and the thermal absorber (that depends on the lamination technique) plays a crucial part in the efficiency and this may deteriorate with the time. Manufacturing the absorber plate along with the cooling channel as a single extruded piece with an improved lamination technique for silicon cells on the thermal absorber may improve the durability and the performance of the collector.

Another notable limitation that needs to be addressed for this collector is the absence of testing data under stagnation conditions and as well as the performance deterioration of the silicon solar cell under constant concentrated radiation. These issues will need to be addressed, especially when they are to be integrated in buildings in general, as replacing or repairing them are not straight forward as the retrofitted collectors.

Finally, although the performance of the collector can be improved by optimising the design parameters, seamless integration of this collector in to the building and making it aesthetically pleasing could be a challenging task worth investigating.

References

Anderson, B. 1977, "*Solar energy: fundamentals in building design*" McGraw-Hill, New York

Anderson, T.N., Duke, M and Carson, J.K., 2009a, "Convection suppression in a triangular-shaped enclosure", *Computational Thermal Sciences,* Vol. 1, pp 309-321

Anderson, T.N., 2009, "*Investigation of thermal aspects of building integrated photovoltaic/thermal solar collectors*", PhD Thesis, The University of Waikato.

Anderson, T.N. and Duke, M., 2007, "Analysis of a photovoltaic/thermal solar collector for building integration", *Proceedings of SB07 NZ Conference,* November 2007, Auckland

Anderson, T.N., Duke, M., Morrison, G.L. and Carson, J.K., 2009b, "Performance of a building integrated photovoltaic/thermal (BIPVT) solar collector", *Solar Energy,* Vol. 83, pp. 445-455

Andrews, J. W., 1981, "*Evaluation of flat-plate photovoltaic/thermal hybrid systems for solar energy utilization"*, Brookhaven National Laboratory, Virginia

AS/NZS., 2007, "*Test methods for solar collectors part 1 Thermal performance of glazed liquid heating collectors including pressure drop"*, Standard Australia and Standard New Zealand, Homebush

Asan, H. and Namli, L., 2001 “Numerical simulation of buoyant flow in a roof of triangular cross-section under winter day boundary conditions” *Energy and Buildings*, Vol 33, pp. 753-757

Berber, S., Kwon, Y.K. and Tomanek, D., 2000, “Unusually high thermal conductivity of carbon nanotubes”. *Physical Review Letters*, Vol 84, pp. 4613-4616.

Brenner, H. and Condiff, D.W., 1974, “Transport mechanics in systems of orientable particles. IV. Convective transport”, *Journal of Colloid and Interface Science*, Vol 47, pp. 199-264

Brogren, M., 2004, “*Optical efficiency of low-concentrating solar energy systems with parabolic reflectors*” PhD thesis, Uppsala University, Uppsala

Brogren, M. and Karlsson, B., 2002, “Low concentrating water cooled PV-thermal hybrid systems for high latitudes”. *Proceedings of Photovoltaic Specialists Conference*, 2002, pp. 1733-1736

Cellura, M., Grippaldi, V., Brano, V. L., Longo S. and Mistretta, M., 2011, “Life cycle assessment of a solar PV/T concentrator system”. *Proceedings of Fifth International Conference on Life Cycle Management*, Berlin, pp. 28-31

Cengel, Y. A. 2007, “*Heat & mass transfer: a practical approach*”, McGraw-Hill, New York

Chapin, D. M., Fuller, C. and Pearson, G., 1954, "A new silicon p-n junction photocell for converting solar radiation into electrical power", *Journal of Applied Physics***,** Vol. 5, pp. 676-677

Chein, R. and Chuang, J., 2007 "Experimental microchannel heat sink performance studies using nanofluids", *International Journal of Thermal Sciences*, Vol. 46, pp. 57-66

Choi, S. and Eastman, J.A., 1995, "Enhancing thermal conductivity of fluids with nanoparticles" *Proceedings of ASME International Mechanical Engineering Congress & Exposition*, Argonne, Illinois

Choi, S., Zhang, Z., Yu, W., Lockwood, F. and Grulke, E., 2001 "Anomalous thermal conductivity enhancement in nanotube suspensions", *Applied Physics Letters*, Vol 79, pp. 2252-2254

Chow, T.T, He, W. and Ji, J., 2006, "Hybrid photovoltaic-thermosyphon water heating system for residential application", *Solar Energy*, Vol 80, pp. 298-306

Coventry, J.S., 2005, "Performance of a concentrating photovoltaic/thermal solar collector", *Solar Energy*, Vol 78, pp. 211-222

Cox, C. and Raghuraman, P., 1985 "Design considerations for flat plate photovoltaic/thermal collectors", *Solar Energy*, Vol 35, pp. 227-241

Da Silva, R. M. and Fernandes, J.L.M., 2010, "Hybrid photovoltaic/thermal (PV/T) solar systems simulation with Simulink/Matlab", *Solar Energy*, Vol 84**,** pp. 1985-1996

Daghigh, R., Ibrahim, A., Jin, G.L., Mat, S., Othman, M.Y., Ruslan, M.H., Salleh, M.H.M. and Sopian, K. 2009, "Hybrid photovoltaic thermal (PV/T) air and water based solar collectors suitable for building integrated applications", *American Journal of Environmental Sciences*, Vol 5, pp. 618-624

Ding, Y., Chen, H., He, Y., Lapkin, A., Yeganeh, M., Siller, L., and Butenko, Y. V. 2007, "Forced convective heat transfer of nanofluids", *Advanced Powder Technology*, Vol 186 , pp. 813-824

Dubey, S., Sarvaiya, J. N., and Seshadri, B., 2013, "Temperature Dependent Photovoltaic (PV) Efficiency and Its Effect on PV Production in the World – A Review", *Energy Procedia*, Vol 33, pp. 311-321

Duffie, J. A., and Beckman, W. A. 2006, "*Solar Engineering of Thermal Processes*", Wiley, New York

Eastman, J., Choi, U., Li, S., Soyez, G., Thompson, L., and Di Melfi, R., 1999, "Novel thermal properties of nanostructured materials", *Journal of Metastable and Nanocrystalline Materials*, Vol 2, pp. 629-634

Eicker, U. 2006, *"Solar technologies for buildings"*, John Wiley & Sons, Chichester, England

Flack, R., 1980., "The experimental measurement of natural convection heat transfer in triangular enclosures heated or cooled from below", *Journal of Heat Transfer*, Vol 102, pp. 770-772.

Florschuetz, L. 1979, “Extension of the Hottel-Whillier model to the analysis of combined photovoltaic/thermal flat plate collectors”, *Solar Energy*, Vol 22, pp. 361-366

Gajbert, Hall, M., and Karlsson, B., 2007, “Optimisation of reflector and module geometries for stationary, low-concentrating, facade-integrated photovoltaic systems”, *Solar Energy Materials and Solar Cells*, Vol 91, pp. 1788-1799

Gajbert, H., 2008, “*Solar thermal energy systems for building integration*”, PhD Thesis, Lund University, Lund

Gibart, C., 1981, “Study of and tests on a hybrid photovoltaic-thermal collector using concentrated sunlight”, *Solar Cells*, Vol 4, pp. 71-89

Gnielinski, V. 1976, “New equations for heat and mass-transfer in turbulent pipe and channel flow”, *International Chemical Engineering*, Vol 16, pp. 359-368

Godson, L., Raja, B., Mohan Lal, D., and Wongwises, S., 2010, “Enhancement of heat transfer using nanofluids—An overview”, *Renewable and Sustainable Energy Reviews*, Vol 14, pp. 629-641

Goswami, Y. D., 2000, “*Principles of solar engineering*”, Taylor and Francis, Philadelphia

Green, M., Emery, K., Yoshihiro, H., Wilhelm, W. and Ewan, D., 2013, “Solar cell efficiency tables (version 41)”, *Progress in Photovoltaics: Research and Applications*, Vol 21, pp. 1-11

Haddad, Z., Abid, C., Oztop, H. F., and Mataoui, A., 2014, "A review on how the researchers prepare their nanofluids", *International Journal of Thermal Sciences*, Vol 76, pp. 168-189

Hall, M., Roos, A., and Karlsson, B. 2005, "Reflector materials for two-dimensional low-concentrating photovoltaic systems: the effect of specular versus diffuse reflectance on the module efficiency", *Progress in Photovoltaics: Research and Applications*, Vol 13, pp. 217-233

Hamilton, R., and Crosser, O., 1962, "Thermal conductivity of heterogeneous two-component systems", *Industrial and Engineering chemistry fundamentals*, Vol 1, pp. 187-191

Hegazy, A. A. 2000, "Comparative study of the performances of four photovoltaic/thermal solar air collectors", *Energy Conversion and Management*, Vol 41, pp. 861-881

Holtzman, G., Hill, R., and Ball, K. 2000, "Laminar natural convection in isosceles triangular enclosures heated from below and symmetrically cooled from above", *Journal of Heat Transfer*, Vol 122, pp. 485-491

Ibrahim, A., Fudholi, A., Sopian, K., Othman, M. Y., and Ruslan, M. H., 2014, "Efficiencies and improvement potential of building integrated photovoltaic thermal (BIPVT) system" *Energy Conversion and Management*, Vol 77, pp. 527-534

Ibrahim, A., Othman, M. Y., Ruslan, M. H., Mat, S., Zaharim, A., and Sopian, K., 2011, "A pilot study of the building integrated photovoltaic thermal (BIPVT)

collector for commercial applications", *Proceedings of the 4th WSEAS International Conference on Energy and Development*, Malaysia

IEA, 2011a, "*25 Energy Efficiency Policy Recommendations*", International Energy Agency, Paris

IEA, 2011b, "*Solar Energy Perspectives OECD Publication"*, International Energy Agency, Paris

IEA, 2012, "*World Energy Outlook 2012 Executive Summary*", International Energy Agency, Paris

IEA, 2013, "*Transition to Sustainable Buildings Strategies and Opportunities to 2050*", International Energy Agency, Paris

IEA, 2014, "Technology Road Map Solar Photovoltaic Energy", International Energy Agency, Paris

Kalogirou, S. A., 2004, "Solar thermal collectors and applications", *Progress in Energy and Combustion Science*, Vol 30, pp. 231-295

Kanagaraj, S., Varanda, F.R., Zhiltsova, T.V., Oliveira, M.S.A., and Simoes, J.A.O., 2007, "Mechanical properties of high density polyethylene/carbon nanotube composites", *Composites Science and Technology*, Vol 67, pp. 3071-3077

Kandilli, C. 2013. "Performance analysis of a novel concentrating photovoltaic combined system", *Energy Conversion and Management*, Vol 67, pp. 186-196

Karlsson, B., and Wilson, G., 2000, "MaReCo design for horizontal, vertical or tilted installation", *Proceedings of EuroSun 2000*, Copenhagen

Kern Jr, E., and Russell, M., 1978, "*Combined photovoltaic and thermal hybrid collector systems*" Massachusetts Institute of Technology, Lexington

Kline, S.J., and McClintock, F., 1953, "Describing uncertainties in single-sample experiments", *Mechanical Engineering*, Vol 75, pp. 3-8

Kostic, L.T., Pavlovic, T.M., and Pavlovic, Z.T. 2010, "Optimal design of orientation of PV/T collector with reflectors", *Applied Energy*, Vol 87, pp. 3023-3029

Kunnemeyer, R.., Anderson, T.N., Duke, M., and Carson, J.K. 2014. "Performance of a V-trough photovoltaic/thermal concentrator", *Solar Energy*, Vol 101, pp. 19-27

Lee, J., and Mudawar, I., 2007, "Assessment of the effectiveness of nanofluids for single-phase and two-phase heat transfer in micro-channels", *International Journal of Heat and Mass Transfer*, Vol 50, pp. 452-463

Li, X., Zhu, D., and Wang, X. 2007, "Evaluation on dispersion behaviour of the aqueous copper nano-suspensions", *Journal of Colloid and Interface Science*, Vol 310, pp. 456-463

Li, Y., Zhou, J. E., Tung, S., Schneider, E., and Xi, S., 2009, "A review on development of nanofluid preparation and characterization", *Powder Technology*, Vol 196, pp. 89-101

Liu, J., Rinzler, A. G., Dai, H., Hafner, J. H., Bradley, R. K., Boul, P. J., Huffman, C. B., 1998, "Fullerene pipes", *Science*, Vol 280, pp. 1253-1256

Mallick, T. K., Eames, P. C., Hyde, T. J., and Norton, B., 2004, "The design and experimental characterisation of an asymmetric compound parabolic photovoltaic concentrator for building facade integration in the UK", *Solar Energy*, Vol 77, pp. 319-327

Maruyama, S. 2002, "A molecular dynamics simulation of heat conduction in finite length SWNTs", *Physica B: Condensed Matter*, Vol 323, pp 193-195

Maxwell, J. C, 1881, "*A treatise on electricity and magnetism*", (2nd edition ed., Vol. 1), Clarendon Press, Oxford

McDaniels, D. K., Lowndes, D. H., Mathew, H., Reynolds, J., and Gray, R., 1975, "Enhanced solar energy collection using reflector-solar thermal collector combinations", *Solar Energy*, Vol 17, pp. 277-283

Munari Probst, M. C., and Roecker, C., 2007, "Towards an improved architectural quality of building integrated solar thermal systems (BIST)", *Solar Energy*, Vol 81, pp. 1104-1116

Nelson, I.C., Banerjee, D., and Ponnappan, R., 2009, "Flow loop experiments using polyalphaolefin nanofluids", *Journal of Thermophysics and Heat Transfer*, Vol 23, pp. 752-761

Nieto de Castro, C. A., Murshed, S. M. S., Lourenço, M. J. V., Santos, F. J. V., Lopes, M. L. M., and França, J. M. P, 2012, "Enhanced thermal conductivity and

specific heat capacity of carbon nanotubes ionanofluids", *International Journal of Thermal Sciences*, Vol 62, pp. 34-39.

Norton, B. 2014, "*Harnessing Solar Heat*", Springer, New York

Notton, G., Cristofari, C., Mattei, M., and Poggi, P. 2005, "Modelling of a double-glass photovoltaic module using finite differences", *Applied Thermal Engineering*, Vol 25, pp. 2854-2877

Pak, B. C., and Cho, Y. I., 1998, "Hydrodynamic and heat transfer study of dispersed fluids with submicron metallic oxide particles", *Experimental Heat Transfer*, Vol 11, pp. 151-170

Parida, B., Iniyan, S., and Goic, R. 2011, "A review of solar photovoltaic technologies", *Renewable and Sustainable Energy Reviews*, Vol 15, pp. 1625-1636

Petter, B., Breivik, C., and Drolsum, R. 2012, "Building integrated photovoltaic products: A state-of-the-art review and future research opportunities", *Solar Energy Materials and Solar Cells*, Vol 100, pp. 69-96

Photon Engineering, FRED Software Knowledge Base, fred-kb.photonengr.com (cited 10/09/2015)

Piratheepan, M., and Anderson, T. N., 2015, "Natural convection heat transfer in façade integrated solar concentrators", *Solar Energy*, Vol 122, pp. 271-276

Playwithcarbon.com. Retrieved 22/05/2014, from http://www.playwithcarbon.com/carbon-nanotubes-1l/

Qiao, L., 1996, *A Study of Triton X Series Nonionic Surfactant Solutions*, PhD Thesis, University of Auckland, Auckland

Quaia, S., Lughi, V., Giacalone, M., and Vinzi, G., 2012, "Technical-economic evaluation of a Combined Heat and Power Solar (CHAPS) generator based on concentrated photovoltaics", *Proceedings of International Symposium (SPEEDAM) 2012*, Sorrento, Italy

Quesada, G., Rousse, D., Dutil, Y., Badache, M., and Hallé, S., 2012, "A comprehensive review of solar facades. Transparent and translucent solar facades", *Renewable and Sustainable Energy Reviews*, Vol 16, pp. 2643-2651

Rabl, A. 1976, "Comparison of solar concentrators", *Solar Energy*, Vol 18, pp. 93-111

Rashmi, W., Khalid, M., Ismail, A., Saidur, R., and Rashid, A., 2013, "Experimental and numerical investigation of heat transfer in CNT nanofluids", *Journal of Experimental Nanoscience*, Vol 10, pp 545-563

Rastogi, R., Kaushal, R., Tripathi, S. K., Sharma, A. L., Kaur, I., and Bharadwaj, L. M., 2008, "Comparative study of carbon nanotube dispersion using surfactants", *Journal of Colloid and Interface Science*, Vol 328, pp. 421-428

Reijenga, T., 2000, "Photovoltaics in the built environment", *Proceedings of 2nd World Solar Electric Buildings Conference*, Sydney

Rittner, E., 1954, "Use of pn junctions for solar energy conversion", *Physical Review*, Vol 96, pp. 1708

Rosell, J. I., Vallverdu, X., Lechon, M. A., and Ibanez, M., 2005, "Design and simulation of a low concentrating photovoltaic/thermal system", *Energy Conversion and Management*, Vol 46, pp. 3034-3046

Royne, A., Dey, C. J., and Mills, D. R., 2005, "Cooling of photovoltaic cells under concentrated illumination: a critical review", *Solar Energy Materials and Solar Cells*, Vol 86, pp. 451-483

Saha, S. C. 2011. "Unsteady natural convection in a triangular enclosure under isothermal heating", *Energy and Buildings*, Vol 43, pp. 695-703

Salmun, H., 1995, "Convection patterns in a triangular domain", *International Journal of Heat and Mass Transfer*, Vol 38, pp. 351-362

Sandnes, B., and Rekstad, J., 2002, "A photovoltaic/thermal (PV/T) collector with a polymer absorber plate, Experimental study and analytical model" *Solar Energy*, Vol 72, pp 63-73

Schoen, T., Prasad, D., Ruoss, D., Eiffert, P., and Sorensen, H., 2001, "Task 7 of the IEA PV power systems program–achievements and outlook", *Proceedings of the 17th European Photovoltaic Solar Conference*, Germany

Sharaf, O. Z., and Orhan, M. F., 2015, "Concentrated photovoltaic thermal (CPVT) solar collector systems: Part I–Fundamentals, design considerations and current technologies", *Renewable and Sustainable Energy Reviews*, Vol 50, pp. 1500-1565

Singh, H., and Eames, P. C., 2011, "A review of natural convective heat transfer correlations in rectangular cross-section cavities and their potential applications to

compound parabolic concentrating (CPC) solar collector cavities", *Applied Thermal Engineering*, Vol 31, pp. 2186-2196

Skoplaki, E., and Palyvos, J. A., 2009, "On the temperature dependence of photovoltaic module electrical performance: A review of efficiency/power correlations", *Solar Energy*, Vol 83, pp 614-624

Tanaka, H., 2011, "Solar thermal collector augmented by flat plate booster reflector: Optimum inclination of collector and reflector". *Applied Energy*, Vol 88, pp. 1395-1404

Tiwari, A., and Sodha, M., 2007, "Parametric study of various configurations of hybrid PV/thermal air collector: experimental validation of theoretical model". *Solar Energy Materials and Solar Cells*, Vol 91, pp. 17-28.

Tripanagnostopoulos, Y., 2007, "Aspects and improvements of hybrid photovoltaic/thermal solar energy systems", *Solar Energy*, Vol 81, pp. 1117-1131

Tripanagnostopoulos, Y., Nousia, T., Souliotis, M., and Yianoulis, P., 2002, "Hybrid photovoltaic/thermal solar systems", *Solar Energy*, Vol 72, pp. 217-234

United Nations Population Division, 2004, "*World population to 2300*", United Nations, New York

Varol, Y., Oztop, H. F., and Yilmaz, T. 2007, "Natural convection in triangular enclosures with protruding isothermal heater", *International Journal of Heat and Mass Transfer*, Vol 50, pp. 2451-2462

Vokas, G., Christandonis, N., and Skittides, F. 2006, “Hybrid photovoltaic–thermal systems for domestic heating and cooling—A theoretical approach”, *Solar Energy*, Vol 80, pp. 607-615

Welford, W. T., Winston, R., and Sinclair, D. C. 1980. “The optics of nonimaging concentrators: light and solar energy”, *Physics Today*, Vol 33, pp. 56

Wenham, S. R., Green, M. A., Watt, M. E., and Corkish, R., 2012, “*Applied photovoltaics”,* Earthscan, London

Williams, W., Hu, L.-W., and Buongiorno, J., 2008, “Experimental investigation of turbulent convective heat transfer and pressure loss of alumina/water and zirconia/water nanoparticle colloids (nanofluids) in horizontal tubes”, *Journal of Heat Transfer*, Vol 130, pp. 042-412

Xie, W. Y. A., 2012, “A Review on Nanofluids: Preparation, Stability Mechanisms, and Applications”, *Journal of Nanomaterials*, Vol 2012, pp. 17

Xuan, Y., and Roetzel, W., 2000, “Conceptions for heat transfer correlation of nanofluids”, *International Journal of Heat and Mass Transfer,* Vol 43, pp. 3701-3707

Yang, Y., Zhang, Z. G., Grulke, E. A., Anderson, W. B., and Wu, G., 2005, “Heat transfer properties of nanoparticle-in-fluid dispersions (nanofluids) in laminar flow”, *International Journal of Heat and Mass Transfer*, Vol 48, pp. 1107-1116

Yousefi, T., Veisy, F., Shojaeizadeh, E., and Zinadini, S. 2012, “An experimental investigation on the effect of MWCNT-H2O nanofluid on the efficiency of flat-

plate solar collectors", *Experimental Thermal and Fluid Science*, Vol 39, pp. 207-212

Zacharopoulos, A., Eames, P. C., McLarnon, D., and Norton, B., 2000, "Linear dielectric non-imaging concentrating covers for PV integrated building facades", *Solar Energy*, Vol 68, pp. 439-452

Zanesco, I., and Lorenzo, E. 2002, "Optimisation of an asymmetric static concentrator: the PEC-44D", *Progress in Photovoltaics: Research and Application*, Vol 10, pp. 361-376

Zhang, X., and Xu, P., 2015, "Field experimental study of a novel solar photovoltaic/thermal (PV/T) system", *Proceedings of Solar World Congress 2015*, Daegu, Korea

Zondag, H., De Vries, D., Van Helden, W., Van Zolingen, R., and Van Steenhoven, A., 2003, The yield of different combined PV-thermal collector designs, *Solar Energy*, Vol 74, pp. 253-269

Zondag, H. A., 2008, "Flat plate PV-Thermal collectors and systems: A review", *Renewable and Sustainable Energy Reviews*, Vol 12, pp. 891-959

Zondag, H. A., de Vries, D. W., van Helden, W. G. J., van Zolingen, R. J. C., and van Steenhoven, A. A., 2002, "The thermal and electrical yield of a PV-thermal collector", *Solar Energy*, Vol 72, pp. 113-128

Appendix A: Uncertainty analysis

To determine the uncertainties associated with the experiments Kline and McClintock's procedure (Kline and McClintock 1953) was used. According to the procedure, when R is a function of the independent measured variables $X_1, X_2 \ldots X_i \ldots X_n$, R can be written in general terms of Equation a1.

$$R = R\,(X_1, X_2 \ldots . X_i \ldots X_n) \tag{a1}$$

For a series of independent measurements, if the probability density function of the Xi is Gaussian in distribution, the uncertainty of R due to each measurement can be written as Equation a2 in terms of the sensitivity coefficients (partial derivatives).

$$\delta R_{X_i} = \frac{\partial R}{\partial X_i}\delta X_i \tag{a2}$$

The combined effect of a series of such measurements on the function R (W) can be expressed by Equation a3

$$W = \left[\sum_{i=1}^{n}\left(\frac{\partial R}{\partial X_i}\delta X_i\right)^2\right]^{1/2} \tag{a3}$$

A.1 Uncertainty analysis of the experiment relation to the geometrical concentration ratio confirmation

As elaborated in the experiment earlier, the concentration ratio was measured by taking the ratio between the open circuit current measurements with and without the reflector as shown in Equation a4. Hence, the uncertainties associated with the concentration ratio experiments are mainly caused by the ammeter reading, which has an uncertainty of ±3%.

$$C = I_c/I_a \qquad \text{(a4)}$$

Hence the error coefficients associated with the calculation are

$$\frac{\partial C}{\partial I_c} = \frac{1}{I_a}$$

$$\frac{\partial C}{\partial I_a} = -\frac{I_c}{I_a^2}$$

By substituting the values and taking rms, the overall uncertainty can be calculated as ±3.3%. The value is conservatively taken as 4% in order to account for the resistance of the connecting wires if there is any. As shown in Figure 65 most of the experimental values closely agree with the theoretical values.

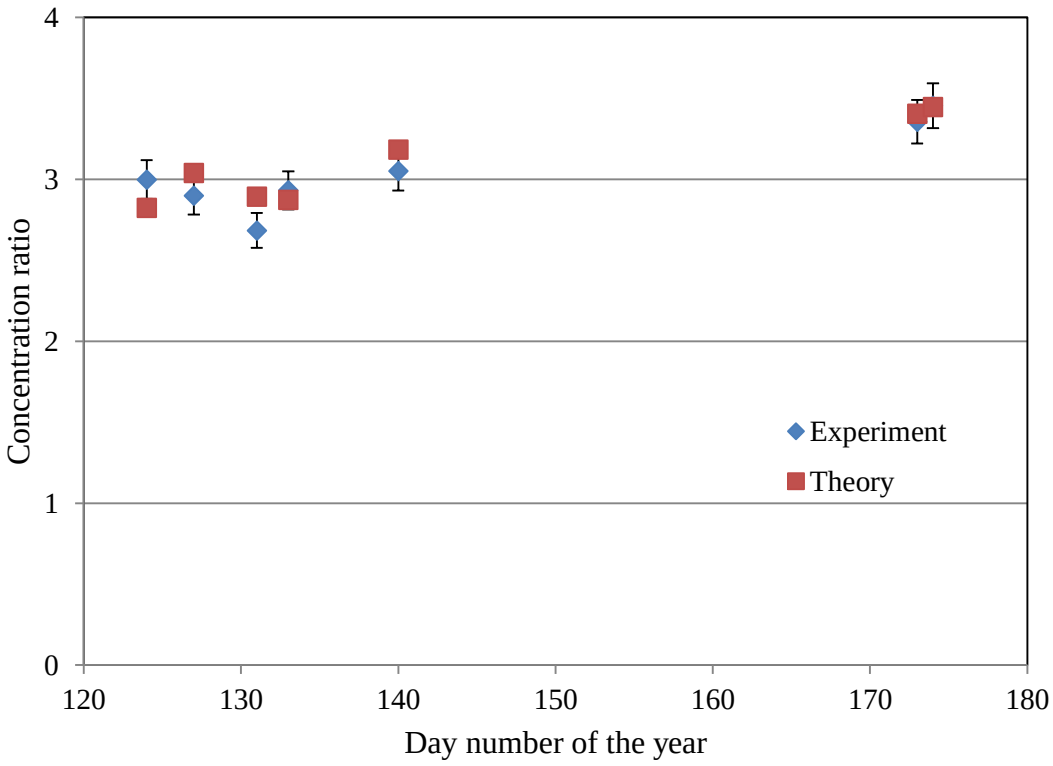

Figure 65 Experimental concentration ratio and calculated concentration ratio with the uncertainty values

A.2 Uncertainty analysis in natural convection heat transfer coefficient measurements

Calculating the heat losses due to conduction and radiation as well as the measurements uncertainties related to the energy input and the thermocouples readings. According to the manufacturer, the uncertainties associated with the thermocouple measurements are ±1.8%.

When calculating the heat losses by conduction using Fourier's law, the uncertainty is a function of area of the interest (A), combined thermal conductivity of the wood and insulation (k), insulation thickness (L) and the temperature difference across the insulation (T_i-T_a). Here T_i is the temperature of the hot wall and the T_a is the temperature of the cold wall.

Assuming the uncertainties arising due to A, k and the L are negligible; the uncertainties due to the temperature measurements of T_i and T_a can be expressed as in Equation a5.

$$w_{Q_{conduction}} = \left[\left(\frac{\partial Q}{\partial T_i}\, w_{T_i}\right)^2 + \left(\frac{\partial Q}{\partial T_a}\, w_{T_a}\right)^2\right]^{1/2} \qquad \text{(a5)}$$

Here $\left(\frac{\partial Q}{\partial T_i}\right) = \frac{kA_i}{L}$

And $\left(\frac{\partial Q}{\partial T_a}\right) = -\frac{kA_i}{L}$

By substituting the values of the measurements, the associated maximum uncertainty of the conduction losses from the test rig are approximately ±3.8 % in the worst case scenario (i.e both hot and cold plate temperatures are the same). As the temperature of the hot wall increases (which is the actual case in the experiment)

the associated uncertainty will decrease. However, the uncertainty $W_{Q\ conduction}$ is conservatively taken as 4%.

As discussed in the experiment, the uncertainty associated with discounting the radiation losses was calculated as less than 4%. Hence $W_{Q\ radiation}$ accounted for ±4% in determining the uncertainty in convection heat transfer. Furthermore, uncertainty associated with the power measurements (Q_e) of the electrical power meter MS6115 is ±1%.

By combining the above independent uncertainties, the uncertainty associated with the convection heat measurements can be expressed as in Equation a6.

$$w_{Q\ convection} = \left[{w_{Q\ coduction}}^2 + {w_{Q\ radiation}}^2 + {w_{Qe}}^2\right]^{1/2} \quad \text{(a6)}$$

By substituting the values calculated earlier in this equation, $W_{Q\ convection}$ is found to be approximately ±6%.

Finally, the uncertainty associated with the calculation of the natural convection heat transfer coefficient (h_c) can be calculated by finding the individual uncertainties of each variable in Equation a7.

$$h_c = Q_{convection} / \left(\left(A_{\ h}\ (T_h - T_i)\right)\right) \quad \text{(a7)}$$

If the uncertainties associated with the measurement of A_h is assumed to be negligible, the combined uncertainty related to convection heat transfer coefficient can be written as in Equation a8 using Equation a3.

$$w_{h_c} = \left[\left(\frac{\partial h_c}{\partial Q_{convection}}\ w_{Q_{convection}}\right)^2 + \left(\frac{\partial h_c}{\partial T_h}\ w_{T_h}\right)^2 + \left(\frac{\partial h_c}{\partial T_c}\ w_{T_c}\right)^2\right]^{1/2} \quad \text{(a8)}$$

Here

$$\frac{\partial h_c}{\partial Q_{convection}} = \frac{1}{A_h\,(T_h - T_c)}$$

$$\frac{\partial h_c}{\partial T_h} = -\frac{Q_{convection}}{A_h (T_h - T_c)^2}$$

$$\frac{\partial h_c}{\partial T_i} = \frac{Q_{convection}}{A_h\,(T_h - T_c)^2}$$

Terms associated with the temperature measurements are negligible as the uncertainty values of temperature measurements are relatively low compare to the uncertainties related to the convection term. Hence the resultant uncertainty associated with the calculation of convective heat transfer coefficient will be approximately ±6%.

From the Equation a9

$$Nu = \frac{h_c L}{k} \qquad \text{(a9)}$$

If the error associated with the measurements of characteristic length and the conduction of the air is negligible, the error associated with the calculation of Nusselt number is ±6%. Similarly, the uncertainties associated with the calculation of Rayleigh number can be accounted for by the uncertainties due to temperature measurements, which is approximately ±4%. As shown in Figure 66, calculated experimental values are within the range of values calculated by CFD.

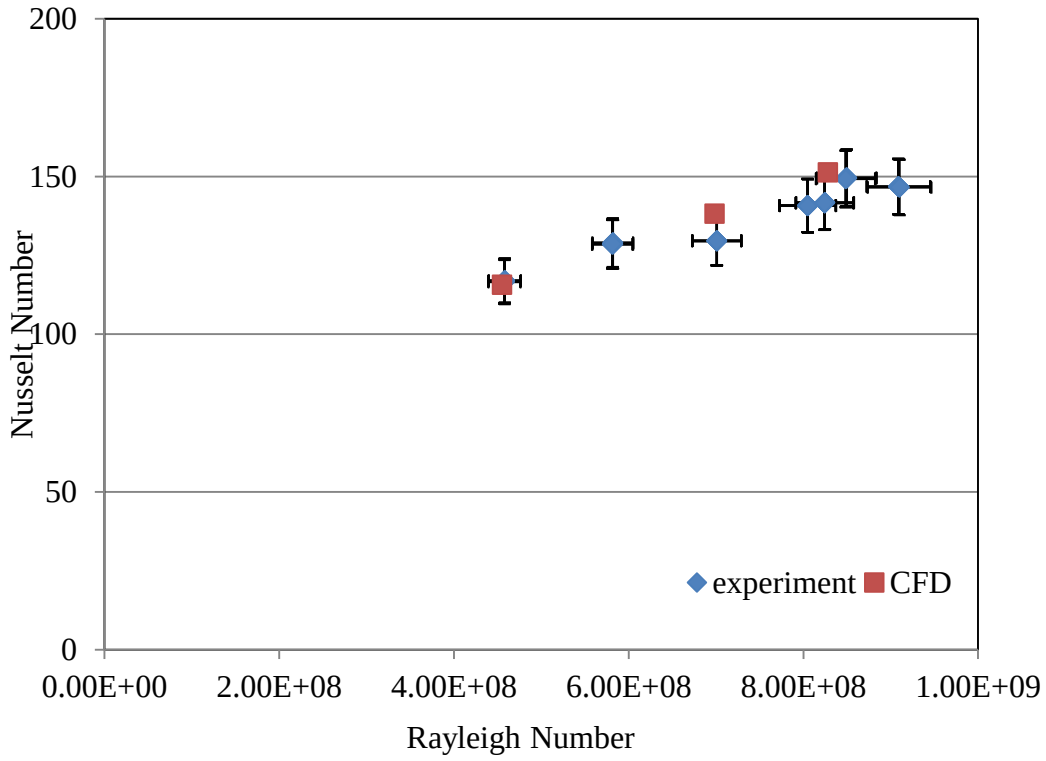

Figure 66 Nusselt vs Rayleigh number for experimental and CFD analysis with the uncertainty values

A.3 Uncertainties associated with final module testing

The standard uncertainty of the thermocouples was given as 1.8% by the manufacturer; hence uncertainty was conservatively taken as ±2%. The uncertainty related to the Parker liquid variable area flow meter reading was given by ±2%. Although, the reading was taken throughout the testing, as the reading involved a manual observation this was conservatively taken as ±4%. To measure the beam radiation, Delta-T SPN1 type sunshine pyranometer with ±5% standard deviation was used.

As discussed in the collector testing, the collector efficiency is given by Equation a10,

$$\eta_{tot} = \eta_{thermal} + \eta_{elect} \quad \text{(a10)}$$

Here $\eta_{elect} = \eta_{NOCT}\left(1 - \beta\left(T_{pm} - NOCT\right)\right) * S$

And $\eta_{thermal} = \frac{mC_p\,(T_o - T_i)}{G_{total}}$

Here T_{pm},m,T_o,T_i and G_{total} are measured variables subjected to uncertainties. Compared to uncertainties associated with the thermal efficiency $\eta_{thermal}$ the uncertainties associated with the electrical efficiency calculation η_{elect} appear to be very small, and were ignored. Hence the uncertainty related to the combined efficiency η_{tot} can be assumed as same as the uncertainty associated with the thermal efficiency measurements.

Hence the uncertainty coefficients can be given in terms of the following partial derivatives.

$$\frac{\partial \eta_{tot}}{\partial m} = \frac{C_p\,(T_o - T_i)}{G_{total}}$$

$$\frac{\partial \eta_{tot}}{\partial T_o} = \frac{mC_p}{G_{total}}$$

$$\frac{\partial \eta_{tot}}{\partial T_i} = \frac{-mC_p}{G_{total}}$$

$$\frac{\partial \eta_{tot}}{\partial G_{total}} = \frac{-mC_p\,(T_o - T_i)}{G_{total}^2}$$

Using the above functions, the final uncertainty associated with the efficiency measurements $W_{\eta total}$ can be given by Equation a11.

$$w_{\eta_{total}} = \left[\left(\frac{\partial \eta_{tot}}{\partial m} w_m\right)^2 + \left(\frac{\partial \eta_{tot}}{\partial T_o} w_{T_o}\right)^2 + \left(\frac{\partial \eta_{tot}}{\partial T_i} w_{T_i}\right)^2 + \left(\frac{\partial \eta_{tot}}{\partial G_{total}} w_{G_{total}}\right)^2\right]^{1/2} \quad \text{(a11)}$$

By substituting the relevant values, the uncertainty in the total efficiency of the final module efficiency is approximately 7%. As shown in the Figure 67 the experimental values closely agree with the efficiency predicted by the model.

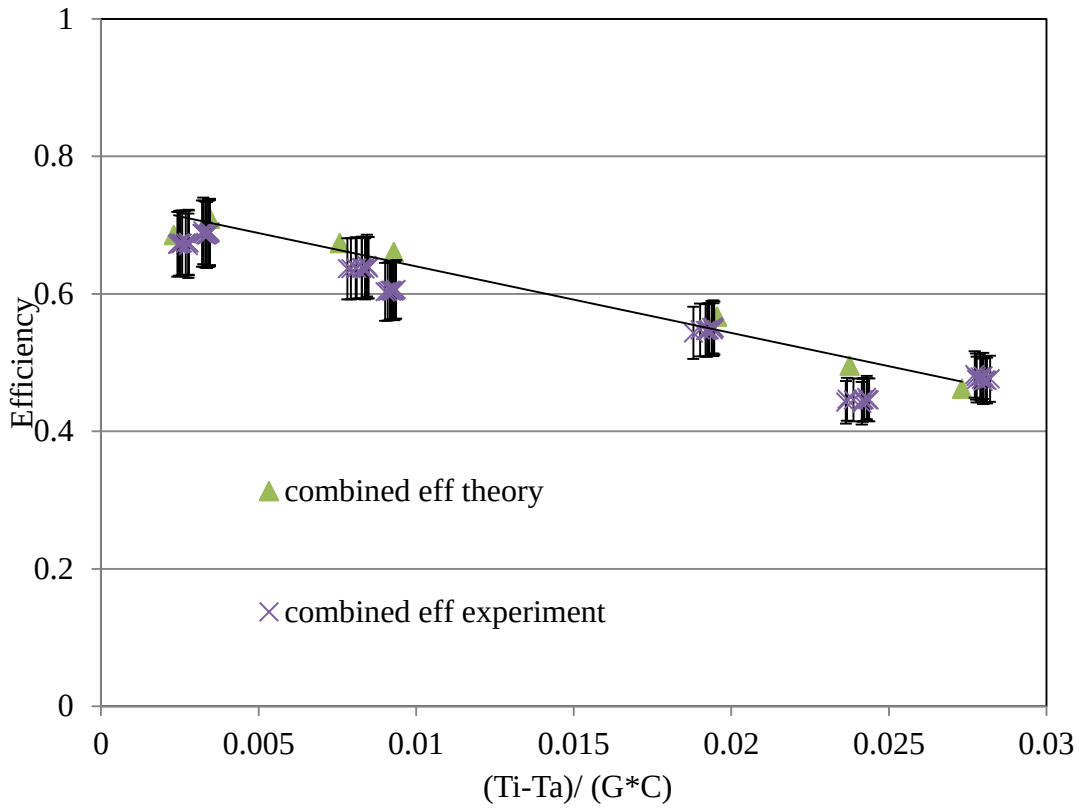

Figure 67 Experimental and theoretical efficiencies of façade integrated collector

A.4 EES code used for the simulation of the collector

```
Function IFTest(alpha)
IF (alpha<50) THEN
c=(cos(alpha+20)*(tan(alpha+20)+Tan(20)))/sin(alpha)*0.9+1/cos(20)
else
IF(alpha<70) and (alpha>50) THEN
c=(cos(alpha+20)*(3+Tan(20)))/sin(alpha)*0.9+1/cos(20)
else
c=(1-3*tan(alpha-70)) *(sin(20+alpha))/(sin(alpha))
endIF
endif
IFtest=c
end
c=Iftest(alpha)
alpha=arcsin(sin(La)*sin(di)+cos(La)*cos(di)*cos(HRA))
La=-36.84
di=23.45*sin((360*(284+n)/365))
```

LST=LT+TC/60

HRA=15*(LST-12)

TC=4*(174.76-15*12)+ET

ET=(9.87*sin(2*b)-7.53*cos(b)-1.5*sin(b))

b=360/365*(n-81)

LT=12

"Re=(4*m_flowrate)/(pi*d*mu)"

mu=Viscosity(Water,T=T_avg-273,P=1.01e2)

Re=m_flowrate/(d*mu)

"Darcy friction factor"

friction_factor=1/(1.8*log10(6.9/Re))^2

"Gnielinski relation"

Nusselt=((friction_factor/8)*(Re-1000)*Pr)/(1+12.7*(friction_factor/8)^0.5*(pr^(2/3)-1))

Pr=Prandtl(Water,T=T_avg-273,P=1.01e2)

"Thermal_conductivity=mu*C_p/Pr"

thermal_conductivity=Conductivity(Water,T=T_avg-273,P=1.01e2)

h_fl=(Nusselt*Thermal_conductivity)/d

T_avg=(T_o+T_i)/2

Q=m_flowrate*c_p*(T_o-T_i)

Q=A*F_r*(tau_alpha*G*C-U_L*(T_i-T_a))

{Q=A*(G*C-U_L*(T_pm-T_a))}

F_r=(m_flowrate*C_p)/(A*U_L)*(1-exp((-A*u_l*F_prime)/(m_flowrate*c_p)))

F=tanh (M*(w-d)/2)/(M*(w-d)/2)

m=sqrt(U_L/(k_abs*L_abs+K_pv*L_pv))

F_prime=U_L^(-1)/(W*(((U_L*(D+(W-D)*F))^(-1))+((pi*D*h_fl)^(-1))+(1/(w*h_pva))))

h_convection=(((Conductivity(Air_ha,T=(((T_pm+T_g)/2)-273),P=1.01e2)*0.67*((9.81*(1/(T_pm+T_g)/2)*(T_pm-T_g)*L^3))/(Viscosity(Air_ha,T=(((T_pm+T_g)/2)-273),P=1.01e2)/(Density(Air_ha,T=(((T_pm+T_g)/2)-273),P=1.01e2))))^0.36)/L)*(200/600)^1.75

h_rad=sigma#*(T_pm^4-T_g^4)/(((1-Epsilon_c)/(A*Epsilon_c))+((1/A*(0.2+0.638-0.6)/(0.2*2)))+((1-Epsilon_g)/(A_g*Epsilon_g)))

R_2=1/(H_convection+h_rad)

R_3=1/((sigma#*epsilon_g*(T_g_prime^2+T_a^2)*(T_g_prime+T_a)+((h_w^3+

h_nat^3)^(1/3))))

h_w=2.8+3*V

h_nat=1.78*(T_g_prime-T_a)^(1/3)

(T_g_prime-T_a)/R_3=(T_g-T_g_prime)/R_4

(T_pm-T_g)/R_2=(T_g-T_g_prime)/R_4

R_1=2.165/A_prime

U_L=1/(R_2+R_3+R_4)+1/R_1

R_4=0.04/0.96

T_pm=T_i+(Q/A)/(F_r*U_L)*(1-F_r)

eta_thermal=F_r*(s*tau_alpha+(1-s)*Tau_beta) -F_r*U_L*(T_i-T_a)/(G*C)

plot=(T_i-T_a)/(G*C)

Eta_now=(m_flowrate*c_p*(t_o-T_i))/(A*G*C)

s=0.7

"electrical efficiency"

eta_elctrical=eta_ref*(1-0.004*(T_pm-298))*s

eta_ref=0.175

E_power=eta_elctrical*c*G*S*A

G_electrical=c*G*S*A

eta_tot=eta_thermal+eta_elctrical

*Few data range and equations are purposefully altered to avoid unauthorised copying